PhD Program in Biomolecular Sciences

Department of Cellular, Computational and Integrative Biology – CIBIO

38th Cycle

lncRNA *RPPH1* in melanoma: novel functions as cargo of tumor-derived Extracellular Vesicles

Tutor:

Prof. Maria Caterina MIONE
University of Trento

Advisor:

Prof. Manuela BASSO
University of Trento

Ph.D. Thesis of

Federica BUSI

University of Trento

Academic Year 2024/2025

Declaration of authorship

I, Federica Busi, confirm that this is my own work. The use of all material from other sources has been properly and fully acknowledged.

Federica Busi

Table of Contents

Abbreviations

AP-1	Activator Protein-1
AS	Anti-sense
ATG5	Autophagy Related 5
BP	Base pair
BRAF	v-raf murine sarcoma viral oncogene homolog B1
CARD	Caspase Activation and Recruitment Domain.
Cas 9	CRISPR-associated protein 9
CCR	Colorectal Cancer
CD-n	Cluster of Differentiation *n*
cDNA	Complementary DNA
CHT	Caudal Hematopoietic Tissue
CRC	Colorectal Cancer
CRISPR	Clustered Regularly Interspaced Short Palindromic Repeats
crRNA	CRISPR RNA
CSF1R	Colony Stimulating Factor 1 Receptor
CTD	C-terminal domain
CU-CPT4a	N-[(3-chloro-6-fluorobenzo[b]thiophene-2-yl)carbonyl]-D-phenylalanine
DAMP	Damage Associated Molecular Pattern
DN	Diabetic Nephropaty
DNA	Deoxyribonucleic Acid
dpf	Days post fertilization
Ds/ssRNA	Double strand/single strand RNA
EGFR	Epidermal Grow Factor Receptor
EIF5B	Eukaryotic Translation Initiation Factor 5B

EMT	Epithelial to Mesenchimal Transition
ESCRT	Endosomal Sorting Complex Required for Transport
EV	Extracellular Vesicle
Gal-3	Galectin-3
GAPDH	Glyceraldehyde-3-Phosphate Dehydrogenase
GFP	Green Fluorescent Protein
GO	Gene Ontology
gRNA	Guide RNA
GSEA	Gene Set Enrichment Analysis
HPSC	Human Pluripotent Stem Cells
HRA1	Hypoxia response Attenuator 1
iDRIP	Identification of Direct RNA-Interacting Proteins
Ifit-n	Interferon-induced protein with tetratricopeptide repeats *n*
IFN	Interferon
IFNAR1/2	Interferon Alpha and Beta Receptor Subunit 1/2
IKK	IκB kinase
IL-n	Interleukin-*n**
ILV	Intra Luminal Vesicles
IRF-n	Interferon Regulatory Factor *n*
ISEV	International Society of Extracellular Vesicles
ISG*n*	Interferon-Stimulated Gene *n**
kDa	Kilo Dalton
Kita	KIT proto-oncogene, receptor tyrosine kinase a
KO	Knock Out
LGP2	Laboratory of Genetics and Physiology 2
lincRNA	Long Intergenic non-coding RNA

lncRNA	Long non-coding RNA
LPS	Lipopolysaccharide
LRR	Leucine-Rich Repeat
M6A	N^6-methyladenosine
MALAT 1	Metastasis-Associated Lung Adenocarcinoma Transcript 1
MAPK	Mitogen-Activated Protein Kinase
MAVS	Mitochondrial Antiviral Signaling protein
MDA5	Melanoma Differentiation–Associated protein 5
MFE	Minimum Free Energy
Mg	Magnesium
miRNA	Micro RNA
Mitfa	Microphthalmia-Associated Transcription Factor a
METTL*n*	Methyltransferase *n*
Mpeg	Macrophage Expressed Gene
MRP	Mitochondrial RNA Processing
mTORC	mechanistic Target of Rapamycin Complex
MVB	Multi Vesicular Bodies
MVs	Microvesicles
MyD88	Myeloid Differentiation Primary Response 88
MYO1C	Myosin 1C
NAP1	Nucleosome Assembly Protein 1
NBI	Nickel Based Isolation
NCL	Nucleolin
ncRNA	Non-coding RNA
NF-kB	Nuclear Factor kappa-light-chain-enhancer of activated B cells
NHEM	Normal Human Epidermal Melanocytes

NK	Natural Killer
nt	nucleotides
PAMP	Pattern Recognition Receptros
PBS	Phosphate-Buffered Saline
PD-L1	Programmed Death-Ligand 1
PDX	Patient derived Xenograft
PMA	Phorbol 12-Myristate 13-Acetate
Pol III	RNA Polymerase III
Poly(A)	Polyadenosine
Poly(I:C)	Polyinosinic:polycytidylic acid
PRR	Pattern Recognition Receptor
qPCR	Quantitative Polymerase Chain Reaction
RIG-I	Retinoic acid-Inducible Gene I
RIP1	Receptor-Interacting Protein Kinase 1.
RLR	RIG-I Like Receptors
RMRP	RNA Component of Mitochondrial RNA Processing Endoribonuclease
RNA	Ribonucleic Acid
RNase	Ribonuclease
RNP	Ribonucleoprotein
Rpp n	Ribonuclease P Protein Subunit *n**
RPPH1	Ribonuclease P RNA Component H1
RPR	RNA Component of RNase P
rRNA	Ribosomal RNA
SK-MEL	Sloan-Kettering Melanoma
SLC3A2	Solute Carrier Family 3 Member 2
smiFISH	Single-Molecule Inexpensive Fluorescence In Situ Hybridization

SRAMP	Sequence-based RNA Adenosine Methylation site Predictor
SRSF-n	Serine/Arginine-Rich Splicing Factor *n**
TAM	Tumor Associated Macrophage
TANK	TRAF Family Member-Associated NF-κB Activator
TBK1	TANK-Binding Kinase 1
TCOF-1	Treacle Ribosome Biogenesis Factor 1
TFEB	Transcription Factor EB
TIR	Toll/interleukin-1 receptor/resistance protein
TLRn	Toll Like Receptor *n**
TME	Tumor Microenvironment
TR	Telomerase RNA Component
tracrRNA	Trans-Activating CRISRP RNA
TRAF	TNF Receptor–Associated Factor
TRIF	TIR-domain–containing adapter-inducing interferon-β
TRIM*n*	Tripartite Motif Containing *n**
tRNA	Transfer-RNA
TRPM8	Transient Receptor Potential Melastatin 8
UAS	Upstream Activating Sequence
UMAP	Uniform Manifold Approximation and Projection
VEGF	Vascular Endothelial Growth Factor
WB	Western Blot
WTAP	Wilms' tumor 1-associating protein

**n* stands for different numbers

Abstract

The long non-coding RNA (lncRNA) *RPPH1* is a ribozyme, an RNA molecule with enzymatic activity, and serves as the catalytic component of the RNase P ribonucleoprotein complex. This complex performs the endonucleolytic cleavage of precursor tRNAs at their 5' leader sequences. Increasing evidence suggests that *RPPH1* may also have non-canonical roles in tumor progression, including its presence as an extracellular vesicles (EVs)-associated RNA species. In a recent study, we reported a significant enrichment of lncRNA *RPPH1* in melanoma-derived EVs, both in zebrafish and human models.

Tumor progression depends on dynamic interactions between cancer cells and their surrounding tumor microenvironment (TME). Among the mediators of this communication, EVs have emerged as key carriers of bioactive molecules capable of modulating multiple aspects of cancer biology: tumor-derived EVs can influence tumor initiation, growth, and metastatic dissemination. Recent evidence indicates that the RNA cargo contained within these vesicles contributes to pro-tumorigenic inflammation by activating interferon-mediated immune responses through Pattern Recognition Receptor (PRR) signalling pathways. Notably, the injection of melanoma-derived EVs or synthetic *RPPH1* into healthy zebrafish larvae induces sterile inflammation, consistent with the activation of PRR-dependent signalling in macrophages.

In this PhD work, we investigated the mechanisms underlying the packaging of *RPPH1* into extracellular vesicles in melanoma. We demonstrated that *RPPH1* is upregulated in melanoma cells and abnormally localizes to the cytoplasm. Proteomic analysis of *RPPH1*-associated protein partners in melanoma revealed potential novel functions for this lncRNA beyond its canonical role in the RNase P complex, particularly in RNA metabolism. These findings suggest that such alternative functions may contribute to its selective encapsulation within EVs.

Using both human and zebrafish melanoma models, we further explored the mechanisms through which melanoma-derived EVs induce sterile inflammation. Our results showed that these EVs, likely through their *RPPH1* cargo, activate the RIG-I-like receptor (RLR) pathway in recipient macrophages, triggering an inflammatory response characterized by the upregulation of interferon-stimulated genes (ISGs) and pro-inflammatory cytokines. Single-cell RNA sequencing revealed that this EV-mediated signalling drives the transcriptional reprogramming of macrophages toward a tumor-supportive, pro-inflammatory phenotype, typical of tumor-associated macrophages (TAMs). Notably, this response appears to be primarily confined to a macrophage subpopulation inherently predisposed to endocytosis and EV-trafficking.

Overall, these findings contribute to a deeper understanding of how melanoma cells promote tumor progression, reprogramming the immune cells in the tumor microenvironment through EV-mediated RNA signalling.

CHAPTER 1

Introduction

1. INTRODUCTION

1.1 Long non-coding RNA *RPPH1*

Ribonuclease P RNA Component H1 (*RPPH1*) is a ribozyme, an RNA molecule with catalytic activity and is classified as a long non-coding RNA (lncRNA). LncRNAs are transcripts longer than 200 nucleotides with limited protein-coding potential, yet they play crucial roles in the regulation of diverse biological processes. These include transcriptional and post-transcriptional regulation, epigenetic modifications, and the initiation and progression of various diseases (1).

RPPH1 was the first RNA molecule to be defined as ribozyme, and its discovery by Sidney Altman was pivotal in revealing that RNA molecules can have catalytic functions, fundamentally changing the understanding of molecular biology. This discovery earned him a Nobel Prize in Chemistry in 1989, which he shared with Thomas R. Cech for demonstrating that RNA is not just a passive messenger but can also act as an enzyme.

Human *RPPH1* was initially identified in HeLa cells as a 340 nt long RNA molecule that copurifies with the catalytic activity of RNase P, establishing its functional role within the enzyme (2). In the same publication authors suggested that in the human genome the copy number for *RPPH1* gene could be at most three. While its primary sequence showed little similarity to prokaryotic or lower eukaryotic counterparts, predicted secondary structures revealed conserved domains shared with yeast RNase P RNA highlighting evolutionary constraints that preserve catalytic function despite sequence divergence (2). Only later the genomic structure and transcriptional properties of the human *RPPH1* gene has been characterized, highlighting that the human genome contains a single copy of the *RPPH1* gene and that even though its promoter exhibits features compatible with both RNA polymerase II and III transcription, it seems to be predominantly transcribed by RNA polymerase III (3).

The main function of *RPPH1* is to be the catalytic component of RNase P, which performs the endonucleolytic cleavage of precursor tRNAs at their 5' leader sequences (4). This reaction, which depends on divalent metal ions, generates the mature 5' termini of tRNAs, is their first and essential post-transcriptional modification, which is fundamental for their biological function (5) (***Figure 1***). For a long time, the RNase activity as part of the RNase P complex has been recognised has the only studied function for the lncRNA *RPPH1*. Nevertheless, more recently, novel functions have been highlighted for *RPPH1*, independently of RNase P. In senescent fibroblast *RPPH1* is upregulated and it accumulates in mitochondria and participate in the destabilization of proliferation-related target mRNAs, thus promoting senescence (6). Other novel functions for *RPPH1* have been discovered in correlation with pathological conditions, such as diabetic nephropathy, in which the lncRNA promotes mesangial cell proliferation and inflammation through interaction with Gal-3 (7).

RPPH1 can interact with various proteins and miRNAs to support cell growth and proliferation, with increasing evidence indicating that these interactions contribute to tumorigenesis and metastasis across multiple cancer types (additional information about non canonical functions of *RPPH1* in cancer are reviewed in section 1.1.2).

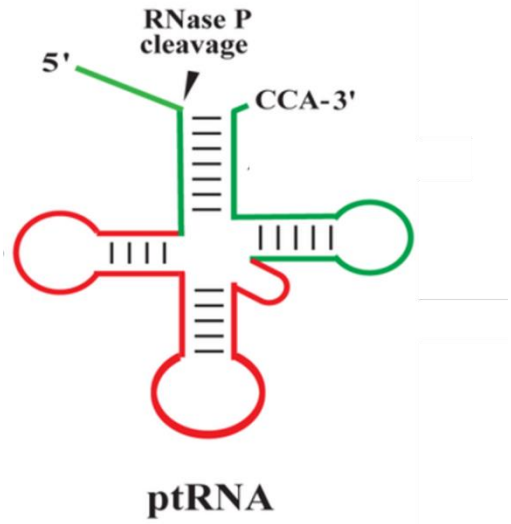

Figure 1. **RNase P substrate.** Representation of a pre-tRNA prior to cleavage by RNase P. The first step of tRNA maturation consists in an endonucleolityc cleavage at the 5' end of the precursor. The black arrow indicates the site of cleavage. *Adapted from (8).*

1.1.1 The canonical function of *RPPH1* as catalytic component of RNase P

Ribonuclease P (RNase P) is an essential endoribonuclease, that was first discovered in bacteria and then found to be highly conserved in all domains of life (9). RNase P catalyses the first and most crucial step in tRNA maturation in all organisms. It cleaves the 5'-end of pre-tRNAs through a precise endonucleolytic cleavage (10). In bacteria it was firstly characterized as a holoenzyme formed by a small protein subunit and a large RNA component, which provides the catalytic function and, *in vitro*, showed all the properties of a complete and functional enzyme also without being associated with the protein counterpart (11). This finding ultimately paved the way for the discovery of ribozymes and the rise of contemporary RNA biology. Many years of studying RNase P, pointed out that the holoenzyme shows surprising differences in composition and structures across different organisms, raising fundamental questions about the evolution in the role of RNA molecules and highlighting a possible transition from an ancient RNA world to the more recent protein-based biology. Indeed, scaling up in evolution and increasing the complexity of organisms, RNase P exhibits a corresponding rise in structural complexity. Indeed, in archaea and eukaryotes, unlike in prokaryotes, RNase P is composed of several protein components that are necessary for the

stabilization of the RNA component that still maintains its catalytic function in the complex (12).

In the human RNase P holoenzyme, the RNA subunit *RPPH1*, is surrounded by eleven proteins forming the largest RNase P ribonucleoprotein complex described so far. Devoid of protein components, *RPPH1* exhibits only limited pre-tRNA processing activity compared to its bacterial counterparts (13). The protein component of human RNase P consists of Pop1, a single protein component, and three subcomplexes: the Rpp20–Rpp25 heterodimer, the Pop5–Rpp14–$(Rpp30)_2$–Rpp40 heteropentamer, and the Rpp21–Rpp29–Rpp38 heterotrimer. These subcomplexes are organised to form a structure shaped as a clamp that tightly grips *RPPH1* (***Figure 2***). Overall, the complex is organized around *RPPH1*, which interacts with all the proteins, that wrap around the RNA moiety to stabilize it in an extended conformation, which allows the correct positioning of the catalytic core (14). This arrangement allows the precise placement of the two Mg^{2+} ions essential for catalysis, as RNase P functions as a metalloenzyme (15).

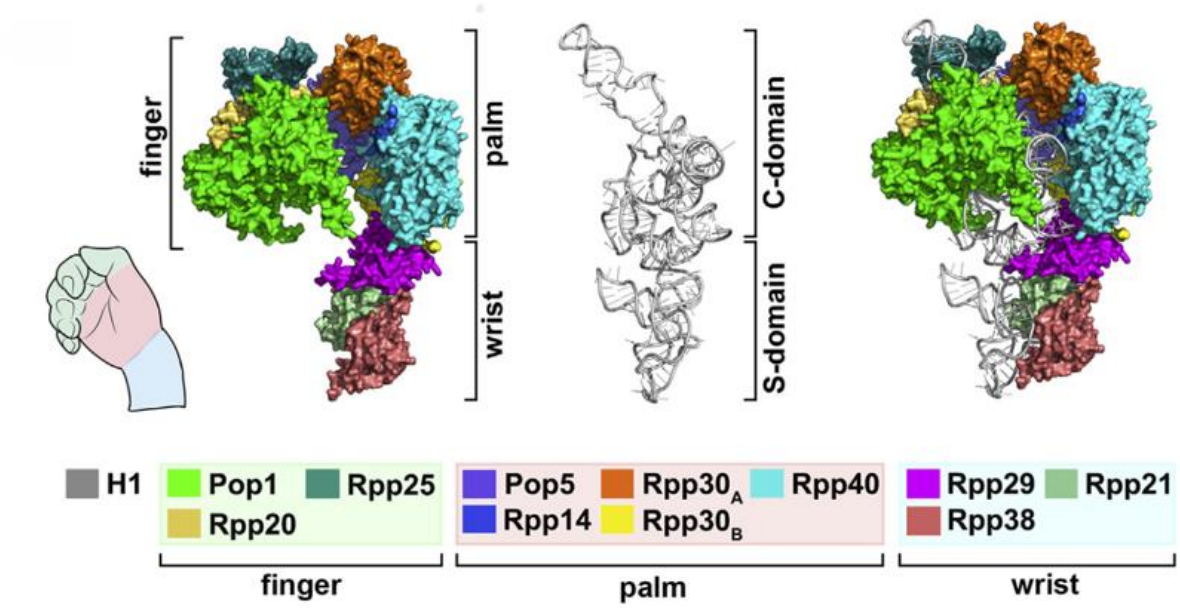

Figure 2. **Three-dimensional structure of the human RNase P**. Structural conformation of RNase P. The proteins of the complex assemble into a right-hand-shaped clamp composed of three modules: finger, palm, and wrist. This clamp securely grips *RPPH1*. The C domain of *RPPH1* contains the conserved catalytic core, fits precisely into the narrow pocket formed between the palm and finger of the clamp, with only the tip of one branch protruding outward. *Adapted from (14).*

Over time it has emerged that RNase P does not process only tRNAs, although they are its main substrates, but is also involved in the maturation of other non-coding RNA species. For example, in *S. cerevisiae*, the hidden-in-reading-frame antisense-1 RNA (*HRA1*) was identified

and validated *in vitro* as an RNase P substrate (16). Moreover, several small-nucleolar RNAs (snoRNAs) were found to copurify with RNase P, further supporting its involvement in processing noncanonical RNA substrates (17). In humans, RNase P has been demonstrated to participate in the maturation of the lncRNA *MALAT1* simultaneously maturing the 3' of the nuclear-retained lncRNA *MALAT1* and generating a small RNA that is then transported in the cytoplasm (18).

Given RNase P's essential role across all organisms and its remarkable functional versatility, considerable efforts over the years aimed at uncovering the full range of processes in which RNase P is involved. Human RNase P play a crucial role in transcription coupled with RNA Polymerase III (Pol III), being recruited at active transcription sites, binding itself to the chromatin of some genes (tRNAs and *5S* rRNA) and being required for the transcription of those genes by Pol III (19). Several studies found evidence of an involvement of RNase P components in genome assembly and stability, being for example recruited to DNA damage sites (20). Moreover, RNase P shares protein subunits with two other vital eukaryotic ribonucleoprotein enzymes, the RNase MRP and telomerase, while their catalytic RNA components are unique (*RMRP* and *TR* respectively), leading to a crosstalk between these complexes.

A cognate endoribonuclease, RNase MRP, is present in eukaryotes and shares nine out of ten protein subunits with RNase P. It was originally characterized as a nuclease that cleaves primers for mitochondrial DNA replication, but subsequent studies revealed its additional role in pre-rRNA processing (21). RNase P and MRP appear to be evolutionary related, displaying several similarities also in the catalytic mechanism of action. The enzymatic function of RNase MRP also resides in an RNA moiety. *RPPH1* and MRP RNA (*RMRP*) are largely unrelated in sequence, yet they share similar secondary structures, particularly in the folding of their catalytic core regions (22). In yeast, three of the RNase P complex proteins are also essential for telomerase activity, binding to the RNA subunit of telomerase. In fact, their reduction causes mature telomerase to be sequestered in the cytoplasm, preventing it from accessing its nuclear substrates (23).

Overall, RNase P emerges as a multifunctional and evolutionarily adaptable ribonucleoprotein, whose roles extend far beyond tRNA processing to fundamental processes in RNA metabolism, transcription, and genome stability.

1.1.2 *RPPH1* in cancer

lncRNAs can modulate gene expression at multiple levels: in the nucleus, they recruit chromatin modifiers to regulate transcription (24) or influence RNA splicing (25); in the cytoplasm, they affect mRNA stability or translation by base-pairing with mRNAs or acting as competitive miRNA sponges (26). As key regulators of several biological processes,

dysregulation of lncRNAs has been found to be associated with several cancer hallmarks, such as cell proliferation and apoptosis as well as migration and invasion during tumor development, thus influencing the remodelling of the tumor microenvironment (TME) and metastases formation (27).

In this context *RPPH1* has been found to be dysregulated in different cancers and to participate in disease progression. In hepatocellular carcinoma, *RPPH1* overexpression correlates with tumor growth and metastases (28). Surprisingly, *RPPH1* has been recently identified also as circular RNA (*circRPPH1*) that localises in the cytoplasm. *circRPPH1* is overexpressed in triple negative breast cancer (29) in which it promotes the malignant behaviour of cancer cells, correlating with poor prognosis (30).

In tumors, *RPPH1* has also been detected as cargo of extracellular vesicles (EVs). Growing evidence suggests that lncRNAs constitute a relevant component of exosomes, with the ability to regulate different functions in recipient cells. However, as the RNase P-related function of *RPPH1* has been the most studied for a long time and consistent with its nuclear localization, *RPPH1* has been rarely reported as EVs cargo until recent years and almost exclusively in the context of tumors.

In colorectal carcinoma, *RPPH1* enhances tumor cell migration and invasion both *in vitro* and *in vivo*, by being transmitted by exosome to macrophages in the TME to mediate their M2 polarization (31). A very recent report unveiled a central role of *RPPH1* in breast cancer metastases formation, also highlighting its potential as therapeutic target. The authors discovered that the hypoxic environment of breast cancer, upregulates the expression of *RPPH1* and promotes its packaging in EVs, influencing the maintenance of stemness and aggressive traits in cancer cells and promoting angiogenesis in endothelial cells (32). In our laboratory, we recently reported a specific accumulation of the lncRNA *RPPH1* in zebrafish melanoma-derived EVs, an enrichment that we also confirmed in a human cell model of melanoma (33). More information about this point is introduced in section 1.5.2.1. Considering all of the above, *RPPH1* appears as a multifunctional lncRNA whose dysregulation and extracellular trafficking via EVs contribute to tumor progression, metastasis, and microenvironment remodelling, underscoring its potential as both a biomarker and a therapeutic target in cancer.

1.2 Extracellular Vesicles

Extracellular Vesicles (EVs) are lipid bilayer-enclosed structures secreted by a wide variety of cell types into the extracellular space, as well as in biological fluids. Initially, they were considered mainly as a mechanism for the disposal of unwanted compounds and cellular debris. Over the years, however, EVs have emerged as more than just waste carriers and are now recognized as fundamental mediators of paracrine cell-to-cell and inter-organ communication, playing a pivotal role in the exchange of biomolecules and in the regulation of numerous physiological and pathological processes.

EVs exert their biological functions by transporting specific molecular cargoes from the cell of origin to recipient cells, thereby delivering precise information that can influence cellular behaviour and function. Proteins, lipids and nucleic acids can be carried inside vesicles, or even on their surface, and act as biomolecular signals (34).

EVs exhibit wide heterogeneity in both size and molecular composition, which is influenced by their cell of origin, the physiological or pathological state of the cell, and environmental stimuli. Consequently, their classification has always been challenging and often relied on diverse criteria, and this has contributed to many misconceptions in the literature. For this reason, in 2023 the International Society of Extracellular Vesicles (ISEV) published a guide on minimal requirements to study EVs (35).

The most common classification of EVs, which is also recognised by ISEV (35), is based on their biogenesis, and distinguish between Ectosomes, also known as microvesicles (MVs) and Exosomes.

1.2.1 EVs Biogenesis

Ectosome biogenesis starts with the outward budding of the plasma membrane. Mature MVs are then shed from the surface of cells, following a strictly regulated pinching and scission process that results in their release directly into the extracellular space (***Figure 3***). MVs formation specifically requires cholesterol, and its depletion prevents their release (36); additionally, extracellular factors, such as an hypoxic environment, can enhance MVs shedding (37).

Nevertheless, it is difficult to define MVs formation by a single biogenetic mechanism, as they represent in turn a highly heterogeneous subpopulation of EVs. This heterogeneity is also reflected by the size range of ectosomes that span from 50 nm to 1000 nm in diameter (38).

What is clear, is that in the biogenesis of MVs an important role is played by the plasma membrane that operates as an extremely organized connection between intra and extracellular signals. To date, research has focused on the understanding of the organization of the plasma membrane into domains that are well defined based on their lipid composition, phospholipid organization, and protein-mediated bending (39).

Exosomes, instead, derive from the endosomal compartment and have a size range between 40- 160 nm in diameter, so they are considered small EVs (34).
Endosomes, that originates from the invagination of the plasma membrane, are organized into distinct compartments: early and late endosomes. Early endosomes can fuse with endocytic vesicles, directing their contents toward degradation, recycling, or secretion. Late endosomes, meanwhile, accumulate intraluminal vesicles (ILVs) formed by inward budding of the endosomal membrane, during which cytosolic proteins, nucleic acids, and lipids are sorted into these small vesicles. Late endosomes containing numerous ILVs are called multivesicular bodies (MVBs), which can either fuse with lysosomes for degradation or with the plasma membrane to release ILVs as exosomes into the extracellular space (40) (***Figure 3***). Thus, the formation of ILVs is the beginning of exosomes biogenesis. It requires firstly the enrichment of the endosomal membrane in tetraspanins, secondly the recruitment of the endosomal sorting complexes required for transport (ESCRTs) (41).

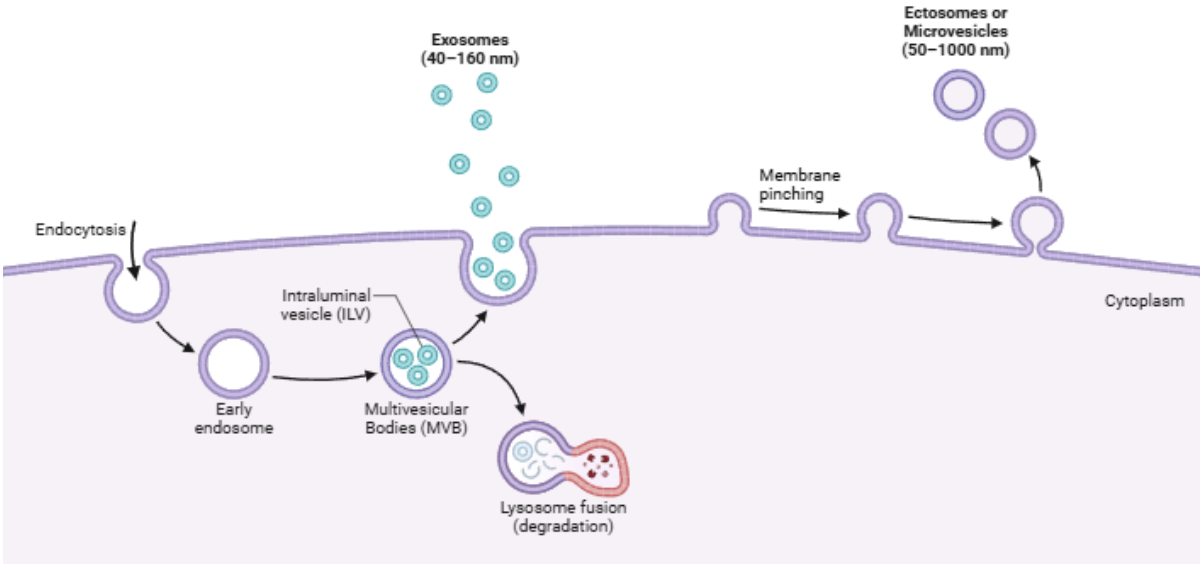

Figure 3. **Biogenesis of Extracellular Vesicles**. The two major categories of EVs are ectosomes and exosomes. Ectosomes are released through plasma membrane budding and are in the size range of ~50 nm to 1000 nm. Exosomes originate from the endosomal pathway by the formation of MVBs, which contain ILVs. *Made with Biorender,com.*

Even if this mechanism is well characterized, emerging evidence are highlighting how even this subpopulation of vesicles can involve several steps, leading to an intrinsic heterogeneity also within exosomes.
The increasing interest in the study of cell-derived particles, is bringing out the internal diversity of extracellular vesicles, adding new structures to the pool of known EVs, such as apoptotic bodies, large vesicles released by cells undergoing apoptosis (42), migrasomes,

released by migrating cells (43) and even oncosomes, large vesicles released by tumor cells in a similar way to MVs (44).

1.2.2 Biological content and roles of EVs

As carriers of biomolecular signals, EVs can exert a variety of functions both in physiologic and pathological contexts, functions that are tightly linked with their biological content.
The cargo composition of EVs is highly specific and depends on several factors such as the type of vesicle, the cell of origin and environmental stimuli. It comprises lipids, proteins and nucleic acids, besides a plethora of different metabolites (45), each of which can be localized either inside EVs, in the vesicular lumen, transmembrane or associated with their outer membrane, forming what is commonly known as the EVs biomolecular corona (46). The biomolecular corona is a complex network of dynamic interaction established between molecules found in the extracellular space, as well as during EVs formation, with the components of the EV membrane, thereby becoming a portion of EV-related molecules, even if not physically included in them. Of note, the components of the biomolecular corona have demonstrated to participate to EV signalling in recipient cells, similarly to their cargoes (47). Mechanism through which different molecules are loaded in EVs are currently a field of great interest, as alterations in EV cargo may reflect the onset or progression of pathological conditions. Consequently, considerable research efforts have been directed towards this field. Although many aspects of EV cargo sorting and several EV components still require further investigation, several recurrent as well as context-specific patterns have been elucidated to date (***Figure 4***).

Lipids
The lipidic composition of EVs has been thoroughly investigated in a variety of settings, as lipids are key components of EVs, not only forming the membrane that allows the transport of cellular molecules in a protected space, but also because their composition intrinsically influences EVs behaviour and functions (48). Overall, the lipid composition reflects the features of membranes of the originating cells. Nevertheless, some studies highlighted that some lipids are more specifically associated with different types of EVs. For example, MVBs derived EVs exhibit a higher enrichment of phosphatidylserine prominently exposed to the extracellular environment than the plasma membrane, promoting their uptake by recipient cells (49). On the other hand, the lipid composition of MVs, reflects their origin from the budding of the plasma membrane and shows an enrichment in ceramides and sphingomyelins (50). Of note, as pathological conditions influence the biomolecular composition of EVs, the lipidic components are likewise affected. For example, it has been reported that EVs derived from breast cancer cells show an enrichment in sphingolipids and glycerophospholipids compared to their parental cells, and this distinctive lipid profile has shown strong potential as a biomarker for breast cancer diagnosis (51).

Proteins

As with all molecules that characterize EVs, the protein fraction of EV cargo generally reflects the cell of origin, while also being influenced by the context in which the EVs are released. For instance, pathological conditions can modulate the selective loading of specific proteins into EVs. Therefore, a comprehensive characterization of the EV protein composition remains difficult, owing to the variety of isolation methods and the heterogeneity of EV populations. However, commonly found proteins in EVs are those related to their biogenesis. Proteins involved in vesicle formation, such as RAB proteins and components of the ESCRT complex, which is also involved in the loading of ubiquitinated proteins in vesicles (52), are commonly associated with EVs. Given their process of origin, MVs specifically are usually enriched in cytoskeletal proteins, as well as cytoskeleton-associated proteins (53). Also, proteins associated to the plasma membrane or the endosomal membranes, are common components of EVs, such as, tetraspanins, which are almost invariably detected in EVs, and especially in exosomes; indeed, proteins such as CD81, CD63, CD9, Alix and Flotillin are widely used as canonical EVs markers, while performing their characterization (35). As tetraspanins are transmembrane proteins, usually found on endosomes, lysosomes and plasma membranes, strictly involved in the organization of membranes microdomain, they are usually localized in EVs membrane also participating to the formation of the EVs biomolecular corona with their external portion (54).

The protein corona of EVs forms spontaneously on the outer surface of EVs, both during vesicle biogenesis, where corona components may associate with vesicles already within multivesicular bodies, and after EV release into the intercellular space or biological fluids. The protein corona differs from EV protein cargo, as cargo molecules are either enclosed within the EV lumen or constitute an integral part of the vesicle membrane. In contrast, the corona is composed of proteins that associate with the EV surface through indirect and dynamic interactions with membrane lipids and membrane-associated proteins. (46). Elements that have been found in EVs corona are for example proteins like cytokines, chemokines, growth factors, lipoproteins and enzymes. The protein corona of EVs provides insight into both the cells from which they originate and the environment in which they are released. Indeed, in EVs isolated from blood or serum, the corona reflects interactions with this complex biological milieu and is often enriched in plasma proteins such as albumin and fibrinogen (55). Importantly, since the behaviour of EVs once they are realised, is influenced by the formation of the EV protein corona, the fate of EV signalling cargoes, and consequently their functions *in vivo*, is strongly influenced by the protein composition of the EV corona (56).

Nucleic Acids

EVs can contain a variety of nucleic acid species, being particularly enriched in RNAs, a discovery that dates back to less than 20 years ago (57). Nucleic acid cargos of EVs are mostly short ncRNAs, such as tRNAs and miRNAs. Indeed, most of the RNAs molecules that have been recognised as EVs cargo do not exceed 200 nt in length, with only a small fraction reaching

bigger sizes. Therefore, intact mRNAs or lncRNAs are relatively rare and are often fragmented both in exosomes and in microvesicles (58). Nevertheless, these types of cargoes, even if sporadically found in their full length, demonstrated to have a central role in the modulation of the response to EVs by recipient cells. In fact, mRNAs can be translated, as well as lncRNAs can interact with their regulatory partners in recipient cells. This highlights how deeply signals coming from EVs are able to influence the activity of their target cells.
Additionally, EVs can carry a diverse composition of genetic material, including both genomic and mitochondrial DNA (59). This discovery is even more recent and constituted a milestone in the exploration of EVs with the finding of DNA associated to EVs isolated from the blood of a pancreatic cancer patient (60). This discovery unveiled that the potential of these small particles not only relies in their biological functions but that can also constitute a powerful tool in diagnostic.

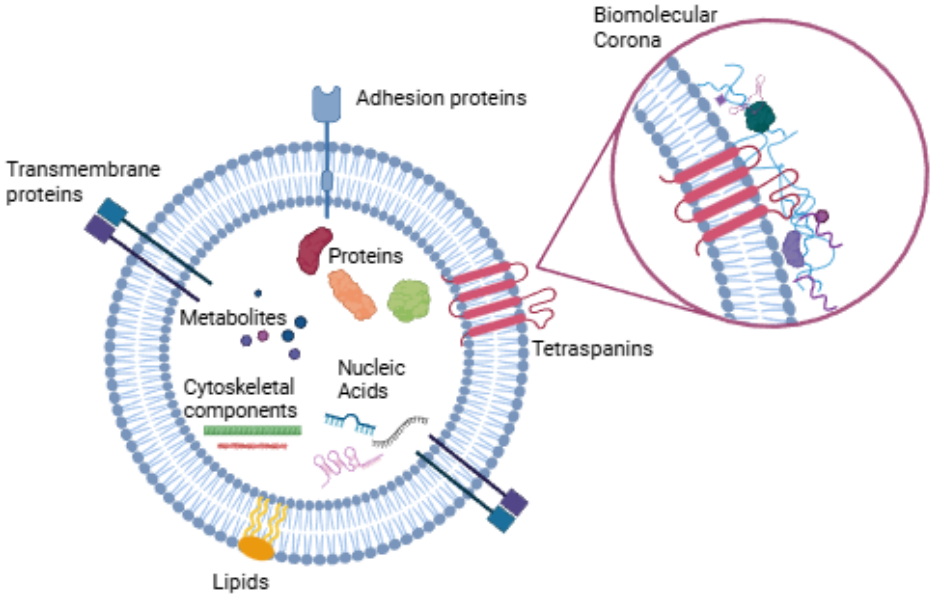

Figure 4. **Schematic overview of extracellular vesicles (EVs) biomolecular cargoes.** EVs contain a heterogeneous cargo, including metabolites, lipids, proteins (both in the lumen and in the membrane) and nucleic acids (RNA, DNA), which mirrors their cellular source and biological functions. Their surface is surrounded by a biomolecular corona composed of associated molecules, including proteins, lipids, metabolites and possibly nucleic acids, that modulate vesicle stability, distribution in biological systems and interactions with target cells. *Made with Biorender.com.*

1.2.2.1 lncRNAs transported by EVs

lncRNAs are increasingly recognised as an important class of EV cargo, contributing to intercellular communication by modulating regulatory networks in recipient cells. Numerous studies have demonstrated that EV-associated lncRNAs retain the capacity to interact with their regulatory partners following transfer, thereby influencing cellular behaviour (58). Notably, EV-associated lncRNAs are emerging as valuable diagnostic biomarkers in liquid biopsies, particularly in oncology. Indeed, several circulating lncRNAs exhibit expression levels in liquid biopsy samples that mirror those observed in tumor tissues, supporting their potential use as diagnostic and prognostic indicators across multiple cancer types (61).

Multiple models have been proposed and supported by evidence, to explain the selective incorporation of RNA molecules into EVs, both considering the transcripts enrichment within EVs relative to their abundance in donor cells, as well as the intrinsic physicochemical and structural characteristics of RNA molecules. A particularly abundant RNA, if localized nearby the EVs biogenesis site, can be passively internalized by vesicles during their formation. Although spontaneous packaging of specific lncRNAs has not been reported, this type of mechanism as already been described for other RNA species. Indeed, comparative analyses of miRNA expression in donor cells and their corresponding EVs have revealed a strong correlation, suggesting that miRNAs present at higher levels within cells are frequently detected at elevated levels in EVs (62). This evidence supports the hypothesis of a possible passive enrichment also for lncRNAs in EVs, since there are several lncRNA species that are found to be expressed at high rates in cells, especially in pathological conditions, such as cancer. In this context lncRNAs are increasingly being demonstrated to be enriched in tumor-derived EVs, regulating pro-tumorigenic functions (63). To allow passive loading in EVs, lncRNA enhanced cytoplasmic stability is fundamental, as it increases the likelihood that these molecules are present at the appropriate subcellular location at the relevant time for vesicle incorporation.

Active enrichment in EVs, on the other hand, implies a specific mechanism for incorporating lncRNAs. Several molecular features can be involved in lncRNA loading into extracellular EVs, such as defined RNA motifs and structural elements, the recruitment of RNA-binding proteins (RBPs), chemical modifications of RNA or post-translational regulation of EV-associated proteins. A particular interest has been given to RBPs or other interacting proteins as drivers for the incorporation of lncRNAs in EVs. For example, it has been demonstrated the enrichment of lncRNAs presenting binding motifs for the RBP HNRNPA2B1, which depletion impacts levels of lncRNA EV cargoes (64). In bladder cancer, EV-enriched lncRNA LNMAT2, loaded by the interaction with hnRNPA2B1, is reported to be involved in lymphangiogenesis, and so in metastatic promotion, modulating gene expression in recipient cells (65). Nonetheless, despite increasing insights into the mechanisms governing lncRNA incorporation into EVs, our understanding of these processes remains limited, and many aspects of these mechanisms are still largely unknown, as well as almost nothing is known

about the distribution of RNA molecules within the different compartments of EVs (lumen, associated to membrane components, corona).

To date the confirmed participation of lncRNA to the EV corona, which is considered to be mainly formed by proteins and lipids, has never been confirmed. However, the study of the corona is still limited by technical limitations of EV isolation methods, and together with the proved presence of extracellular and circulating RNA molecules (61), we cannot exclude the participation also of lncRNA molecules to the formation of the EV corona. Of note, the presence of RNA molecules on the external surface of EVs has recently been confirmed. Using a range of single-vesicle analytical approaches, RNA was demonstrated to be associated with the surface of EVs. Notably, these RNAs colocalize with EVs upon entry into recipient cells, suggesting that surface-associated RNAs may contribute to EV-mediated functions and highlighting a previously unrecognized mechanism for intercellular RNA signal exchange (66).

Overall, although current knowledge of lncRNAs as EV cargoes remains limited, particularly with respect to the mechanisms governing their selective incorporation into these vesicles, the investigation of lncRNA roles and functions in the context of EVs is emerging as a pivotal area of research. This is especially relevant to the study of cancer pathogenesis and progression, as well as to diagnostic applications, thereby conferring increasing interest and significance to the field.

Given the extraordinary variety of EVs cargos, they can be involved a multiplicity of functions, starting from the first stages of development. EVs are released by most cells from early embryonic stages and play key roles in intercellular communication, transporting nutrients and signalling molecules during morphogenesis. Studies, particularly on stem cell cultures, have shown that EVs, such as microvesicles from mouse embryonic stem cells, can influence processes like embryo implantation (67). Many cells inhabiting the blood circulation, such as platelets, macrophages and neutrophils, have been found to shed MVs that carry fundamental pro-coagulatory signals (68).
Pivotal functions of EVs have been reported in several diseases and pathogenic contexts. For example, in myocardial injuries microRNAs transported in epicardial-derived EVs carry a pro-regenerative molecular signal to cardiomyocytes (69). Moreover, cancer cell–derived EVs serve as a specialized form of intercellular communication, promoting cell growth and survival, modulating the tumor microenvironment, and enhancing invasion and metastasis. Additional details about EVs involvement in cancer are reviewed in section 1.2.3 below.

1.2.4 Extracellular Vesicles in cancer

Tumor pathogenesis and progression need active communication between cells involved in the process, including their neighbouring cancer cells and the surrounding microenvironment. In the last decades, studies on EVs in cancer have shown that EVs are key players in these interactions.

Many studies characterizing tumor-derived EVs have demonstrated a strong association between tumor-secreted EVs and cancer hallmarks, some broadly shared among cancer-derived EVs and others tumor type-specific. EVs have been reported to promote reprogramming of recipient cells toward a malignant phenotype for example by transporting factors that sustain proliferative signalling and help cells evade apoptosis, such as mir-21 that has been reported in this role in breast cancer as well as in colon adenocarcinoma and lung cancer (70–72). Tumor-secreted EVs also contribute to angiogenesis by delivering pro-angiogenic effectors, such as VEGF that has been identified on the surface of EVs derived from ovarian, colorectal and renal cancer (73). On the other hand, the EGFRvIII mutation, specific to glioblastoma, has been detected in extracellular vesicles derived from patients' cerebrospinal fluid and serum (74). These are just few examples that highlight the remarkable diagnostic potential of EVs, as they can carry tumor-specific signatures that are detectable in accessible body fluids, paving the way for minimally invasive biopsies. This and the fact that tumor-derived EVs are consistently found to be released in biofluids, such as blood, has positioned the study of these particles as highly significant in the diagnostic field, in particular for liquid biopsies (75).

The study of EVs-associated cancer hallmarks is not restricted to the identification of diagnostic biomarkers but broaden the analysis of their functions to disease onset and progression. In fact, several studies demonstrated the involvement of tumor-derived EVs in influencing tumor growth as well as the metastatic process (76) (***Figure 5***).

An example are prostate cancer-derived exosomes that, carrying *miR-125b*, *miR-130*, *miR-155*, and *H-RAS* or *K-RAS* mRNAs, are able to reprogram adipose stem cells, promoting tumor development (77). EVs can also facilitate invasion and metastasis through extracellular matrix remodelling and pre-metastatic niche formation. As in breast cancer where transfer of *miR-105* by cancer-derived EVs destroys vascular endothelial barriers to promote metastasis, targeting the tight junction protein ZO-1 in endothelial cells, thereby increasing vascular permeability (76) (78)

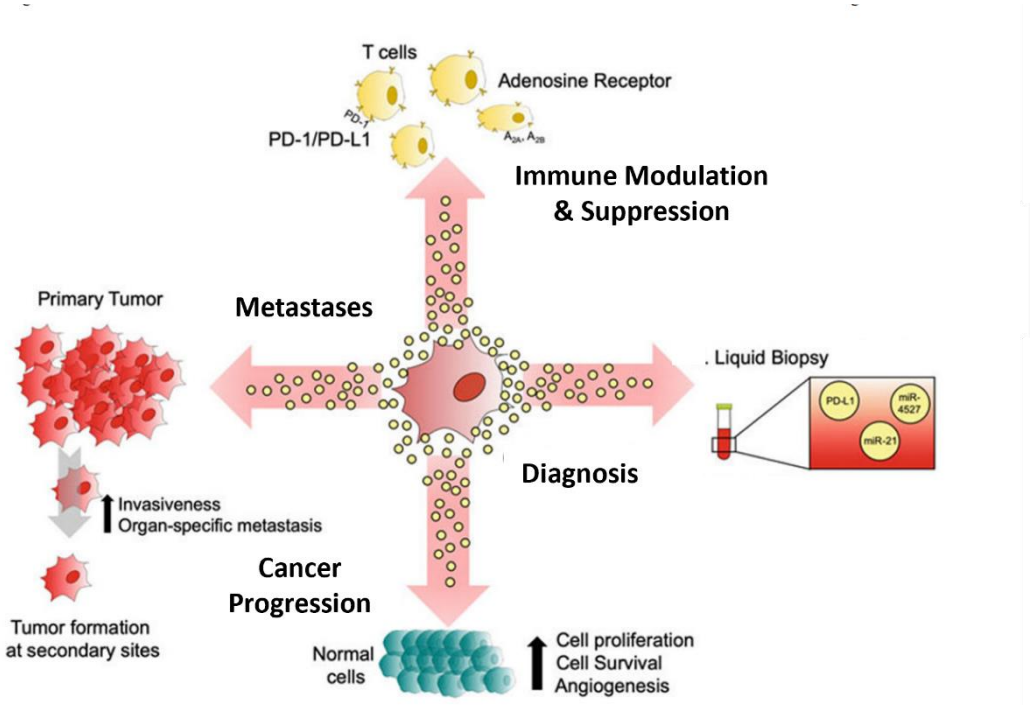

Figure 5. **Roles of tumor-derived EVs**. Schematic representation of the major roles of EVs derived from cancer cells. EVs play crucial roles in cancer progression, metastases formation, immune modulation, and can be exploited in diagnosis. *Adapted from (76).*

Tumor-derived EVs do not only influence the local environment around tumor cells, but they are also released in the blood circulation. The intravascular dynamics of EVs are central to the metastatic cascade, as their ability to disseminate and arrest at specific vascular sites dictates the establishment of metastatic foci. For example in an in vivo model of melanoma, EVs released in blood vessels can be up taken by epithelial cells and patrolling macrophages, stimulating an immune response by macrophages, that contributes to pre-metastatic niche formation (79). Notably, EVs carrying surface PD-L1 bind to PD-1 on T cells, inducing their exhaustion and suppressing anti-tumor activity. In glioblastoma, PD-L1-enriched EVs inhibit CD8+ T cell function, mimicking immune checkpoint signalling and enabling systemic immune escape. High levels of EV-bound PD-L1 have also been linked to poor responses to PD-1/PD-L1 immunotherapy (80). EVs mediated immune escape and metastases promotion can be also regulated though mechanism of innate immunity, such as RNA sensing pathways. In fact members of the Toll-like Receptors family have been reported to be implicated in the response to RNA molecules transported by tumor-derived EVs in macrophages, triggering NF-κB signalling and increases secretion of inflammatory cytokines, creating an inflammatory environment that supports metastasis formation (81).

Overall, growing evidence highlights the central role of extracellular vesicles in both tumor initiation and progression, not only through direct regulation of tumor cells, but also by shaping the tumor microenvironment and modulating immune responses. Understanding the diverse functions of EVs in cancer will provide deeper insight into disease mechanisms and open new avenues for therapeutic intervention.

1.3 RNA sensing pathways of the innate immune system

The innate immune response constitutes the host's first line of defence against invading pathogens acting rapidly and non-specifically to contain infection. A key mechanism involved in innate immunity relies on the recognition of pathogen-associated molecular patterns (PAMPs) by pattern recognition receptors (PRRs), a class of receptors capable of directly recognizing molecular structures that are specific of pathogens. In a pathogenic context PRRs can be also activated by endogenous molecules, released by the host's stressed, damaged or dying cells, known as damage-associated molecular patterns (DAMPs) (82). RNA sensing pathways participate in this mechanism by recognising viral or endogenous pathogenic RNA molecules through several receptors positioned in different subcellular compartments and that can recognise different type of RNA molecules. These receptors serve two principal functions: the specific recognition of ligands and the initiation of intracellular signalling cascades. RNA sensing is mediated by two main classes of receptors: RIG-I-like receptors (RLRs), which detect viral RNA in the cytosol, and Toll-like receptors (TLRs) such as TLR3, TLR7, and TLR8, which sense RNA within endosomes.

Not all cells express RNA-sensing receptors uniformly. RLRs, for example are broadly expressed across many cell types such as epithelial cells, fibroblasts, endothelial cells, and immune cells, providing a widespread cytosolic antiviral defence. In contrast, RNA-sensing TLRs display a more restricted expression pattern. TLR3 is found in dendritic cells, macrophages, and some epithelial cells, whereas TLR7 and TLR8 are mainly expressed in dendritic cells, monocytes, and B cells. Unlike RLRs, these TLRs are localized in endosomes and play specialized roles in detecting extracellular or endocytosed viral RNA (83).

Activation of RNA-sensing pathways triggers a cascade of signalling events that rapidly activate the production of cytokines and chemokines, which result in inflammatory cell activation and recruitment. More specifically, these signalling pathways activate the production of type I interferons (IFN-α/β) and pro-inflammatory cytokines, which establish an antiviral state in both the infected and neighbouring cells. Additionally, these pathways promote the upregulation of co-stimulatory molecules and chemokines, facilitating the recruitment and activation of innate immune cells such as dendritic cells, macrophages, and natural killer (NK) cells. These passages are critical for the subsequent priming and differentiation of T cells (84). In this way, RNA sensing serves as a bridge between PAMPs or DAMPs detection and the initiation of adaptive immune responses, ensuring a rapid and coordinated defence.

1.3.1 RIG-I like Receptors Pathway

Retinoic acid inducible gene I (RIG-I), melanoma differentiation-associated protein 5 (MDA5) and Laboratory of genetics and physiology 2 (LGP2) are the three cytosolic receptors belonging to the family of RLRs. RIG-I, MDA5 and LGP2 share a common DExD/H-box RNA helicase domain, as well as the C-terminal domain (CTD), which are essential for the

recognition of specific RNA structures. In addition, RIG-I and MDA5 contain two caspase activation and recruitment domain (CARD), which are responsible for recruiting the downstream signalling components. LGP2 lacks the CARD domain, therefore is not able to initiate the downstream signalling cascade on its own, but seems to be involved in modulating the response of the other two receptors (85).

Although members of the RLR family share a similar structural architecture, they recognize their ligands through distinct ligand-recognition domains. Both RIG-I and MDA5 detect double-stranded RNA (dsRNA), with RIG-I preferentially sensing relatively short dsRNA molecules (<1000 bp), whereas MDA5 is more effective in detecting long dsRNA chains (>1000 bp) (86). Additionally, RIG-I specifically recognizes the 5'-triphosphate ends of single stranded RNA molecules, a structural feature typically generated during viral RNA synthesis by viral polymerases. In contrast, host-derived RNAs undergo extensive post-transcriptional modifications, most notably 5'-end capping and various nucleoside modifications. These processing events effectively mask endogenous RNAs from RIG-I surveillance, thereby preventing inappropriate activation of innate immune signalling against endogenous RNAs (87).

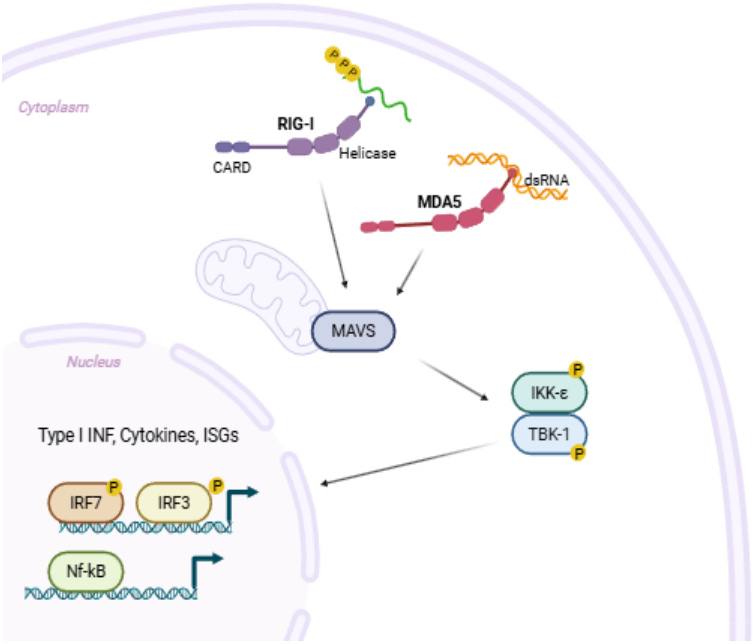

***Figure 6*. RIG-I Like Receptors Pathway.** Two cytosolic receptors, RIG-I and MDA5, detect viral or endogenous RNA species: RIG-I recognizes short dsRNA and RNA bearing 5'-triphosphates through its helicase, while MDA5 binds directly to long dsRNA molecules. Upon ligand binding, both receptors signal to the mitochondrial adaptor protein MAVS. MAVS subsequently activates downstream kinases, including TBK1 and IKKε, which phosphorylate the transcription factors IRF3 and IRF7. Activated IRF3 and IRF7 translocate into the nucleus, where they drive the transcription of type I interferons and interferon-stimulated genes (ISGs), establishing an antiviral state. *Made with Biorender.com.*

Once RIG-I and MDA5 recognised their ligands, they undergo a conformational change that exposes their CARD domain, which interacts with the CARD domain of their first common downstream effector MAVS, on the mitochondrial outer membrane. MAVS activation subsequently recruits and stimulates key kinases involved in inflammatory signalling: TBK1, and IKK-ε. These kinases activate through phosphorylation members of the Interferon Regulatory Factor (IRF) family, IRF-3 and IRF-7, as well as the transcription factor NF-κB. Activation of these transcription factors drives the expression of type I interferons (IFN-α, IFN-

β) a broad array of pro-inflammatory cytokines and Interferon Stimulated Genes (ISGs) (88) (***Figure 6***). The production of IFN-α, IFN-β, and pro-inflammatory cytokines establishes a positive feedback loop, reinforcing the expression of RLRs, type I IFNs, and a suite of interferon-stimulated genes that sustain the antiviral and pro-inflammatory response (89).

1.3.2 Toll-like receptors

Toll-like receptors (TLRs) are trans-membrane pattern recognition receptors that play a central role in the innate immune system of vertebrates. Engagement of TLRs with their ligands triggers signal transduction pathways that leads to the activation of immune cells involved in inflammation and promotes the transcription of genes encoding pro-inflammatory cytokines.

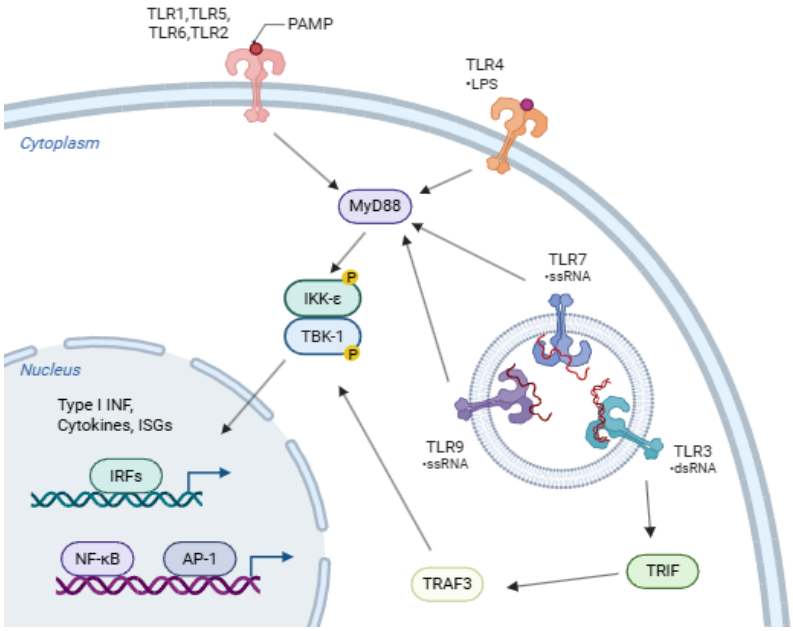

Figure 7. **Toll-like receptor (TLR) signalling pathways.** Cell surface TLRs (TLR1, TLR2, TLR5, TLR6, and TLR4) recognize PAMPs, such as lipopolysaccharide (LPS). Endosomal TLRs (TLR3, TLR7, TLR9) recognise single-stranded RNA (ssRNA), and double-stranded RNA (dsRNA). Ligand recognition induces recruitment of adaptor proteins, including MyD88 (for most TLRs) and TRIF (for TLR3) as well as TRAF3. These adaptor molecules activate downstream kinases such as TBK1 and IKKε, which phosphorylate transcription factors IRFs, NF-κB, and AP-1. Once translocated into the nucleus, these transcription factors drive the expression of type I interferons (IFN-α/β), cytokines, and interferon-stimulated genes (ISGs), thereby initiating an inflammatory response. *Made with Biorender.com*.

To date, ten functional TLRs (TLR1–10) have been identified in humans. Structurally, TLRs are type I transmembrane glycoproteins composed of an extracellular domain, a transmembrane region, and an intracellular signalling domain. The extracellular region is characterized by leucine-rich repeats (LRRs) that mediate ligand recognition, while the intracellular Toll/IL-1 receptor (TIR) domain, is responsible for downstream signal transduction (82).

Each TLR initiates distinct signalling cascades that culminate in the production of cytokines, chemokines, and interferons (IFNs), molecules essential for pathogen clearance and the activation of immune responses. The subcellular localization of TLRs is closely linked to the types of ligands they recognize and the mechanisms by which recognition occurs. Cell-surface TLRs, including TLR1-6 and TLR10, form homo- or heterodimers and primarily detect structural components of pathogenic microorganisms such as lipids, lipoproteins, and proteins. In

contrast, endosomal TLRs, such as TLR3, TLR7, TLR8, and TLR9, are typically expressed as homodimers and are specialized in sensing nucleic acids (90). While TLR9 is activated by the recognition of CpG-rich DNA molecules, TLR7 and TLR8 sense ssRNA molecules and TLR3 is primarily activated by dsRNAs, as such they constitute integral elements of the RNA-sensing pathways (91).

TLR3 mainly localizes on the membrane of exosomes, although some expression at the plasma membrane has been reported in certain cell types (92), and it is widely expressed not only in immune cells, such as macrophages and dendritic cells, but also in other cell types such as fibroblast and epithelial cells (93). Upon activation, TLR3 recruits the adaptor protein TRIF, on which it relies exclusively, in contrast to other Toll-like receptors that activate a different adaptor, MyD88. The TLR3–TRIF axis initiates an intracellular signalling cascade involving the adaptor proteins TRAF3, and several kinases such as TANK, TBK1, IKKε, RIP1 and NAP1. These signalling mediators activate through phosphorylation the transcription factors IRF3/7, NF-κB, and AP-1, which in turn drive the production of type I interferons, proinflammatory cytokines, and chemokines (***Figure 7***). Through this mechanism, TLR3 signalling plays a pivotal role in orchestrating the innate immune response to viral infection (94).

1.3.3 RNA sensing activation in cancer

In the tumor microenvironment, the activation of an innate response can play a double-faced role, since it can either promote a pro-tumorigenic inflammation, pushing immune cells towards an immune-suppressive phenotype, or induce a tumour-suppressive response by cells of the immune system. In fact, persistent activation of RLRs or endosomal TLRs can lead to sustained production of cytokines such as IL-10, TGF-β, and type I IFNs, which can influence macrophages polarization toward an M2 phenotype and promote the recruitment of regulatory T-cells in the TME, obtaining overall an immunosuppressive effect (95) that can facilitate tumor progression. Moreover, IL-6, that can be produced downstream of RNA sensor activation, promotes tumor cell proliferation, survival, invasion thereby supporting metastasis (96), as it happens in non-small-cell lung cancer (97).

On the other hand, many studies highlighted how targeting the activation of RNA sensors can activate an anti-tumorigenic response by cells of the immune system. Stimulation of TLR3 with an agonist has been reported to reprogram macrophages from an M2 to an M1 phenotype, suppressing tumor growth via the IFN-α/β. TLR3 agonists can also activate NK cells, promoting antitumor immunity and inhibiting melanoma lung metastasis (98).

What emerge from the diversity of responses that can be obtained by activating RNA sensing pathways in tumours, is that the final effect on tumor progression is extremely specific and may be influenced by several parallel factors in the TME. Therefore, it is crucial to understand how activation of RNA-sensing pathways, by tumour-specific derived DAMPs may influences disease progression and the related microenvironment. Such knowledge could provide valuable insights for developing targeted therapeutic strategies.

1.4 Zebrafish as a model for human disease

The zebrafish (*Danio rerio*) is a small freshwater teleost fish native of South Asia. Adults typically measure 2–3 centimetres in length and are easily recognized by the characteristic horizontal stripes along their bodies, which give them their common name "zebrafish." This species has been widely used in developmental biology research and, more recently, has become an important experimental model for studying various human diseases. Its growing popularity in biomedical research is due to numerous advantages, such as genetic tractability, rapid development, and physiological similarities to humans.

Compared to mammalian models, zebrafish are much easier and more cost-effective to maintain and breed. They can be housed in tanks within automated aquatic systems, which greatly reduces the space required for animal care. In addition, zebrafish require smaller amounts of food and experimental compounds, making them an efficient and economical choice for large-scale studies.

External fertilization contributes to the attractiveness of zebrafish as a model organism. A single mating can produce hundreds of fertilized eggs, enabling high-throughput experiments with strong statistical power within just a few days. Moreover, the external development of embryos facilitates direct observation and manipulation during the earliest stages of embryonic and larval development. In addition, transparency during early development allows for high resolution live imaging of cell biology events.

In 2013, the first zebrafish genome assembly was published, and it has been continuously updated up to the most recent versions available today, marking a major milestone in the use of this species as a model organism. Approximately 70% of human genes are shared with zebrafish, and about 82% of human disease-related genes have at least one zebrafish orthologue (99). The availability of a well-annotated genome has opened the way for precise genetic manipulations, enabling researchers to model and investigate a wide range of human diseases, including cancer.

1.4.1 Zebrafish immune system

Zebrafish genetic and regulatory networks controlling haematopoiesis and the immune system share many similarities with the mammalian counterpart, in fact molecular mechanisms driving the haematopoietic process are highly conserved between humans and zebrafish. Haematopoiesis is a highly regulated process controlled by numerous signalling pathways that guide blood cell development from early progenitor stages through the final stages of differentiation. In mammals, the division of the immune system into innate and adaptive branches arises from haematopoietic programs originating from specialized blood progenitors, which are generated through an endothelial-to-hematopoietic transition during embryonic development (100). Zebrafish haematopoiesis take place in two consecutive waves during embryonic development, and it relies in a very well conserved mechanism (101).

The first wave starts at 11-18 hours post fertilization (hpf) and it is responsible for the generation of myeloid and erythroid cells. At 30 hpf, during the second wave, definitive haematopoiesis takes place giving rise to haematopoietic stem and progenitor cells (HSPCs), responsible for the generation of adult blood cells. HSPCs then produces embryonic macrophages, neutrophils and monocytes (102). Adaptive immunity do not develop until 4-6 weeks post fertilization (wpf), following the maturation of CD4+ and CD8+ lymphocytes, happening at 3 wpf, and B-cells, which develop in the kidney marrow (***Figure 8***). Therefore, innate immunity can be studied during the early embryonic and larval stages of zebrafish, before the occurrence of T- and B-cell responses (103).

The innate immune system serves as the host's first line of defence against infection; its primary role is to detect invading pathogens early and initiate an appropriate proinflammatory response. The innate immune system relies on PRRs to detect evolutionarily conserved structures on pathogens, known as PAMPs and endogenous pathogenic molecules so called DAMPs. The main families of PRRs present in humans, such as Toll-like Receptors and RIG-I like receptors, are conserved in zebrafish, as well as their downstream signalling pathways, confirming the zebrafish an excellent model to study infections and immunity.

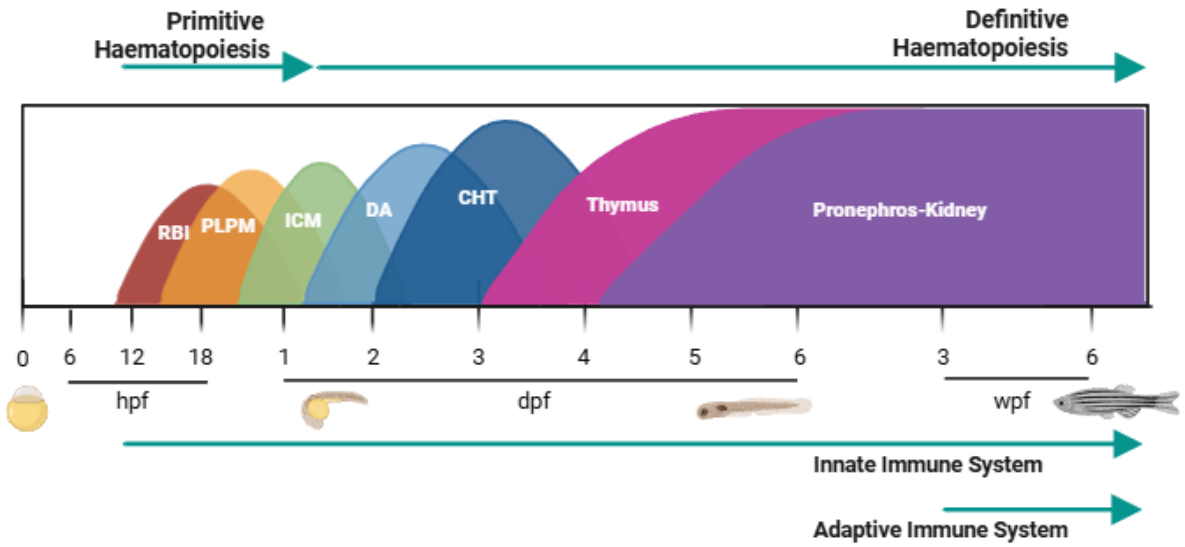

***Figure 8*. Development of the immune system and haematopoiesis in zebrafish**. Immune system development begins during early embryogenesis with primitive haematopoiesis, initiating at 11 hours post-fertilization (hpf). Progenitors of the myeloid and erythroid lineages arise from distinct regions of the lateral plate mesoderm: myeloid cells are formed in the rostral blood islands (RBI) and erythroid cells originate from a specific area in the posterior lateral plate mesoderm (PLPM), the intermediate cell mass (ICM). By approximately 2 days post-fertilization (dpf), definitive hematopoietic stem cells (HSCs) are generated in the dorsal aorta (DA) and subsequently migrate to the caudal hematopoietic tissue (CHT). In the final stage of hematopoietic development, HSCs relocate to the thymus and the pronephros (the embryonic kidney), where they undergo terminal differentiation and maturation. Adaptive immunity develops with the maturation of CD4+/CD8+ lymphocytes, which starts at 3 weeks post fertilization (wpf). *Made with Biorender.com, adapted from (101)*

1.4.2 RIG-I Like Receptors in zebrafish

The RIG-I Like Receptors Pathway is highly conserved among vertebrates. Consistently, most of the components of the pathway being identified in the zebrafish genome. Although zebrafish possess two variants of RIG-I and MDA5 (104) they operate in the innate immune pathway similarly to their mammalian homologs.

RIG-I is conserved in zebrafish with all its functional domains, and its preservation of its involvement in the signalling pathway mediated by Nf-kB and the interferon response has been demonstrated (105). According to the most recent annotations, RIG-I is encoded by a single gene in the zebrafish genome but is expressed as two splicing variants. The first, RIG-Ia, includes a 114-nucleotide insertion in the second CARD domain, which has no known homology with sequences in other fish species or mammals. The second, RIG-Ib, retains both structural and functional homology with the mammalian counterpart. While RIG-Ib is considered the primary functional isoform, RIG-Ia is thought to enhance RIG-Ib–mediated signalling, potentially fine-tuning the antiviral response (106).

A single *mda5* ortholog has been identified in zebrafish, but it gives rise to two distinct splicing variants. The longer isoform, MDA5a, has a protein length comparable to that of mammals, suggesting a conserved function, an idea supported by its established role in antiviral responses (107). The second variant, MDA5b, is significantly shorter, lacks part of the helicase domain, and appears to enhance MDA5a-mediated signalling (87). Notably, both zebrafish MDA5 variants retain the conserved DExD core and two CARD domains, indicating preservation of key functional elements (108). As well as in mammals, the role of LGP2 in zebrafish remains unclear, but two isoforms of LGP2 have been identified in zebrafish and its structure closely resembles the one of the zebrafish MDA5 (109). Also, teleost MAVS conserves its adaptor function and contains similar protein domains as in mammals (110).

The downstream signalling, even if with its specificities, retains a well conserved mechanism, with innate immune response related interferons (IFNs) classified into group I and group II. Although they are not true homologs of mammalian type-I IFNs and have distinct receptors, their expression is activated through similar mechanisms, the activation of IRF3 expression via STAT signalling, IRF7 activation through phosphorylation, and participate in the generation of a positive feedback loop that reinforces and propagates the signal (111). Overall, the RIG-I-like receptor pathway in zebrafish is largely conserved, with key components functioning like in mammals while showing some fish-specific adaptations

1.4.3 Toll-like Receptors in zebrafish

The Toll-like receptor (TLR) protein family is evolutionarily conserved from insects to mammals, but the signalling pathways mediated by TLRs in fish display distinctive features. In zebrafish, putative orthologs of mammalian TLRs have been identified, alongside several fish-specific family members, suggesting both conservation and diversification of TLR functions in

vertebrate immunity. While in humans TLRs are a family of 10 proteins, (112), in zebrafish a family of 20 putative variants has been identified (113). Among zebrafish TLRs, 10 are orthologs to the humans', while others belong to a fish specific sub-family of receptors.

Because teleost fish underwent an additional genome duplication, zebrafish possess duplicate counterparts of some mammalian TLRs, such as *tlr4ba*/*tlr4b* (for TLR4), *tlr5a*/*tlr5b* (for TLR5), and *tlr8a*/*tlr8b*. While homologs of mammalian TLR6 and TLR10 are absent in fish, they possess unique receptors such as TLR18 and TLR14 that are likely to be their functional substitutes (114).

Importantly, also the specificity for some ligands appears to be conserved between zebrafish and mammals; for example, TLR3, TLR5, and TLR9 recognize double-stranded RNA, flagellin and unmethylated CpG DNA, respectively, as the humans counterparts (111). On the other hand, the fish-specific TLR22 recognises dsRNAs and the immunostimulant Poly(I:C) (115), being a functional homolog for TLR3, while TLR4 in zebrafish is unable to recognise LPS (116), highlighting that, even if TLR-mediated mechanisms are conserved across vertebrates, zebrafish have also evolved specific adaptations in the development of their RNA sensing pathways.

Receptors of these pathways are not the only component conserved, but also downstream signal propagation and activation of pro-inflammatory factors. Zebrafish possess orthologs of the key adaptor proteins and signalling molecules described in mammals, including MyD88, that is the most studied adaptor in zebrafish for its key role in defence against microbial infection, and TRIF which overexpression in zebrafish leads to the production of INFs suggesting that zebrafish *trif* is a true homolog of the mammalian gene, as well as the central intermediators interferon regulatory factors (IRFs) and the signal transducers and activators of transcription (STATs) (114). On the whole, the TLRs and their associated signalling pathways are broadly conserved in zebrafish, yet the emergence of fish-specific receptors reflects unique evolutionary adaptations.

1.4.4 Extracellular Vesicles in Zebrafish

EVs as membrane-enclosed microparticles are secreted by the majority of cells across all domains of life (117). The field of EVs is relatively recent and given their recognized importance as mediators of intercellular communication, research efforts have historically focused on the identification, characterization, and functional analysis of EVs in mammalian systems. For this reason, relatively little is known about EVs in aquatic animals. Nevertheless, multiple types of EVs have been successfully isolated and characterized from various zebrafish tissues and cultured cell lines. These studies have employed a range of EV isolation approaches, including differential centrifugation and density gradient centrifugation (118) , which are methodologies widely established and validated in mammalian EV research, highlighting the similarities of these particles in their physical features.

Extracellular vesicles secreted by different intestinal cell types in zebrafish have been characterized, providing evidence for their cellular origin and for the ultrastructural distribution of exosomes within distinct intestinal cell populations (119). A very recent study isolated and characterized dynamic changes in the extracellular vesicle population of zebrafish larvae during early development, revealing an increase in EV abundance and stage-specific alterations in EV composition. These changes were analysed at multiple time points between 24 and 96 hpf. Notably, Alix, an established component of the ESCRT-III pathway, was detected in EVs purified from zebrafish larvae (120). As the ESCRT-III machinery is a well-characterized mechanism involved in vesicle biogenesis in humans (121), this finding suggests that EV formation mechanisms are evolutionarily conserved.

The transparency and small size of zebrafish also allowed the investigation in vivo of endogenous EVs dynamics, with single cell precision. A membrane-tethered fluorescent reporter system was used to enable fluorescent labelling of extracellular vesicles in both larval and adult zebrafish. This approach revealed that multiple cell types, including endothelial cells and cardiomyocytes, actively produce EVs *in vivo*, revealing also morphological differences between larval and adult zebrafish EVs (122). Similarly, targeted expression of CD63-pHluorin in zebrafish embryos, allowed the establishment of an *in vivo* model to study EVs functions. This approach in combination with imaging techniques and proteomic analyses enabled the characterization of EV biogenesis, composition, transfer, uptake, and fate at the level of individual endogenous vesicles. A subpopulation of EVs displaying exosome-like features was identified in zebrafish larvae, these EVs are released from the yolk syncytial layer into the bloodstream. These exosomes are subsequently captured, internalized, and degraded by patrolling macrophages and endothelial cells in the caudal vein plexus (CVP) (123).

Overall, although much remains to be understood about the roles of EVs in zebrafish development and physiology, significant progress has been made in recent years, particularly at the technical level, with the development of tools and systems to study these processes. Moreover, the advantages of zebrafish as a model for *in vivo* observation of cellular dynamics have enabled not only the study of endogenous but also of exogenous EVs, such as tumor-derived EVs isolated from cultured cells or tumor masses, allowing a better understanding of their dynamics and functions. For example, it has been possible to define that the pro-tumoral activity of circulating EVs isolated from the triple-negative breast cancer line 41T, is enhanced by low-flow regimes in the blood circulation, thanks to the combination of a system of microfluidics with an *in vivo* approach in zebrafish (124). Exogenous EVs isolated from zebrafish melanoma cells were used to study for the first time the dynamics of EVs released in the circulation in vivo. It was observed that circulating EVs were rapidly internalized by endothelial cells and patrolling macrophages and subsequently trafficked to degradative compartments. Furthermore, tumor EVs were found to activate macrophages and promote metastatic progression, highlighting the utility of the zebrafish embryo as an *in vivo* model for tracking tumor EVs and investigating their contribution to the formation of metastatic niches (125).

1.5 Cutaneous Melanoma

Cutaneous melanoma is a skin malignant tumor originating from melanocytes, pigment-producing cells that arise from the neural crest. Despite representing only a small fraction of all skin cancers, melanoma is the most aggressive form due to its strong metastatic potential and is responsible for most of skin cancer–related deaths (126).

BRAF mutations are the most common genetic alterations in melanoma, with over 90% of cases involving most frequently a V600E substitution. Mutant *BRAF* drives constitutive activation of the MAPK pathway, promoting aberrant cell proliferation and inhibition of apoptosis, ultimately leading to tumor formation and frequent acquisition of additional alterations. With a less frequent incidence, other MAPK pathway mutations occur, such as *NRAS* (127). The identification of these hotspot mutations enabled the development of effective targeted therapies over the years and have markedly improved survival outcomes in melanoma patients. However, the clinical benefits are often limited by the rapid emergence of resistance, attributed to the intrinsic plasticity of melanoma cells and the complexity of the surrounding tumor microenvironment (TME) (128). The TME is a complex and continuously evolving ecosystem composed not only by cancer cells, but also by many other players such as immune cells, stromal cells, blood vessels, and extracellular matrix, that together can actively promote cancer progression (129).

Due to the lethality of cutaneous melanoma, a huge effort has been done in the development of drugs and therapies to treat it, with immunotherapies, pioneered in the treatment of melanoma, leading to a more durable remission. However, despite these advances, nearly half of patients still succumbed to the disease within five years (130). Understanding the genetic, molecular, and cellular pathobiology not only of melanoma cells but also of the components of the TME is essential for advancing diagnostics and developing new therapies. In this context in vivo models constitute a powerful tool to study melanoma in its whole complexity. Over the past two decades, zebrafish have emerged as an effective and well-established model to advance our understanding not only of melanoma onset and progression but also provided the basis for therapeutic development (131).

1.5.1 Modelling melanoma in zebrafish

Over the years, zebrafish have become an important model organism for studying human disease and development. Their genetic similarity to humans, transparent embryos, and an anatomical organization that resembles the human one in several systems make them well suited for biomedical research. Zebrafish have been used to model a wide range of diseases, including solid tumours such as melanoma. Two main approaches have been established to model melanoma: the generation of genetically modified lines that express human oncogenes

under pigment cell–specific promoters or xenografting human or mouse tumor cells into zebrafish to study tumor growth and progression.

Xenografts

The modelling of xenograft tumours in zebrafish relies in the transplantation of fluorescently tagged melanoma cells at different developmental stages. In recent years, zebrafish xenografts have become a powerful model not only for studying cancer progression but also for screening potential anti-cancer compounds (132). Depending on the biological question it is possible to transplant different types of melanoma cells. An approach can be to transplant human or mouse derived melanoma cell lines. For example, in a recent study, the effects of melanoma cells on peripheral neurons have been characterized. The xenograft model was obtained by transplanting a primary-melanoma derived human cell line in the swim bladder of zebrafish larvae (***Figure 9***), and helped in defining how catecholamines can promote melanoma progression toward a more aggressive phenotype (133).

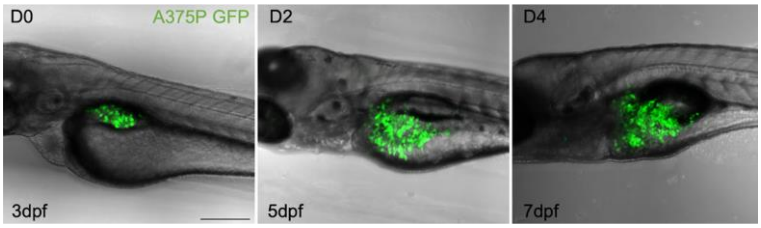

Figure 9. **Xenograft model of melanoma.** Zebrafish larvae transplanted in the swim bladder with the melanoma human cell line A375P-GFP. Image shows the growth of the transplanted cell mass grow in vivo in a 5 days' time span. *Adapted from (133).*

A second option can be to perform patient-derived xenografts (PDX) by directly transplanting in zebrafish, cancer cells obtained from the surgical resection of primary or metastatic tumour from patients. This approach enables personalized drug screening in a context that closely resembles human tumours, improving the likelihood of selecting effective therapies and reducing the risk of treatment failure. It has been reported that zebrafish PDX models for pancreatic ductal adenocarcinoma can accurately predict patient response to adjuvant chemotherapy (134).

Zebrafish melanoma transgenic lines

Among the many advantages that make zebrafish a powerful model organism for studying diseases, the ability to easily manipulate its genome is particularly important. The ability to express human melanoma oncogenes in the melanocyte lineage has enabled the development of various melanoma transgenic models in zebrafish.

The most common mutation that occurs in human melanoma is $BRAF^{V600E}$ and the first transgenic model of melanoma in zebrafish was developed by expressing the human $BRAF^{V600E}$

under the melanocyte-specific promoter *mitfa.* Mosaic $BRAF^{V600E}$ expression in zebrafish produced nevus-like melanocytic spots, but the *Tg(mitfa:BRAFV600E)* line developed melanoma at a higher rate in a p53 loss of function ($p53^{lf}$) background, highlighting cooperation between p53 and BRAF pathways. Additionally, zebrafish with p53 mutant background developed melanomas that are histo-pathologically similar to human melanoma and that are invasive and transplantable by 4 months of age (135).

Another line has been developed by expressing the oncogene $NRAS^{Q61K}$ in a $p53^{lf}$ background (136). Although p53 is mutated in only ~19% of human melanomas, p53 pathway function is often lost through other alterations. Additional models have been developed for less commonly mutated driver genes, including oncogenic HRAS-dependent melanomas. This model will be briefly reviewed in the following paragraph and it's the one used for my PhD thesis project.

1.5.2 Kita-GFP-RAS; p53-/- zebrafish transgenic model of cutaneous melanoma

For the development of a zebrafish model of cutaneous melanoma based on the overexpression of the oncogene HRAS, Santoriello and colleagues (137) used the UAS:Gal4 system, that enables the targeted expression of a transgene in a tissue of interest. In this model the *Et(kita:GalTA4,UAS:mCherry)hzm1* line from (138) is crossed with *the Tg(UAS:eGFP-H-RAS_GV12)io6* line (139) to express the human oncogene $HRAS^{G1V2}$, tagged with GFP, specifically in melanocytes under the control of the *kita* regulatory sequences (***Figure 10***). These fish will thereby be referred to as to *kita-GFP-RAS* from now on. Larvae obtained by crossing the two transgenic lines showed a hyperpigmentation already at 3 days post fertilizatio (dpf), then developed solid, mainly hyperpigmented, tumours within 1-3 months of age (***Figure 11***).

The tumours often developed at the level of the caudal fin. Histological analysis showed the beginning of tumour onset as a disruption of the tissue and melanocytic hyperplasia, and in around 20% of individuals progressing in a more invasive phenotype, resembling the features of human melanoma. Also, under an immunological point of view, zebrafish melanoma expresses the same markers that are commonly used to diagnose human melanoma, such as Melan-a and s100.

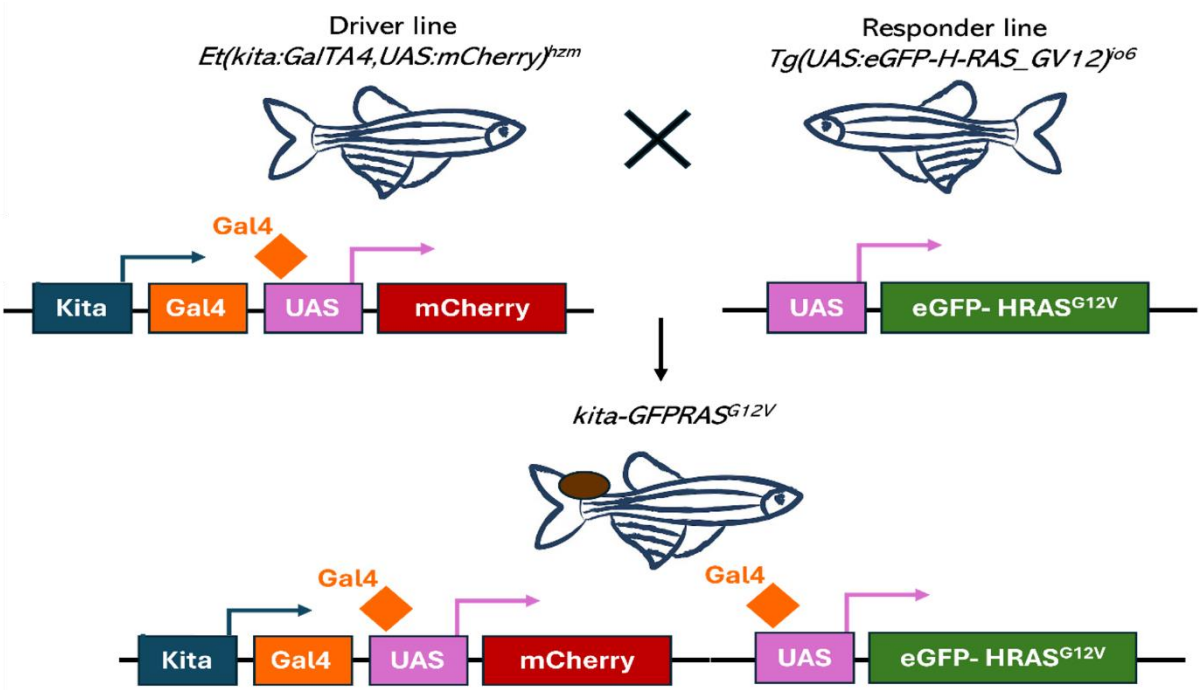

***Figure 10*. The *kita-GFP-RAS* melanoma zebrafish model.** The model is developed using the Gal4-UAS binary system. The crossing of driver and responder lines generates double-transgenic zebrafish in which the trans-activator Gal4 is expressed under the control of *the kita* promoter, while the $HRAS^{G12V}$ oncogene is placed under the control of the UAS promoter. Upon activation, Gal4 binds to UAS and induces the expression of the human oncogene specifically in *kita*-expressing cells. Since *kita* activity is restricted to melanocytes, $HRAS^{G12V}$ expression is confined to this lineage, thereby driving melanoma initiation and progression.

In a *tp53-/-* background, *kita-GFP-RAS* transgenic fish developed rapidly progressing melanomas that required euthanasia within 1–3 months, indicating that loss of p53, even if it's not necessary for the development of a tumour, enhances melanoma development and acts as a modulator in this genetic model.

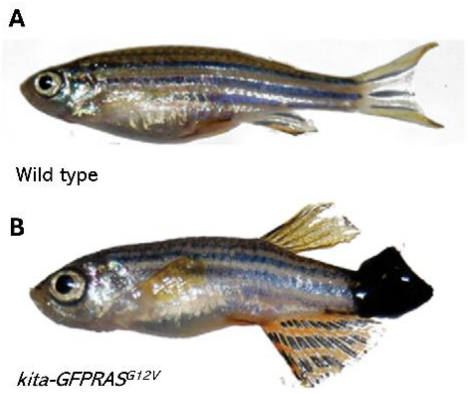

***Figure 11. kita-GFP-RAS* melanoma in zebrafish.** (A) Wild-type zebrafish at 3 months post-fertilization (B) kita-RAS^{G12V} transgenic zebrafish displaying a hyperpigmented tumor in the caudal fin region. *Adapted from (137).*

1.5.2.1 Zebrafish Melanoma-Derived Interstitial EVs Are Carriers of ncRNAs That Induce Inflammation

Recently, in our laboratory we isolated and characterized EVs directly from the tumour mass of *kita-GFP-RAS* individuals (33). To study extracellular vesicles directly from tumour tissue, we adapted the Nickel-Based Isolation (NBI) method, originally developed for isolating EVs from biological fluids (140), to be used on melanoma tissue from adult *kita-GFP-RAS* zebrafish, following gentle dissociation of the tumour into single cells (***Figure 12A***). Characterization revealed that melanoma cells release abundant EVs into the intercellular space, with a predominant size range of 200–220 nm, consistent with small EVs, also defined as exosomes. Importantly, since all tumour cells in our model express GFP on the membrane of tumour cells, we confirmed the melanoma origin of the EVs since at least 45% of isolated EVs were GFP-positive (***Figure 12B-C***).

In the molecular characterization of zebrafish melanoma-derived EVs we focused on the ncRNA content and analysed both zebrafish melanoma tissue and their corresponding EVs using RNA sequencing. Both melanoma tissue and EVs contained similar classes of ncRNAs, though EVs displayed a greater abundance of long intergenic non-coding RNAs (lincRNAs). Overall, 118 transcripts were found to be differentially abundant between melanoma tissues and EVs, with only 17 of these showing higher representation in EVs (***Figure 13A-B***). Among the ncRNAs enriched in EVs, lincRNAs and ribozymes were the most prevalent (***Figure 13C-E***).

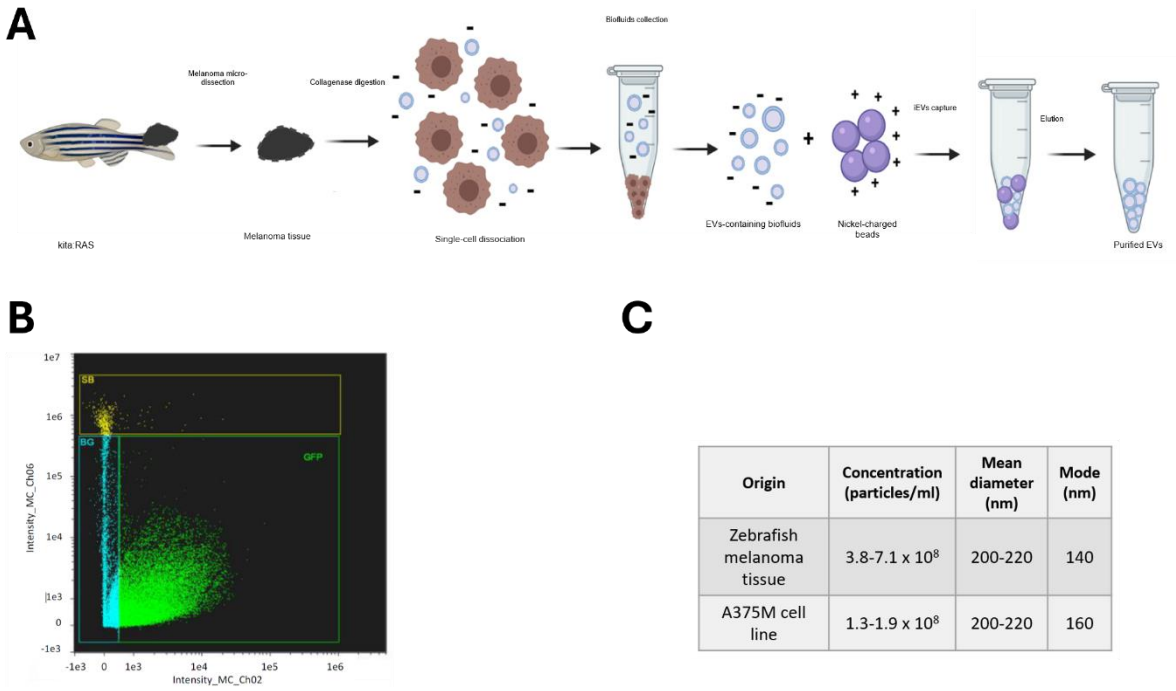

Origin	Concentration (particles/ml)	Mean diameter (nm)	Mode (nm)
Zebrafish melanoma tissue	3.8-7.1 x 10^8	200-220	140
A375M cell line	1.3-1.9 x 10^8	200-220	160

***Figure 12*. Melanoma-derived isolation and characterization A**) Schematic representation of melanoma microdissection, single cells dissociation, and EVs isolation following the NBI method. B) Representative sorting of EVs isolated from kita-GFP-RAS zebrafish melanomas using Imaging Flow Cytometry. C) Table reporting concentration, mean, and mode diameter values retrieved from Nanoparticle Tracking Analysis performed either on kita-GFP-RAS zebrafish melanomas or the A375M human melanoma cell line. *Adapted from (33).*

Through qPCR analysis we confirm that two lncRNAs, which are also classified as ribozymes, were strongly enriched in EVs. These two transcripts are *RPPH1* and *RMRP* which are the catalytic components of the two ribonucleoprotein complexes RNase P and MRP respectively. Of interest, they are rarely reported in extracellular vesicle studies. By extending our investigation to a human model and isolated EVs from the conditioned medium of human melanoma A375M cells (***Figure 12C***); similar to the zebrafish model, the human ortholog of *RPPH1* was more abundant in EVs than in the parental cells, but not *RMRP*. (***Figure 14A, C***).

With the interest of understanding whether this enrichment was specific to melanoma, we examined EVs derived from zebrafish brain tumours induced by the same oncogene (141). Characterization of brain tumour-derived EVs confirmed comparable size distribution and proportions of GFP-positive vesicles relative to melanoma-derived EVs. However, in contrast to the melanoma-derived EVs, these brain tumour EVs did not show enrichment of *RPPH1* or *RMRP*, indicating that their presence in EVs may be specific to melanoma (***Figure 14B***).

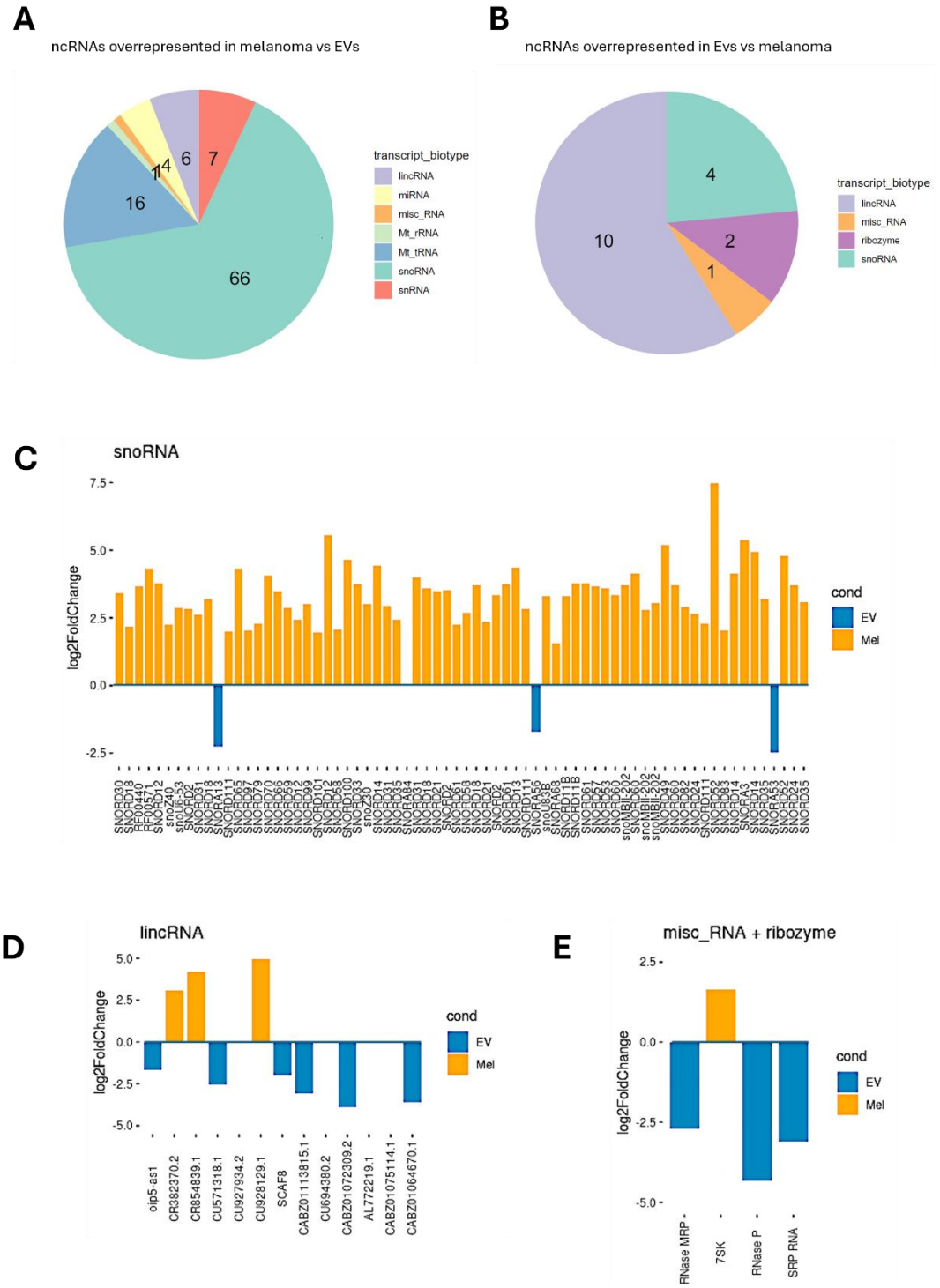

***Figure 13*. Analysis of ncRNA in EVs and melanoma**. **A**) Pie charts representing the different ncRNA species found enriched in melanoma and **B**) in their EVs. **C-E**) Representation of the three main categories of differentially enriched species of ncRNAs (orange bars: enriched in melanoma, blue bars, enriched in EVs) and their identity. *Adapted from (33)*

Size-based separation upon crosslinking of RNA–protein complexes prior to EV isolation, revealed that most of the *RPPH1* and *RMRP* could be amplified from the high molecular weight fraction, suggesting they remain largely intact and likely associated with protein complexes in EVs (***Figure 14D***). In this work we also explored susceptibility of the two ribozymes to enzymatic digestion on isolated EVs, revealing that the majority of *RPPH1* and *RMRP* (67% and 57%, respectively) is susceptible to treatment with RNase A (***Figure 14E***). These results implied that a substantial portion of these ncRNAs is either exposed on the outer surface of EVs or becomes accessible due to EV membrane compromise.

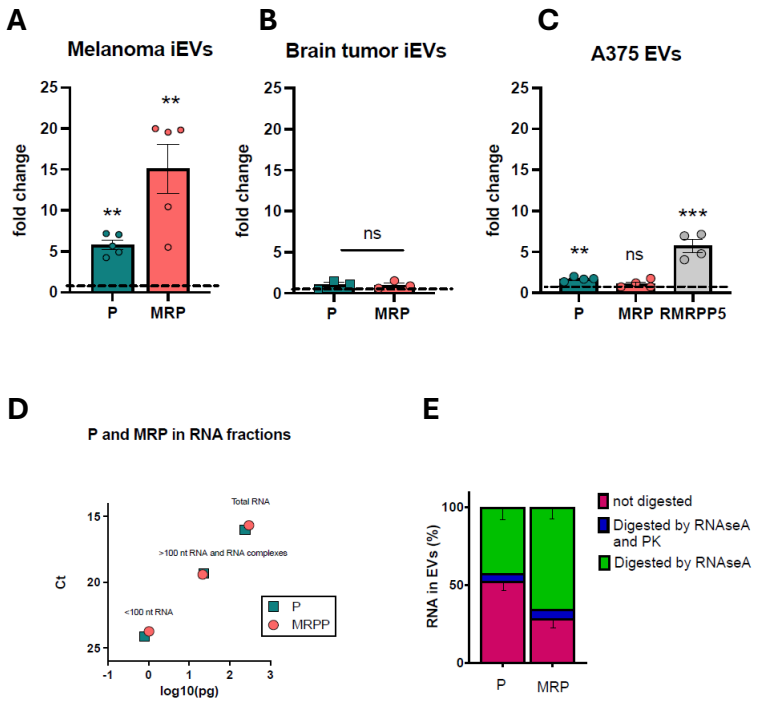

***Figure 14*. qPCR validation of *RPPH1* (P RNA) and *RMRP* (MRP RNA) enrichment** in A) melanoma-derived EVs compared to the expression in melanoma tissue, B) in brain tumour-derived EVs compared to the expression in tumour cells; C) in A375M EVs versus A375M cells. (**D**) Graphic representation of the amount of *RPPH1* and *RMRP* found in the fragmented and RNA–protein complexes fractions and total RNA of A375M EVs, following UV crosslinking. (**E**) Percentages of P and MRP RNA lost in RNaseA digested and RNaseA + proteinase K digested in A375M EVs. *Adapted from (33).*

Given the advancements in immunotherapy for melanoma and since the role of EVs in triggering immune responses was increasingly recognised, the possibility that melanoma-derived EVs can trigger innate immune activation through the delivery of DAMPs was for us of significant interest. So, in the study, we evaluated EVs derived from zebrafish melanoma or their ribozymes cargoes could stimulate components of the innate immune system. To this end, we injected melanoma-derived EVs or in vitro transcribed *RPPH1/RMRP* molecule into the bloodstream of 2- dpf transgenic zebrafish larvae expressing GFP-tagged macrophages or neutrophils.

This experiment revealed a significant increase in macrophage numbers and an alteration in their morphology in EV-injected, while neutrophil numbers remained unchanged (***Figure 15***

A, B, G) Macrophages recruitment is also recapitulated by injection of in vitro transcribed *RPPH1* or *RMRP* (***Figure 15C-F***). This macrophages response was also accompanied by an increased upregulation of ISGs and inflammatory cytokines, which are commonly induced following exposure to Poly(I:C) and serve as markers of antiviral and inflammatory responses (***Figure 15H-I***). These findings underscored the role of tumour-derived vesicles as modulators of the tumor microenvironment and systemic inflammation and point to specific ncRNAs as potential biomarkers or therapeutic targets in melanoma progression.

Overall, the *kita-GFP-RAS* zebrafish model recapitulates key genetic, histological, and immunological features of human melanoma, providing a robust platform to study tumor development, progression, and the role of tumor-derived extracellular vesicles in modulating the microenvironment.

Figure 15. *[Following page]* (**A, B**) Fluorescence stereomicroscope images of 5 dpf *tg(mpeg:GFP)*^{gl222} larvae injected intravascularly with PBS or with melanoma-derived EVs at 2dpf. The caudal hematopoietic tissue (CHT), where counts were performed, is boxed. (**A', B**') High magnification images of macrophages (C-E) Representative images of the CHT regions of 5 dpf *tg(mpeg:GFP)*^{gl222} larvae injected with the indicated molecules. F) Counts of macrophages in the CHT of injected larvae. G) Counts of neutrophils in the CHT of larvae injected with melanoma-derived EVs and controls. **H**) qPCR analysis of the expression of ISGs in larvae injected with the indicated molecules, compared to PBS-injected (horizontal dashed line). **I**) qPCR analysis of the expression Inflammatory cytokines in larvae injected with EVs, compared to PBS-injected (horizontal dashed line). *Adapted from (33).*

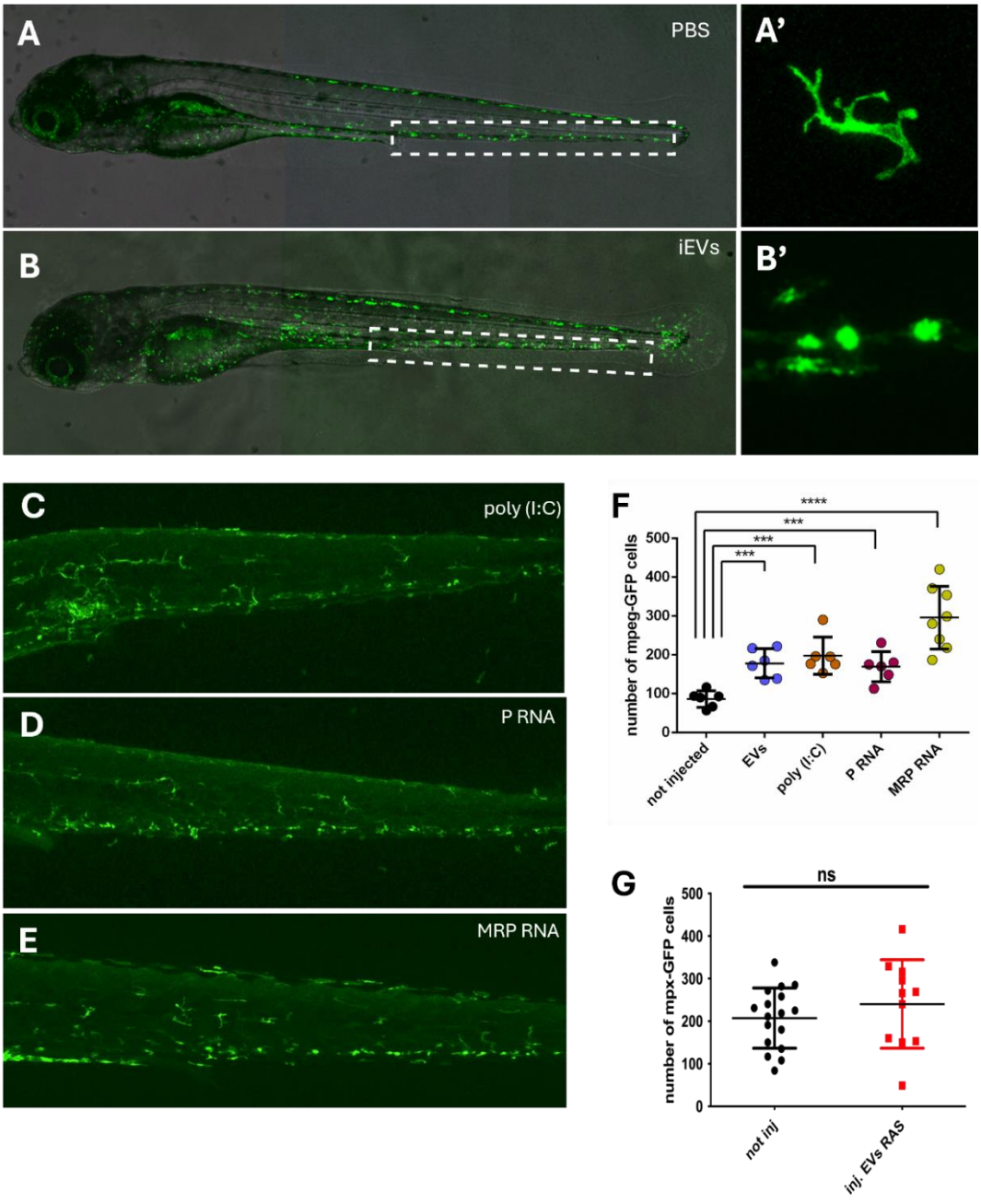
A
PBS
A'
B
iEVs
B'
C
poly (I:C)
D
P RNA
E
MRP RNA
F
number of mpeg-GFP cells
not injected
EVs
poly (I:C)
P RNA
MRP RNA
G
number of mpx-GFP cells
ns
not inj
inj. EVs RAS
H
fold change
ifit10
isg15
EVs
poly (I:C)
P RNA
MRP RNA
I
iEVs injection
fold change
il-8
il-1β
ns

CHAPTER 2

Aims

2. AIMS

Tumor progression relies on active communication between cancer cells and tumor microenvironment (TME). Extracellular Vesicles (EVs), which function as carriers of biomolecules, have been recognized as key mediators of these interactions. In cancer, EVs can influence not only tumor initiation and growth but also the metastatic process. Recent studies suggest that the RNA cargo of tumor-derived EVs can trigger pro-tumorigenic inflammation within the TME by activating interferon-mediated inflammatory responses through Pattern Recognition Receptor (PPRs) pathways. In a recent study, we reported a specific accumulation of the lncRNA *RPPH1* in EVs derived from zebrafish melanoma, an enrichment we also confirmed in a human melanoma cell model (33). *RPPH1* is the catalytic component of the ribonucleoprotein complex RNase P. While little is known about additional functions of *RPPH1*, emerging evidence highlights its involvement in tumor progression, including its role as an EV cargo. In this context, the injection of melanoma-derived EVs or *in vitro*–synthesized *RPPH1* into healthy zebrafish larvae induces sterile inflammation, in a manner consistent with the activation of PPRs in macrophages.

Our hypothesis is that the regulation of *RPPH1* in melanoma cells is altered, affecting the localization and/or functional activity of this lncRNA. This dysregulation promotes its packaging into EVs, which are subsequently released into the TME by malignant cells. EVs enriched in *RPPH1* serve as messengers within the TME, eliciting an innate immune response that primarily targets macrophages. This response is mediated through the activation of innate immune pathways specialized in the recognition of RNA molecules.

To investigate this hypothesis, my PhD thesis focused on four main objectives aimed at dissecting different aspects.

In the first section (section 3.1) we aimed to dissect the potential mechanisms underlying the packaging of *RPPH1* into EVs in melanoma cells. To this end, we employed both human cell systems and zebrafish melanoma models to investigate aspects of *RPPH1* regulation that may distinguish melanoma from non-malignant cells. Specifically, we examined the expression levels of *RPPH1,* its subcellular localization, and possible post-transcriptional modifications, all of which could contribute to differences between malignant and non-malignant contexts. In addition, we analysed the protein interactome of *RPPH1* in melanoma cells to gain insights into potential novel functions of this lncRNA in melanoma biology and to explore possible connections between its protein partners and its incorporation into the vesicular compartment.

Previous investigations demonstrated that melanoma-derived EVs injected into zebrafish larvae induce transcription of interferon-stimulated genes (ISGs) and inflammatory cytokines and a recruitment of macrophages. In the second part, we aimed at identifying the pathway of the innate immune system that is activated by melanoma-derived EVs. In this part (section

3.2) we exploited zebrafish models, to investigate the involvement of candidate pathways, considering both the type of response and *RPPH1* as possible trigger molecule.

In our hypothesis macrophages are the main cellular targets of melanoma-derived EVs. In the third section (section 3.3) we aimed at validating this in a human context by testing whether melanoma-derived EVs elicit in human macrophages a response that is comparable to the one we observed in *in vivo* models and if this response engages the same pathways.

Finally (section 3.4), we aimed at understanding the impact of melanoma-derived EVs on macrophages cell fate. The TME is a highly dynamic and intricate ecosystem, in which macrophages represent the most abundant immune cell population. They actively contribute to cancer initiation and development, and are critically involved in processes such as tumor growth, angiogenesis, metastasis, and evasion of immune surveillance. Emerging evidence highlights that tumor-derived EVs play a pivotal role in shaping macrophage phenotypes by transferring diverse molecular cargos, thereby fostering tumor progression. To investigate the role of EVs determining the activity of macrophages in the TME, in the final section we analysed transcriptional programs that are activated in macrophages in response to melanoma-derived EVs uptake.

CHAPTER 3

Results

3. RESULTS

3.1 Differential Regulation and Enrichment of lncRNA *RPPH1* in Extracellular Vesicles in Melanoma

We hypothesize that the regulation, processing, and functional dynamics of the lncRNA *RPPH1* are dysregulated in melanoma cells compared with non-malignant melanocytes. These tumor-associated alterations may modulate the molecular interactions of *RPPH1*, thereby promoting its selective recruitment and enrichment within extracellular vesicles EVs. Such effects could result from aberrant transcriptional control, altered post-transcriptional processing, or differential association with specific RNA-binding proteins. Collectively, these mechanisms may underlie the preferential packaging of *RPPH1* into melanoma-derived EVs. In this section, we employed multiple experimental melanoma models to investigate these regulatory and functional aspects.

3.1.1 *RPPH1* expression in melanoma cell lines and in zebrafish melanoma

Several studies reported an overexpression of *RPPH1* in different cancers, in which the lncRNA has been proven to participate in tumor progression by various mechanisms (31) (28) (142). Additionally, in colorectal cancer (CCR) the upregulation of *RPPH1*, correlates with its enrichment in exosomes isolated from the blood of CCR patients (31). To investigate the possibility that the enrichment of *RPPH1* in melanoma-derived EVs is due to a dysregulation of the expression of the lncRNA in melanoma cells, we employed different approaches.

Firstly, we analysed whether in zebrafish melanoma in which we previously reported an enrichment of *RPPH1* in extracellular vesicles (33), we detect changes in the expression of *RPPH1*. To do so we performed qPCR for *RPPH1* on RNA extracted from the dissected tumor masses of *kita-GFP-RAS; p53-/-* fishes and compared it to the expression of the lncRNA in healthy tissue. Melanomas in our zebrafish model usually develops on the trunk or the tail of fishes, so for this analysis we collected RNA from the same regions (including skin and muscles) dissected from healthy zebrafishes. Results showed that in zebrafish melanoma, *RPPH1* is up to six-fold more expressed than in the tissue of healthy specimens (***Figure 16A***).

We also examined human cell models of skin cutaneous melanoma. We performed qPCR to evaluate the expression of *RPPH1* in A375M cells, for which we previously reported an enrichment of *RPPH1* in EVs (33) and SK-MEL-5 cells. We used NHEM, a healthy melanocytes cell line as control. Results showed an increased expression of *RPPH1* of around five-fold in A375M in comparison to NHEM. In SK-MEL cells, *RPPH1* expression is increased up to twenty-fold with respect to NHEM (***Figure 16B***).

We also analysed the *RPPH1* transcripts in human cells using Northern blot and detected three bands specifically hybridizing with the *RPPH1* probe. As expected, one band was

observed at approximately 350 bp, corresponding to *RPPH1* size. Unexpectedly, we also detected two distinct bands at approximately 1800 bp and 5000 bp (***Figure 16C***). *RPPH1* signal quantification on the 350 bp band, further confirmed the overexpression of *RPPH1* in A375M and SK-MEL-5 cells compared to NHEM (***Figure 16E***). Of interests, the signal bands at 1800 bp and 5000 bp corresponds to the length size of ribosomal RNA *18S* and *28S* respectively, visible in the agarose gel (***Figure 16D***), that we used to verify RNA loading and integrity as well as to normalize band intensity for band intensity quantification. This result may indicate that *RPPH1* can be found complexed with ribosomal RNAs. These results highlighted a significant overexpression of the lncRNA *RPPH1* in both zebrafish melanoma and human melanoma cells.

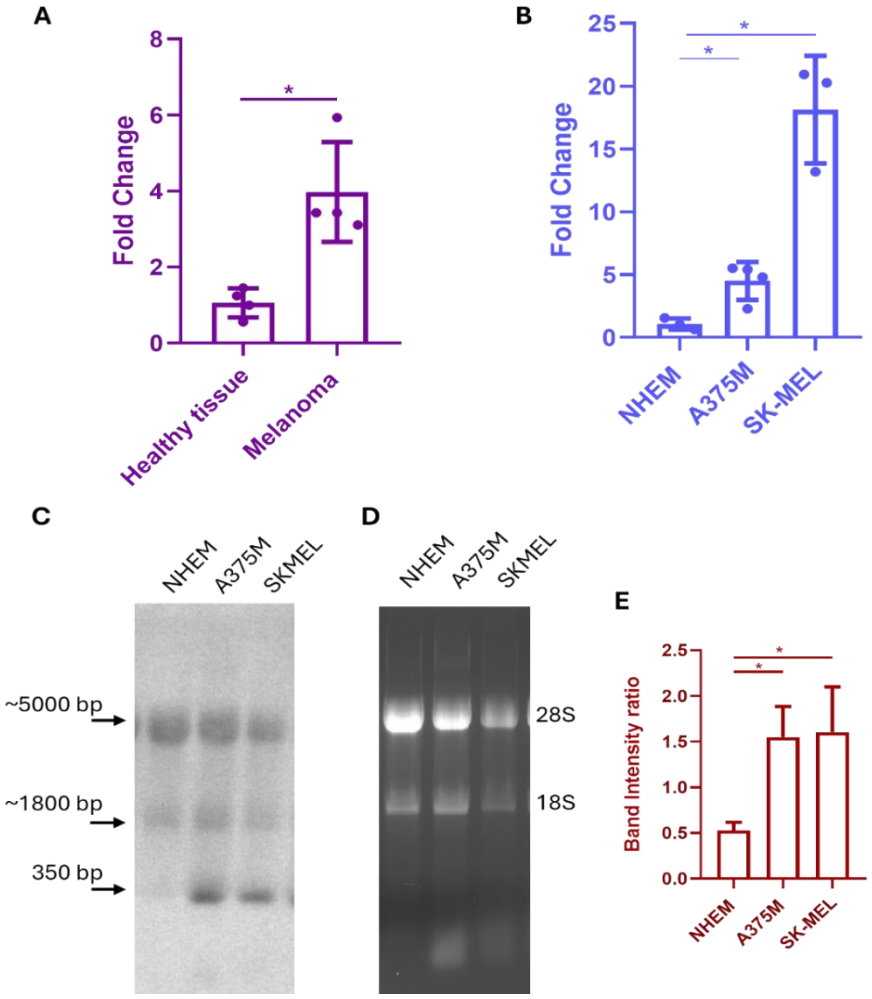

***Figure 16*. Analysis of lncRNA *RPPH1* expression levels. A)** qPCR analysis for *RPPH1* in zebrafish melanoma compared to healthy zebrafish tissue (p=0.02). **B)** qPCR analysis for *RPPH1* in A375M (p=0.01) and SK-MEL (p=0.01) compared to NHEM cells. Results are expressed as Fold Change and represent mean with SD. **C**) Northern Blot for *RPPH1* (arrows) and **D**) relative gel image used for normalization **E**) Northern Blot *RPPH1* bands intensity quantification for NHEM, A375M and SK-MEL. Results are shown as band volume intensity normalized over 28S RNA band on the agarose gel and represent mean with SD. n=3. **= p≤0.05*

3.1.2 *RPPH1* localization in melanoma cells

As the main function of *RPPH1* is exerted within the nuclear RNase P complex, this RNA is expected to localise predominantly in the nucleus. We hypothesize that, to enable its encapsulation into EVs by melanoma cells, *RPPH1* might exhibit an altered localization outside the nucleus compared to non-melanoma cells. To address this, we performed Single Molecule Inexpensive FISH (smiFISH) to visualize *RPPH1* in human cell lines (***Figure 17***). We compared its localization in A375M cells, as a model of human melanoma, and in NHEM cells, as a model of normal human melanocytes. In some NHEM cells, the *RPPH1* signal was clearly nuclear (***Figure 18A-A"***). In contrast, in A375M cells, the *RPPH1* signal was much more pronounced in the cytoplasm (***Figure 18C-C"***). In both cases, the specific signal was strongly reduced following RNase A treatment, leaving only a uniform background signal (***Figure 18B, D***), confirming the specificity of *RPPH1* RNA detection. These results highlighted a different distribution of *RPPH1* in subcellular compartments between healthy melanocytes and melanoma cells, suggesting an abnormal localization outside the nucleus, probably due to a non-canonical function and/or non-canonical molecular partners for this RNA in the cytoplasm in melanoma cells, leading to its accumulation outside the nucleus.

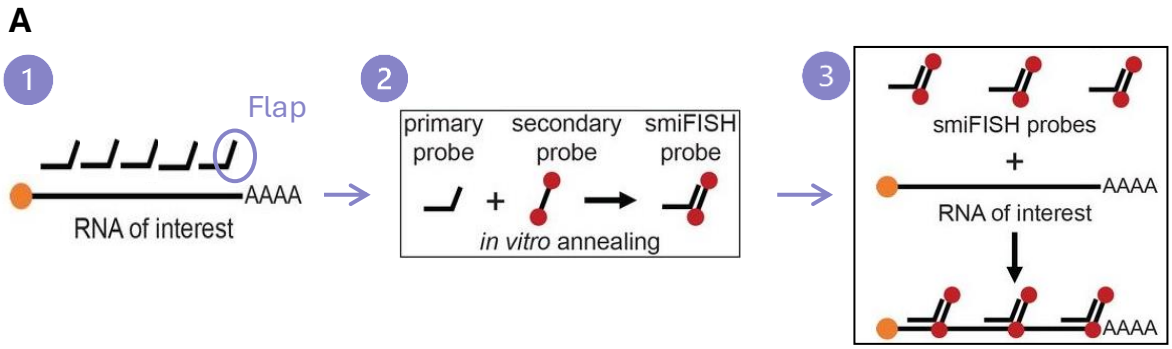

Figure 17. **A)** smiFISH workflow; 1.design of a probeset of 20 nt long probes that cover the full length of the RNA of interest, to which we added a sequence named FLAP (primary probes) that can anneal to the secondary probe; 2. In vitro annealing of primary probes to a fluorescently labelled secondary probe complementary to the FLAP sequence 3. RNA FISH is performed on fixed cells using the previously fluorescently labelled probeset**.** *Adapted from (143*)

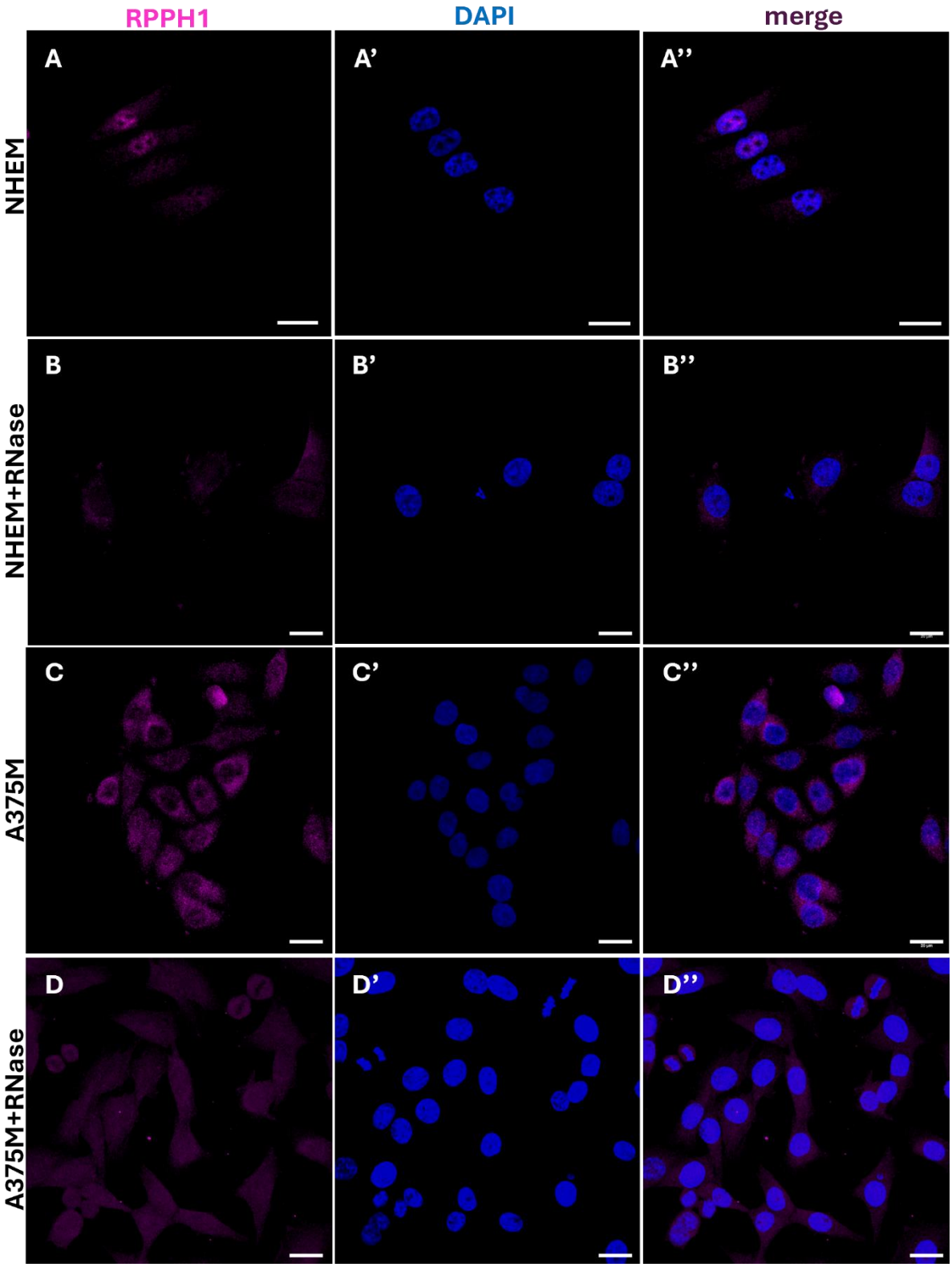

Figure 18. ***RPPH1* smiFISH. A)** Representative images of smiFISH for *RPPH1*, DAPI staining and merge in NHEM, with respective **B**) RNase treated **C)** Representative images of smiFISH for *RPPH1*, DAPI staining and merge in A375M, with respective **D)** RNase treated. Scale bar= 20µm

3.1.3 *RPPH1* post-transcriptional modifications

Among the events that can influence the fate of RNA molecules, post-transcriptional modifications represent key regulatory mechanisms that determine RNA processing, stability, localization, and translation. On this basis, we investigated whether *RPPH1* in melanoma cells undergoes post-transcriptional modifications that could alter its function and/or localization. Two of the most prevalent modifications that can occur on RNA molecules are polyadenylation and N6-adenosine methylation (m6A).

Polyadenylation consists of the addition of a long stretch of adenosine residues, known as the poly(A) tail, to the 3' end of the transcript. This modification is essential for RNA stability, as the poly(A) tail protects RNA molecules from rapid degradation, regulates their half-life, and enhances translation efficiency. For this reason, several classes of RNAs, most notably mRNAs, undergo polyadenylation (144). In contrast, the lncRNA *RPPH1*, like many other RNAs transcribed by RNA polymerase III, does not undergo polyadenylation and is therefore frequently used as a reference RNA for the non-polyadenylated RNA fraction (145).

N6-methyladenosine (m6A) represents the most abundant, widespread, and evolutionarily conserved internal post-transcriptional modification in eukaryotic RNAs. This modification consists of the addition of a methyl group on adenosine residues, and can be installed by different methyltransferase group, such as METTL3, METTL14 and WTAP (146). It is found in both protein-coding RNAs and in several types of noncoding RNAs. m6A influences the fate of RNA molecules by regulating multiple aspects of RNA metabolism, including stability, splicing, and nuclear export. This modification is dynamically controlled by distinct classes of RNA-modifying enzymes, thereby modulating RNA interactions with a variety of protein partners (147). Importantly, aberrant m6A patterns have been implicated in the pathogenesis of diverse diseases, including cancer (148).

With the aim of identifying potential post-transcriptional events that might alter the behaviour of *RPPH1* in melanoma cells, thereby conferring novel functions and/or enabling its packaging into extracellular vesicles, we considered these two fundamental modifications to assess whether the fate of *RPPH1* in melanoma may be influenced by either of them. For this part we used both human and zebrafish models.

3.1.3.1 Polyadenylation

To evaluate if *RPPH1*, or at least a fraction of it, is polyadenylated in melanoma we fractionated total RNA extracted from human cell lines, separating the PolyA+ and a PolyA- fractions. RNA was extracted from control NHEM cells, healthy melanocytes used as controls, and from A375M, as melanoma cells. Fractionated RNA was analysed by qPCR for *RPPH1*, comparing the PolyA+ fraction to the Poly(A)- fraction. *GAPDH* and *18S RNAs* were added to the analysis as controls for Poly(A)+ and Poly(A)- fractions respectively. Results are expressed as fold change over Poly(A)- fraction. This analysis reported that *RPPH1* is very rarely

polyadenylated both in NHEM and A375M cells (***Figure 19A-B***). Moreover, the state of polyadenylation of *RPPH1* is similar in human melanoma cells and healthy melanocytes (***Figure 19C***).

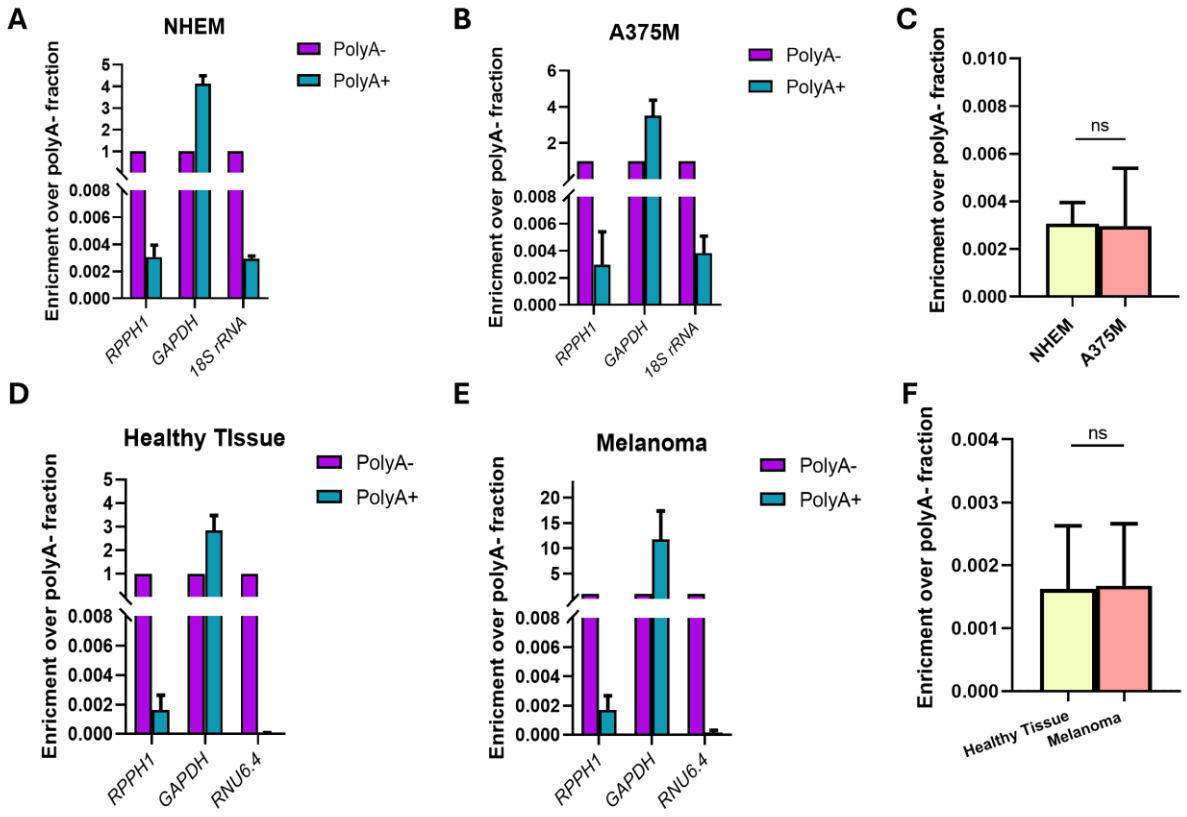

Figure 19. **Human and zebrafish *RPPH1* polyadenylation A)** qPCR analyses of *RPPH1* transcript expressed from poly(A)+ and poly(A)- fractions obtained from total RNA of NHEM and **B)** A375M. Poly(A)+ transcript (*GAPDH*) and a poly(A)- RNA (*18S rRNA*) were included in the analyses. **C)** Comparison of qPCR analysis for Poly(A)+ fractions of NHEM and A375M cells. **D)** qPCR analyses of *RPPH1* transcripts from the poly(A)+ and poly(A)- fractions obtained from total RNA of zebrafish healthy tissue and **E)** zebrafish melanoma tissue. Poly(A)+ transcript (*GAPDH*) and a poly(A)- RNA (*RNU6.4*) were included in the analyses. **F)** Comparison of qPCR analysis for Poly(A)+ fractions of zebrafish healthy tissue and melanoma tissue. Data are shown as Fold Change over poly(A)- fraction and represent mean and SEM. Data were analysed using unpaired t-test (no Gaussian distribution) n = 3. *Significative p-value set at >0.05*

We performed the same analysis in our zebrafish models. Using the *kita-GFP-RAS; p53 -/-* zebrafish melanoma model and healthy control tissue (as in 3.1.1), total RNA was fractionated into Poly(A)+ and Poly(A)– pools. qPCR analysis of *RPPH1* was performed, with *GAPDH* RNA as a Poly(A)+ control and the nucleolar ncRNA *RNU6.4* as a Poly(A)– control. Results showed that, even in zebrafish, *RPPH1* is predominantly detected in the Poly(A)– fraction in both melanoma and healthy tissues (***Figure 19D, E***). Furthermore, no significant differences were observed between the *RPPH1*-associated Poly(A)+ fractions in melanoma and healthy samples (***Figure 19F***).

3.1.3.2 N6-methyladenosine

To verify whether *RPPH1* can undergo m6A modification along its sequence in human cells we used the online tool deepSRAMP (http://www.cuilab.cn/deepsramp/) [7] to predict putative consensus sequences within the human *RPPH1* sequence. The algorithm did not identify any sequence that could serve with high confidence as site for m6A modification. A few positions along the *RPPH1* sequence displayed very low probabilities of being m6A sites, with the highest probability reaching 28% at position 250 (***Figure 20***). Overall, this analysis suggests that m6A modification is very unlikely to occur within the human *RPPH1* sequence.

Although the secondary structure and functions of *RPPH1* are highly conserved across species, the nucleotide sequence itself differs, indicating that the likelihood of this molecule undergoing modifications in other organisms may diverge significantly from what is observed in humans. N6-methyladenosine (m6A) is a conserved modification between humans and zebrafish, where it plays a comparable role in regulating RNA stability and processing. We submitted the zebrafish *RPPH1* sequence to the same prediction tool used for the human transcript in order to evaluate its potential for m6A modifications. The analysis identified four putative m6A sites within the zebrafish sequence, with predicted probabilities ranging from 30% for the least likely site to 61% for the most likely site (***Figure 21***). These analyses indicate that, while human *RPPH1* is highly unlikely to undergo m6A modification, its zebrafish counterpart retains a moderate probability of being modified, highlighting potential specie-specific differences in the epitranscriptomic regulation of this RNA. Nonetheless, it is important to note that these results are based solely on sequence-based predictions, and at present we lack experimental evidence regarding the actual occurrence of m6A modifications of *RPPH1* in living cells.

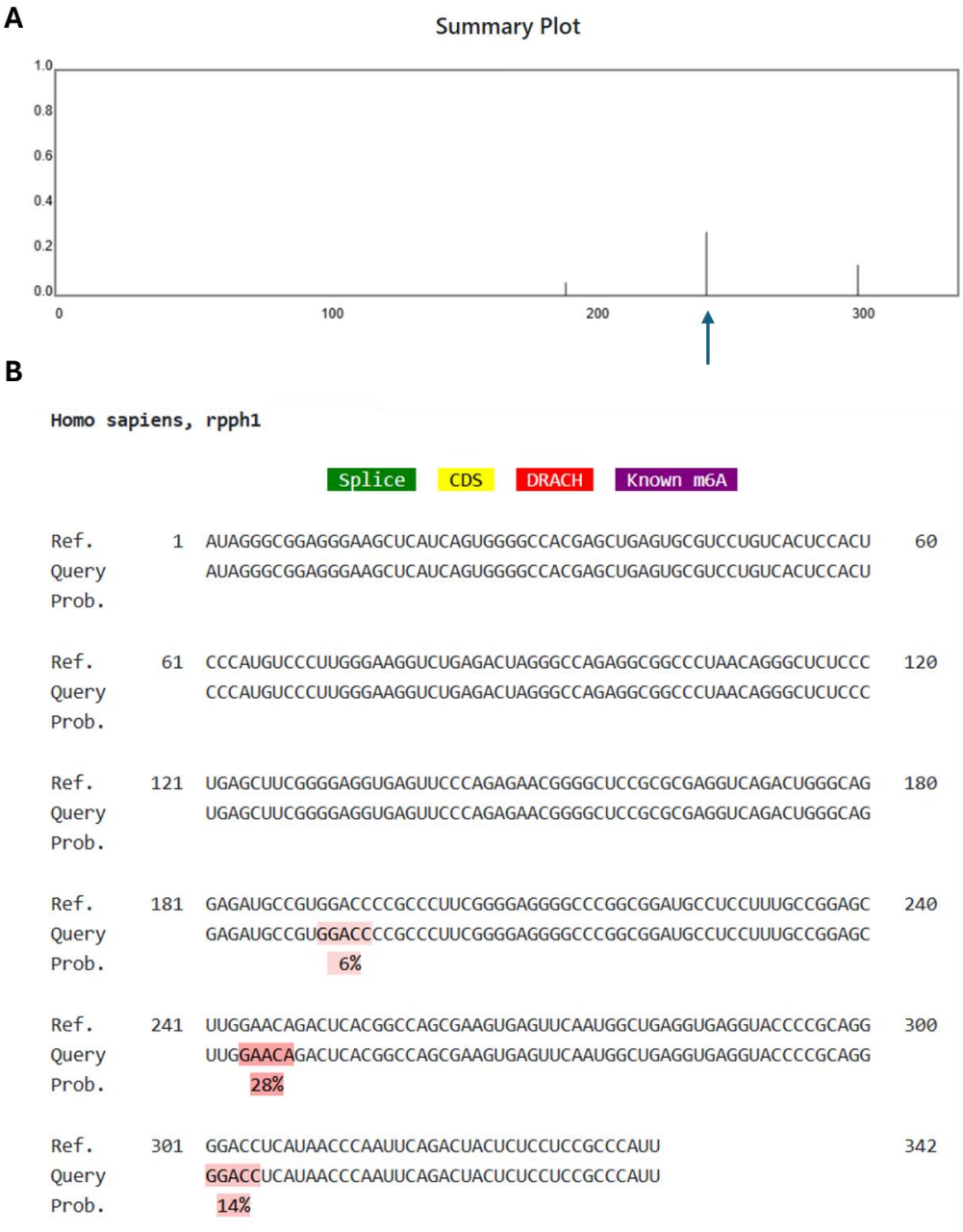

Figure 20. **deepSRAMP output for m6A site prediction on human *RPPH1* sequence. A)** Summary plot showing positions on the *RPPH1* sequences and the relative probability to be a m6A site with the higher rate for position 250, with 28% probability (blue arrow) **B**) Visualization of human *RPPH1* sequence with putative m6A modification sites and relative probability.

A

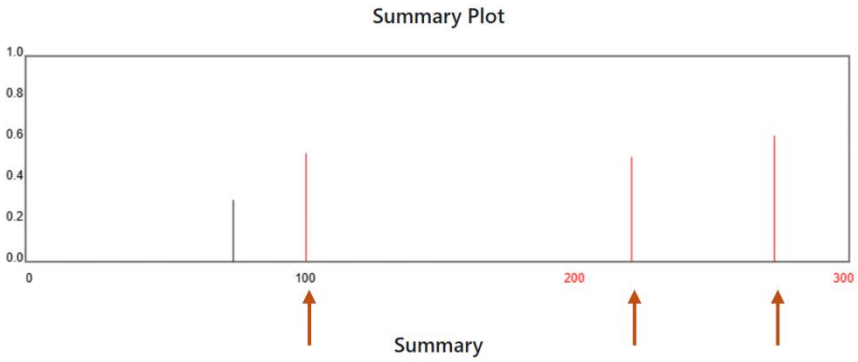

Summary

No.	Position	Query Position	Reference Sequence Position	Motif	Probability
1	105	104	104	GGACA	0.5283509493
2	226	225	225	AAACA	0.5092789531
4	279	278	278	GAACC	0.6126342416

B

Danio rerio, rpph1

Splice CDS DRACH Known m6A

```
Ref.      1  AGUAGCGGAAGGAAGCUCACUGUAGAGGUCACCCACUGAGUGCUCGUCACUCGCCAACAC   60
Query        AGUAGCGGAAGGAAGCUCACUGUAGAGGUCACCCACUGAGUGCUCGUCACUCGCCAACAC
Prob.

Ref.     61  CUCGGGGAAGGUCUGAGACAGGAGCCACUCGCUGUCCUAGCAGGACAUCAUCUGAAUGAU  120
Query        CUCGGGGAAGGUCUGAGACAGGAGCCACUCGCUGUCCUAGCAGGACAUCAUCUGAAUGAU
Prob.                      30%                          53%

Ref.    121  GAGCGAGUGCACAGAAAAUCGGGUCACGCGCGCGAUUCUCGCAGCAGACGUUGAUGCUCG  180
Query        GAGCGAGUGCACAGAAAAUCGGGUCACGCGCGCGAUUCUCGCAGCAGACGUUGAUGCUCG
Prob.

Ref.    181  CACACAUUCAGCGGAUCAACUGAUGCGACGCGCGCAGACUUGGAAACACUCGCGGCUGGC  240
Query        CACACAUUCAGCGGAUCAACUGAUGCGACGCGCGCAGACUUGGAAACACUCGCGGCUGGC
Prob.                                              51%

Ref.    241  GAAUGAGUGCGAUGUGUGAGCUAGCAUAACAUGCUAGAACCCAAUUCAGACUACUCUCCC  300
Query        GAAUGAGUGCGAUGUGUGAGCUAGCAUAACAUGCUAGAACCCAAUUCAGACUACUCUCCC
Prob.                                          61%

Ref.    301  UCCGCUC                                                       308
Query        UCCGCUC
Prob.
```

Figure 21. **deepSRAMP output for m6A site prediction on zebrafish *RPPH1* sequence. A)** Summary and relative plot showing the positions on the zebrafish *RPPH1* sequences and the relative probability to be a m6A site. Identified sites with higher probability highlighted in position 104 with 53%, position 225 with 51 % and position 278, with 61% probability (orange arrows) **B**) Visualization of zebrafish *RPPH1* sequence with putative m6A modification sites and relative probability.

3.1.4 Protein partners of *RPPH1* in melanoma cells

To verify the protein partners of *RPPH1* in melanoma cells, we used a technique known as Identification of Direct RNA Interacting Proteins (iDRiP), on A375M cells. iDRiP is an RNA-centric method that enables the detection of proteins directly interacting with a specific RNA of interest in cultured cells or tissues (***Figure 22A***) (149). We were able to capture *RPPH1* with a 0.5-1.5 % range of efficiency (***Figure 22B***). Although the retrieval efficiency observed for *RPPH1* is modest, this is not unexpected given its highly structured nature. Folded RNAs often exhibit reduced hybridization or pulldown efficiencies due to limited probe accessibility (150). Following RNA–protein isolation, in collaboration with the Proteomic Facility at CIBIO (University of Trento), the protein fraction was analysed by mass spectrometry (MS) to identify proteins co-purified with *RPPH1*. Analysis was conducted by comparing proteins precipitated by using an Anti-Sense (AS) probe (sample) or a Sense probe (control) designed on the regions of the *RPPH1* sequence that are predicted as single stranded (additional information on *RPPH1* secondary structure in section 3.2.1) and so should be accessible. We considered *RPPH1* partners those proteins that showed significant enrichment with the antisense (AS) probe compared to the sense (S) probe, using a statistical cutoff of p-value < 0.05. Using this criterion, our analysis identified 25 proteins (***Figure 22C***) that were significantly enriched and therefore we considered potential *RPPH1* interactors, listed in ***Table 1***, with relative p-value.

We performed Gene Ontology (GO) analysis to investigate whether the identified protein interactors of *RPPH1* in melanoma cells are enriched in specific pathways, with the aim of gaining insight into the putative biological processes in which *RPPH1* may be involved. We examined biological processes, molecular functions, and cellular components. GO enrichment analysis revealed that the most significant biological processes were strongly related to RNA metabolism, with a prominent enrichment in the regulation of mRNA splicing via the spliceosome (***Figure 22D***). Within the cellular component category, the most significant associations were with the cytoskeleton and intracellular membraneless organelles (***Figure 22E***), consistent with the enrichment of proteins involved in the activity of the spliceosome, of which many components are localized in nuclear speckles and Cajal bodies, and with proteins associated to ribosomal biogenesis and activity, such as EIF5B. Regarding molecular functions, the most enriched terms were double-stranded RNA binding and mRNA binding (***Figure 22F***). Taken together, these results highlight a strong involvement of the identified proteins in RNA splicing and RNA binding.

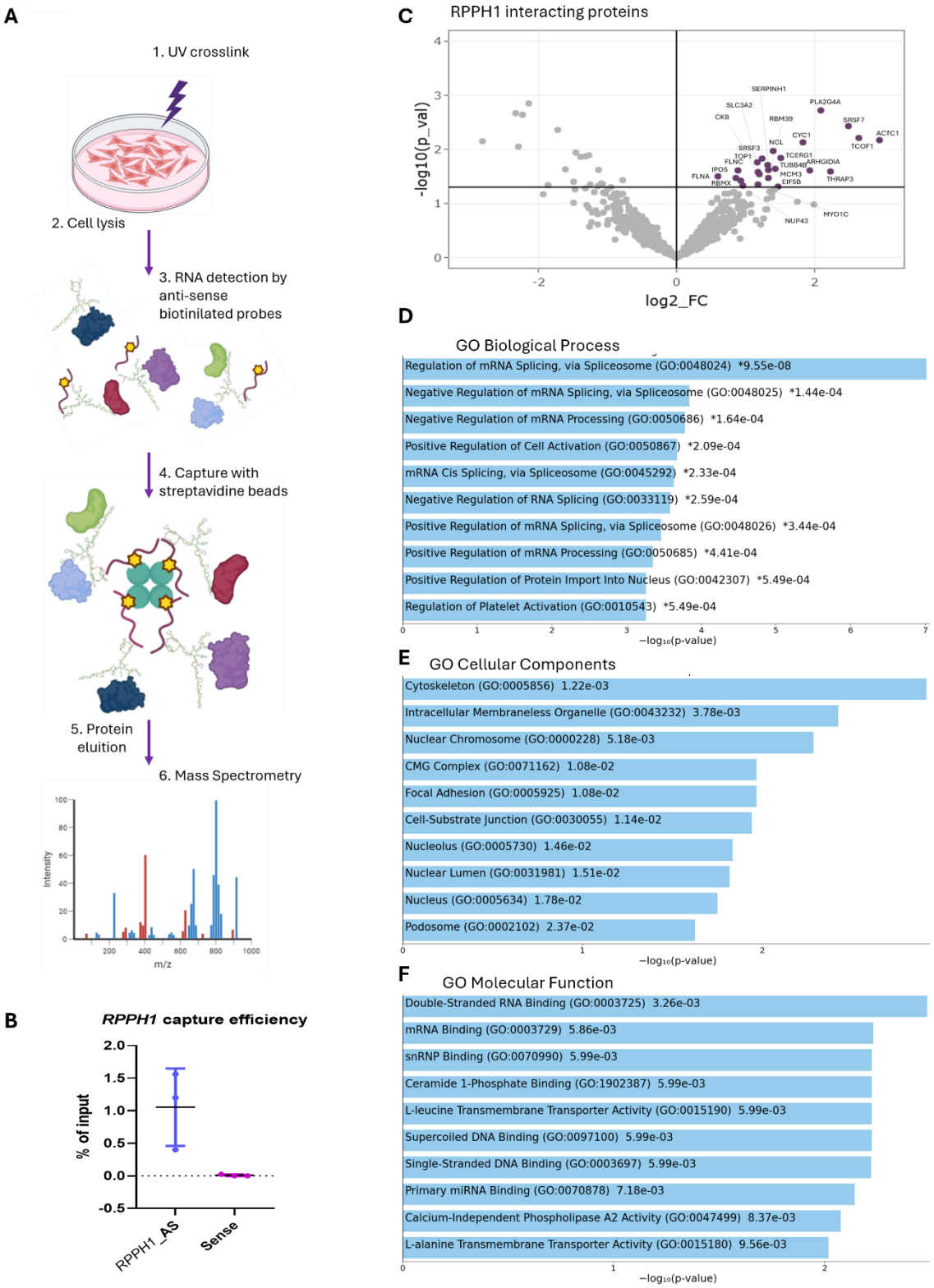

Figure 22. **iDRIP and Proteomic Analysis A)** Schematic workflow of iDRIP (*created with Biorender.com*) **B**) iDRIP capture efficiency for antisense probe (sample) and sense probe (control), expressed as percentage of the input. **C)** Volcano plots showing *RPPH1* interacting proteins enriched with AS probe (purple dots), significantly enriched compared with S controls (n = 3). The threshold for significance is set at a p-value of 0.05. **D**) Graph showing most significative results for GO analysis for biological processes, **E**) Cellular components and **E**) Molecular functions. Analysis performed using EnrichR. *=*adjusted p-value*

Interestingly, we did not find any of the proteins of the RNase P complex in our MS analysis. We hypothesize that this is due to the fact that in the RNase P complex, the catalytic RNA is highly folded and hidden in the core of the complex surrounded by the proteins (151). In fact, the crystallographic structure of Rnase P, shows that just a very limited portion of the RNA is exposed (151). Given that, it is unlikely that our probes to capture *RPPH1* and its bound protein partners are able to find an exposed segment of the RNA when it is in the RNase P complex. This hypothesis correlates with the modest capture efficiency obtained and is further supported by a published study in which it has been performed a co-purification of *RPPH1* and its proteins partners, targeting the RNA molecule. In this work none of the RNase P complex proteins were identified among the co-precipitated proteins (31). Indeed, the identification of *RPPH1* as the RNA component of the RNase P complex was done by targeting the proteins in the complex (2). Further hypotheses on the protein partners of *RPPH1* in and out of the RNaseP complex are presented in the Discussion (section 4.1).

Table 1. Human *RPPH1* protein partners identified through

Accession	Name of the Protein	Symbol	p-value
P68032	Actin, alpha cardiac muscle	ACTC1	0,00669
Q13428	Treacle protein	TCOF1	0,006096
Q16629	Serine/arginine-rich splicing factor 7	SRSF7	0,003734
Q9Y2W1	Thyroid hormone receptor-associated protein 3	THRAP3	0,025474
P47712	Cytosolic phospholipase A2	PLA2G4A	0,001908
P52565	Rho GDP-dissociation inhibitor 1	ARHGDIA	0,024829
P08574	Cytochrome c1, heme protein	CYC1	0,007403
O14776	Transcription elongation regulator 1	TCERG1	0,014425
O60841	Eukaryotic translation initiation factor 5B	EIF5B	0,048677
P68371	Tubulin beta-4B chain	TUBB4B	0,022914
P19338	Nucleolin	NCL	0,010617
Q14498	RNA-binding protein 39	RBM39	0,024102
P25205	DNA replication licensing factor MCM3	MCM3	0,033829
P50454	Serpin H1	SERPINH1	0,019612
P84103	Serine/arginine-rich splicing factor 3	SRSF3	0,014647
P08195	Amino acid transporter heavy chain SLC3A2	SLC3A2	0,028776
O00159	Unconventional myosin-Ic	MYO1C	0,044867
P12277	Creatine kinase B-type	CKB	0,02601
P11387	DNA topoisomerase 1	TOP1	0,017322
Q8NFH3	Nucleoporin Nup43	NUP43	0,04713
P38159	RNA-binding motif protein, X chromosome	RBMX	0,0384
Q14315	Filamin-C	FLNC	0,024646
O00410	Importin-5	IPO5	0,034163
P21333	Filamin-A	FLNA	0,03198

Since our main objective was to identify possible events leading to the encapsulation of *RPPH1* in EVs secreted by melanoma cells, we sought to determine whether its association with one or more of the identified protein partners could correlate with its inclusion in extracellular vesicles. To address this, we searched *Vesiclepedia*, a community-annotated database that collects and organizes information on molecules identified in EVs (152) http://www.microvesicles.org/). Specifically, we queried the database for each of the protein partners of *RPPH1* to assess whether they had ever been reported as cargo in melanoma-derived EVs.

Our analysis revealed that 23 out of 25 proteins have indeed been previously reported in melanoma-derived EVs. *Vesiclepedia* also allows verification of the type of sample from which EVs were isolated and the type of vesicle in which a molecule of interest has been found. Most of the proteins were identified in a study that performed mass spectrometry analysis on EVs derived from a broad panel of melanoma cell lines derived both from primary and metastatic melanomas. However, in that study the vesicle subtype was not specified, and the authors referred to them collectively as generic "EVs" (153) .On the other hand, some of the proteins in analysis have been found specifically both in MVs and Exosomes derived from a both murine and human cell lines, for instance, MYO1C, NCL and SLC3A2 (154) (155) (156). Results of the *Vesiclepedia* search are summarized in ***Table 2.***

In summary, our analyses suggest that the majority of *RPPH1*-interacting proteins are involved in RNA metabolism, splicing, and binding, and that many of these proteins have previously been identified in melanoma-derived extracellular vesicles. These findings support the idea that *RPPH1* may associate with specific protein partners that facilitate its encapsulation into EVs. However, while these analyses provide valuable insights, further experimental validations are needed to understand which protein partner is involved in possible non canonical functions of *RPPH1* in melanoma and whether these interactions influence *RPPH1* packaging in EVs.

Table 2. Vesiclepedia results

Protein	Type of Sample	Type of Vesicles	Reference
ACTC1	SK-MEL-2/SK-MEL-28/ MALME-3M/ UACC-2579	EVs	Hurwitz et al., 2016
TCOF1	SK-MEL-2/SK_MEL_28/ M14/ MDA-MB-435/ UACC-62/ UACC-257	EVs	Hurwitz et al., 2016
SRSF7	SK-MEL-5/UACC-62/LOX IMVI	EVs	Hurwitz et al., 2016 Liang et al., 2014
THRAP3	SK-MEL-2/ SK-MEL-5/M14/LMALME-3M/ LOX IMVI/	EVs	Hurwitz et al., 2016
PLA2G4A	MDA-MB-435	EVs	Hurwitz et al., 2016
ARHGDIA	UACC-62/ UACC-257	EVs	Hurwitz et al., 2016
CYC1	SK-MEL-2/ SK-MEL-5	Exosomes, Microvesicles, EVs	Hurwitz et al., 2016 Liang et al., 2014
EIF5B	SK-MEL-28/ UACC-62/ UACC-257/ LOX IMVI	EVs	Hurwitz et al., 2016
TUBB4B	SK-MEL-2/ SK-MEL-5/M14/ UACC-257	EVs	Hurwitz et al., 2016
NCL	SK_MEL-28,/SK-MEL-5/ SK-MEL-147/M14/ MALME-3M/ MDA-MB-435/ LOX IMVI	Exosomes, Microvesicles, EVs	Hurwitz et al., 2016 Suárez et al., 2021 Liang et al., 2014
RBM39	SK-MEL-2/ SK-MEL-5/M14/ MDA-MB-435	EVs	Hurwitz et al., 2016
MCM3	SK_MEL-2/ SK-MEL-5/ M14	Evs	Hurwitz et al., 2016
SERPINH1	M14/ MDA-MB-435	Evs	Hurwitz et al., 2016
SLC3A2	SK_MEL_5/ SK-MEL-202/ SK-MEL035/ SK-MEL-265/ UACC-62/LOX IMVI/ B16-F10	Exosomes, Microvesicles EVs	Hurwitz et al., 2016 Liang et al., 2014 Perinato et al., 2012
MYO1C	SK_MEL_5/ SK-MEL-202/ SK-MEL035/ SK-MEL-265/M14/ UACC-62/LOX IMVI/ B16-F10	Exosomes, EVs	Hurwitz et al., 2016 Perinado et al., 2012
CKB	SK-MEL-2/ SK-MEL-28/ M14/ LOX IMVI/	Evs	Hurwitz et al., 2016
TOP1	SK-MEL-5/ M14/ MDA-MB-435/ LOX IMVI	Evs	Hurwitz et al., 2016
NUP43	LOX IMVI	Evs	Hurwitz et al., 2016
FLNC	SK-MEL-2/ MDA-MB-435/ UACC-257	Evs	Hurwitz et al., 2016
IPO5	SK-MEL-28/ M14/ MDA-MB-435/ MALME-3M/ LOX IMVI	Evs	Hurwitz et al., 2016
FLNA	UACC-62; UACC-257	Evs	Hurwitz et al., 2016
SRSF3	SK-MEL5/ M14/ MALME-3M/ UACC-62	EVs	Hurwitz et al., 2016 Liang et al., 2014

3.2 Identification of the RNA Sensing Pathway Activated in Response to Melanoma-Derived EVs

Injection of zebrafish melanoma–derived EVs (and synthetic *RPPH1*) into the bloodstream of healthy zebrafish larvae led to increased transcription of ISGs and inflammatory cytokines (33). Our aim here was to identify which innate immune pathways capable of recognizing RNA molecules were activated by melanoma-derived EVs. To address this, we inhibited candidate pathways and then injected melanoma-derived EVs into the bloodstream of the inhibited larvae and analysed the responses that EVs triggered (33). Candidate pathways were selected based on two criteria: (i) the likelihood that EV content could reach the pathway's receptor(s), and (ii) the nature of the ligand.

Given that the lncRNA *RPPH1* is the cargo of melanoma-derived EVs in which we are interested we analysed the secondary structure of *RPPH1* in both human and zebrafish to understand which type of receptor(s) of the innate immune system it could engage.

3.2.1 Study of *RPPH1* secondary structure

This part was performed in collaboration with Stefano Maria Marino, PhD (Laboratory of RNA and Disease Data Science, Cibio, University of Trento).
We analysed the sequence of human *RPPH1* to predict its secondary structure using the minimum free energy (MFE) model. For this purpose, three different RNA secondary structure prediction tools were employed: MXFold (157), ViennaRNA (RNAFold) (158) and RNAstructure (Fold) (159).
The results obtained from these analyses consistently indicated that no extended regions longer than 20 nucleotides can be reliably predicted to adopt a single-stranded RNA (ssRNA) conformation. On the contrary, all three prediction methods revealed that the molecule is predominantly arranged in double-stranded regions. This double-stranded conformation was predicted uniformly across the three tools, highlighting the overall consistency of the results (***Figure 23***).
Nevertheless, a few specific segments of the sequence showed a higher tendency to remain unpaired: these could correspond to transiently extended single-stranded conformations within the structural ensemble. A noteworthy case was identified in the prediction generated by MXFold: here the region spanning positions 310 to 320 (sequence: *AACCCAAUUCAGACUACUCU*) was classified as a putative extended single-stranded region. (***Figure 23A***).

Figure 23. **Human *RPPH1* predicted secondary structure.** Dot-brackets notation for predicted secondary structure of *RPPH1* made with **A**) MXFold (longest single stranded predicted region highlighted in purple), **B**) ViennaRNAfold and **C**) RNAstructure. "." = single strand, ssRNA; "(" and ")" = double strand, dsRNA, in 5'->3' and 3'->5' directions respectively. **D**) Predicted secondary structure profile of human *RPPH1* sequence showed with color-coded pairing probability. White: prob(ssRNA) < 30%, light green: 30% < prob(ssRNA) < 75 %, dark green: 75% < prob(ssRNA). Obtained with ViennaRNAfold.

Overall, these results suggest that human *RPPH1* is largely structured in stable double-stranded regions, with only minor portions potentially adopting transient single-stranded conformations within the structural ensemble

We performed the same type of analysis on the sequence of the zebrafish *RPPH1*, in order to understand if the mainly double stranded structure of this RNA is conserved in zebrafish. Results showed a prediction for the secondary structure that predominantly double stranded, similarly to what we obtained in human (***Figure 24***). The MXFold analysis highlighted the same region of zebrafish *RPPH1* as putative extended single stranded region (***Figure 24A***).

This analysis supports the conclusion that, even being the human and zebrafish sequences of *RPPH1* different, the secondary structure is conserved in both organism (***Figure 25***) and it's predominantly double stranded.

Figure 24. **Zebrafish *RPPH1* predicted secondary structure.** Dot-brackets notation for predicted secondary structure of *RPPH1* made with **A**) MXFold (longest single stranded predicted region highlighted in purple), **B**) ViennaRNAfold and **C**) RNAstructure. "." = single strand, ssRNA; "(" and ")" = double strand, dsRNA, in 5'->3' and 3'->5' directions respectively. **D**) Predicted secondary structure profile of zebrafsih *RPPH1* sequence showed with color-coded pairing probability. White: prob(ssRNA) < 30%, light green: 30% < prob(ssRNA) < 75 %, dark green: 75% < prob(ssRNA). Obtained with ViennaRNAfold.

.

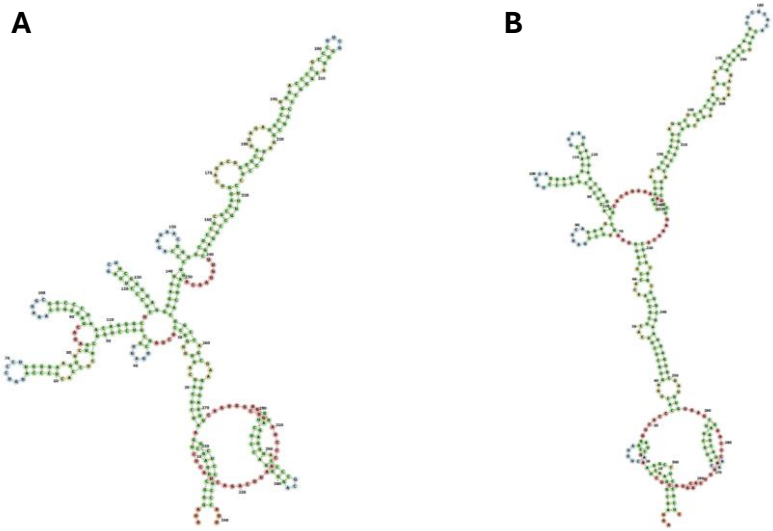

***Figure 25. RPPH1* predicted 2D secondary structure.** MXfold 2D prediction of A) Human and B) Zebrafish *RPPH1* molecules.

3.2.2 Inhibition of candidate pathways

Given the double stranded secondary structure of our ligand of interest, we therefore focused on RNA-sensing pathways that recognize double-stranded RNA. These include the Toll Like Receptor 3 (TLR3) pathway, whose receptor is localized on the membrane of endosomes, subcellular compartments that can be targeted by EV content in recipient cells. In fact, endocytosis is one of the most common and widely studied pathway for EVs uptake and through which EVs release their content in recipient cells, becoming part of the endosomal compartment (160). Moreover, it has been demonstrated that the RNA content of tumor-derived EVs can be recognized by TLR3 in recipient cells. For example, in prostate cancer, *TRPM8* RNA contained in tumor cell–derived EVs activates TLR3 in epithelial recipient cells, thereby contributing to sterile inflammation (161). Other endosomal TLRs capable of recognizing RNA, such as TLR7 and TLR8, are primarily activated by single-stranded RNAs and are therefore unlikely to be triggered by *RPPH1*, which is mostly double stranded.

We also considered the RIG-I like Receptors (RLRs) pathway, in which RIG-I and MDA5 recognize dsRNA in the cytoplasm, where EV-derived RNA may also accumulate through different routes (162) . Moreover, it has been reported in breast cancer that RNA contained within exosomes, predominantly composed of non-coding transcripts, can activate RIG-I in recipient cells, resulting in an interplay between the tumor cells and cells of the TME that promotes tumor growth and therapy resistance (163).

To identify which pathway is involved in the response to melanoma-derived EVs, we inhibited candidate pathways in zebrafish larvae and injected melanoma-derived EVs into the bloodstream of the inhibited larvae. The response that has been previously observed in (33) of increased expression of ISGs and inflammatory cytokines (we considered *isg15, ifit10* and *il1 β*) was then evaluated through qPCR on larval total RNA.

TLR3 was inhibited using CU-CPT 4a, a commercially available specific inhibitor, that selectively targets TLR3 (164). The TLR3 inhibitor was added to the water of zebrafish larvae that were also injected with melanoma derived EVs at 48 hpf (***Figure 26A***).

To date there are no available compounds that can selectively inhibit the RLRs, so we decided to inhibit this pathway by knocking out *mavs*, that encodes for the first main effector downstream of both RIG-I and MDA5 (***Figure 26B***). Additional details regarding the knockout of *mavs* in zebrafish larvae are provided in Section 3.2.2.1.

RNA from injected larvae was analysed by qPCR for the same genes previously shown to respond to EV injection in (33). Inhibition of the TLR3 pathway produced ambiguous results. Upon injection of melanoma-derived EVs, expression of *isg15* and *il1β* was higher in TLR3-inhibited larvae, with both genes showing a significant upregulation compared to non-inhibited controls. In contrast, *ifit10* exhibited the opposite trend, with a significantly reduced response to EV injection in TLR3-inhibited larvae (***Figure 26C-E***). This contrasting and ambiguous result may be attributed to the fact that the TLR family in zebrafish is broader than in humans, including at least another receptor capable of recognizing double-stranded RNA, known as TLR22 (165). The responses of these receptors may not be directly replicable in humans and therefore we did not investigate this discrepancy further, as our goal is to translate these findings to a human context. Our hypothesis is that the overactivation of one of the IRGs may result from the inhibition of TLR3, which causes other endogenous ligands to engage alternative TLRs, artificially enhancing their signalling. Of interest, although downstream effectors of the zebrafish-specific TLR22 appear to overlap with those of TLR3, there is currently no experimental evidence defining the precise transcriptional response triggered by TLR22. It is therefore possible that the genes activated downstream of TLR22 differ, which could explain the distinct responses observed when TLR3 is inhibited.

Inhibition of the RLRs pathway yielded a clearer outcome. In *mavs* knockout larvae, the transcriptional response to melanoma-derived EVs was strongly impaired. Specifically, *isg15*, *ifit10*, and *il1β* were all significantly less expressed in knockout larvae compared to wild-type specimens following EV injection (***Figure 26C-E***). Given the more definitive result obtained by inhibiting the RIG-I receptors pathway, that clearly seems to be involved in the response to melanoma-derived EVs, we decided to focus only on this pathway for the subsequent analysis.

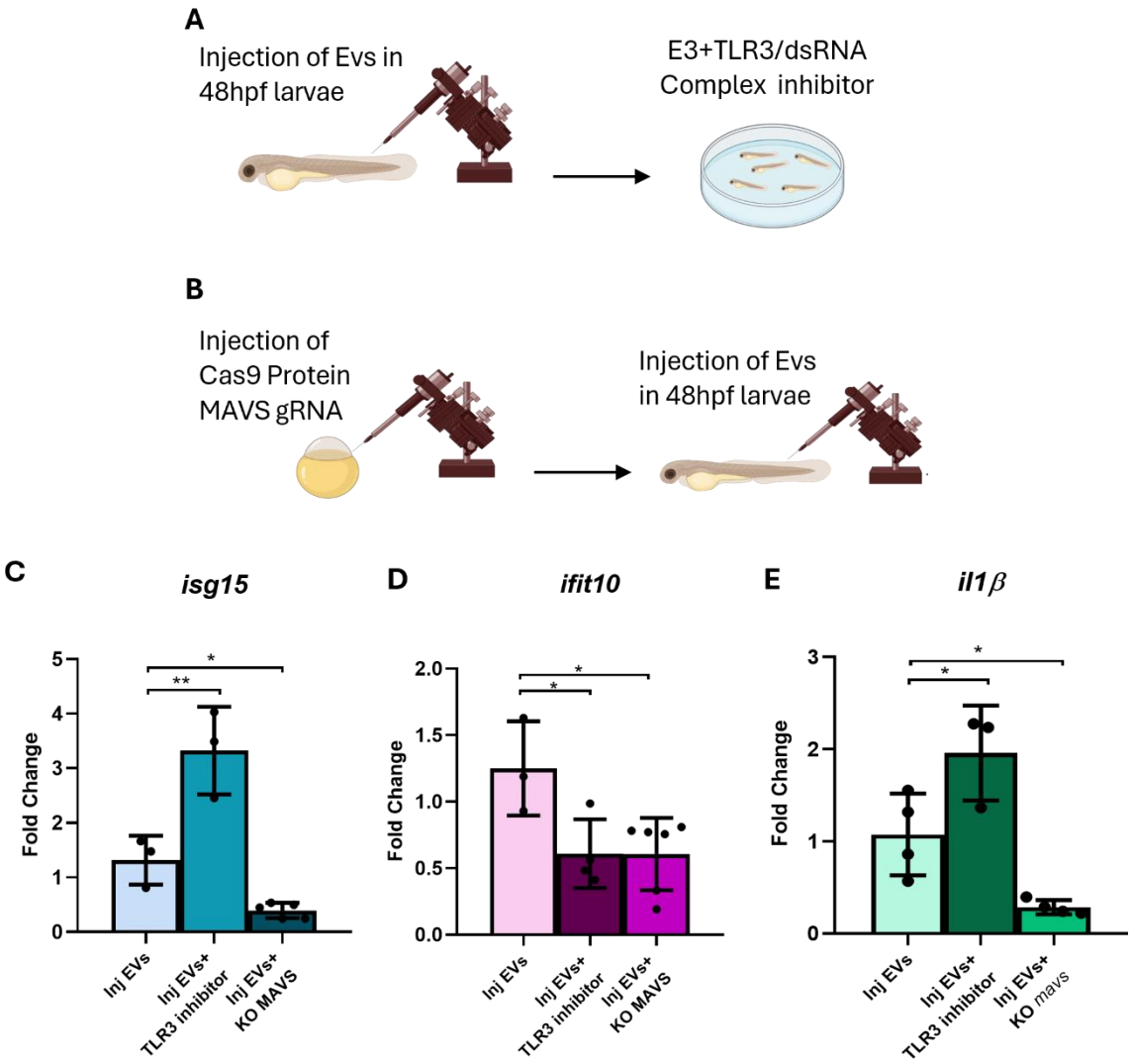

Figure 26. **A**) Schematic representation of the workflow to inhibit TLR3 and **B**) RLRs pathways in zebrafish larvae upon injection of melanoma-derived EVs **C**) Results of qPCR for *isg15*, D) *ifit10* and D) *il1β* in larvae transfused with melanoma-derived EVs and in which TLR3 or RLRs pathway have been inhibited, compared to wild type larvae injected with the same EVs. Results are showed as Fold Change and represent mean with SD. **= p< 0.05, **p< 0.005*

3.2.2.1 mavs Knock-out in zebrafish

To knock out *mavs* in zebrafish larvae, we employed CRISPR-Cas9 technology to generate zebrafish crispants, larvae carrying mosaic mutations in the target gene. The guide RNA (gRNA) targeting *mavs* (gRNAzf01, Table 5.6, Materials and Methods) was co-injected with a gRNA targeting *golden* (gRNAzf02, Table 5.6, Materials and Methods), a pigmentation gene whose loss of function results in defective pigmentation visible in the eye as early as 48 hpf. The *golden* phenotype served as a reporter, allowing us to identify larvae in which the CRISPR system had been efficiently delivered and was functionally active (***Figure 27A***).

Zebrafish embryos were injected with the Cas9 protein together with gRNAzf01 and gRNAzf02 at one cell stage, and then crispant larvae were selected based on the golden phenotype. KO for *mavs* was then evaluated through sequencing of genomic DNA. *mavs* KO was efficiently performed in zebrafish larvae with a KO score of 82,9% (***Figure 27B-C***). We will refer to crispant larvae as *mavs* KO larvae in the following sections. Since we were interested in the response of innate immune cells, specifically macrophages, we evaluated whether the KO of *mavs* affected these cells. We performed *mavs* knockout in a zebrafish transgenic reporter line expressing GFP in macrophages (*tg(mpeg:GFP)*^{gl222}), referred to as *mpeg:GFP*. At 5 dpf we evaluated *mavs* KO larvae and counted GFP+ macrophages in the Caudal Hematopoietic Tissue (CHT). If compared to not-injected *mpeg:GFP* larvae, mavs KO larvae showed a reduced number of macrophages, suggesting that the absence of *mavs* reduces the number of macrophages in the CHT even in the absence of other stimuli. ***(Figure 27D)***. (166)

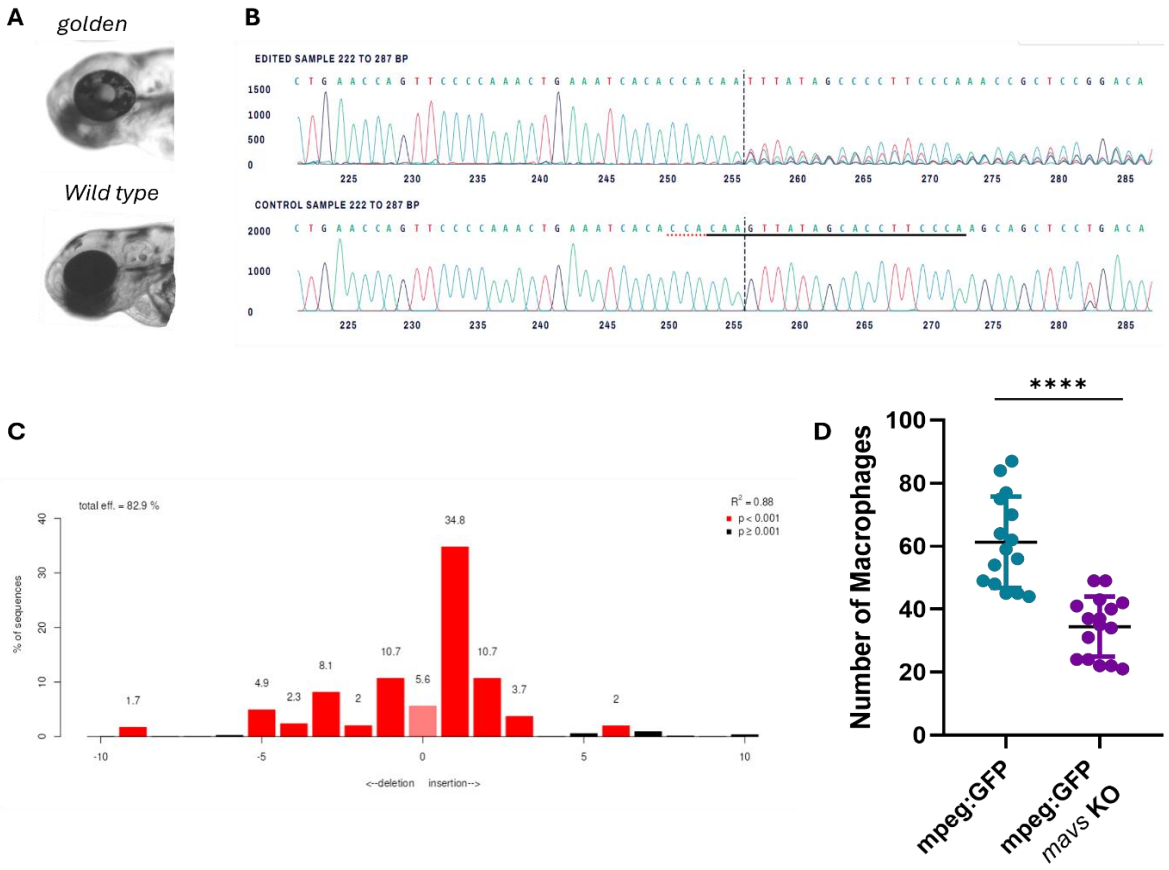

Figure 27. **Zebrafish *mavs* KO larvae**. **A**) Representative image of wild type and golden eye of 48hpf zebrafish larvae *(imaged by Irene Pecchini, Laboratory of Experimental Cancer Biology, Unitn)* **B**) Electropherogram of sequenced larvae showing the *mavs* KO (upper image) compared to wild type sequence (lower image). **C**) Graph showing the *mavs* total KO score and score for each type of mutation present in the crispants larvae, showing a predominance of insertions downstream the gRNA targeted sequence (obtained with TIDE *[Brinkman et al., 2014]*). **D**) Counts of macrophages in the CHT of *mpeg:GFP* larvae compared to *mpeg:GFP mavs* KO larvae (****= p< 0.0001)

3.2.3 Macrophage recruitment by EVs in *mavs* KO larvae

We further investigated the involvement of the RLRs pathway in the response to melanoma-derived EVs by examining the recruitment of macrophages in the CHT, a response that we previously observed to be triggered by the injection of melanoma-derived EVs as reported in (33) and reviewed in section 1.5.2.1. Melanoma-derived EVs were injected into 48 hpf *mavs* KO *mpeg:GFP* larvae and the number of macrophages induced by EVs was compared with that retrieved in *mavs* KO *mpeg:GFP* larvae injected with PBS, as negative control. At 5 dpf (three days post-injection), we quantified macrophages in the CHT of injected larvae. Poly(I:C) injected in *mavs* KO *mpeg:GFP* larvae was used as a positive control, as it is an immunostimulant known to activate multiple RNA-sensing pathways and has previously been shown to elicit the macrophage response under similar conditions [4]. Macrophage counts revealed that injection of melanoma-derived EVs in *mavs* KO larvae, in which the RLRs pathway is inhibited, failed to induce macrophage recruitment compared to control larvae injected with PBS (***Figure 28***), indicating the involvement of RLRs in the response of macrophages to EVs. In contrast, Poly(I:C) maintained its immunostimulatory effect even in *mavs* KO larvae, which may be due to the ability of Poly(I:C) to activate other RNA sensing pathways (167) .

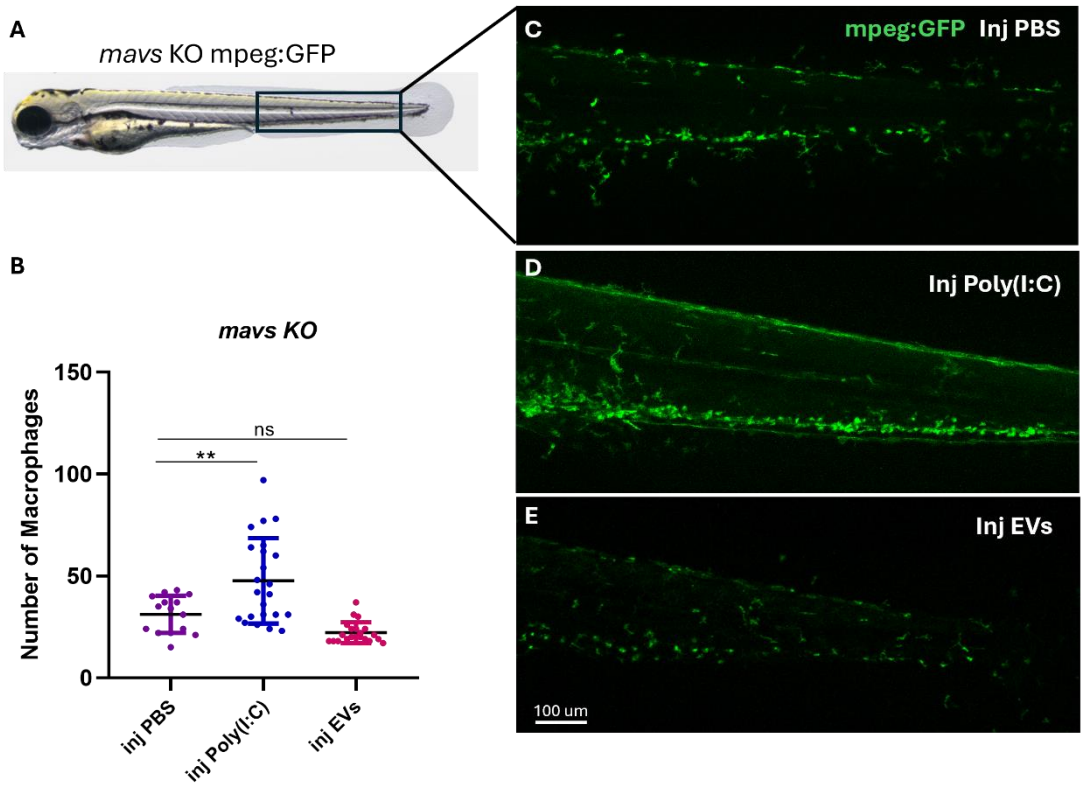

Figure 28. **Number of macrophages in injected crispant larvae**. **A**) Representative image of a 5dpf larva, showing the region of the Caudal Hematopoietic Tissue (CHT) used for the count of macrophages (black rectangle). **B**) Counts of macrophages in the CHT of injected larvae. ** *p< 0.005* **C-E**) Representative confocal images of the CHT regions of 5dpf *mavs* KO larvae injected with PBS, Poly(I:C) and melanoma-derived EVs, as indicated in the images.

3.2.4 Effect of *RPPH1* RNA in RLRs inhibited larvae

To determine if the activation of the RLR pathway by melanoma-derived EVs in zebrafish larvae is mediated by the lncRNA *RPPH1* they carry, we tested whether silencing the pathway through *mavs* KO would also abolish the response induced by injection of *in vitro*–synthesized *RPPH1* molecules, as shown in (33) (reviewed in section 1.5.2.1).

We synthetised zebrafish *RPPH1* molecules (zf*RPPH1*) and injected them in the bloodstream of 48 hpf zebrafish healthy larvae as in (33), and we checked for the same response described in section 3.2.2 and 3.2.3. Analysis of expression of ISGs and cytokines showed that *isg15 and ifit10* are significantly less expressed in *mavs* KO larvae compared to wild type controls injected with zf*RPPH1* RNA (***Figure 29A***). Conversely, there is not a significant difference in the expression *il1β* upon injection of synthetic zf*RPPH1* RNA between *mavs* KO and wild type larvae (***Figure 29B-C***), suggesting that the effect of injected *RPPH1* is not completely abolished by the silencing of the RLRs pathway, in terms of the activation of the expression of cytokines.

We also investigated the response of macrophages to zf*RPPH1* injection in *tg(mpeg:GFP)*^{gl222} *mavs* KO larvae. Macrophage counts revealed no significant increase in cell number three days post-injection compared to PBS-injected controls (***Figure 29D-F***). These suggest that MAVS (and RLRs signalling) is responsible for the increase in macrophage number observed upon synthetic zf*RPPH1* RNA injection, in wild-type larvae (33), (reviewed in section 1.5.2.1).

It is important to consider that the use of in vitro–transcribed RPPH1 may intrinsically activate immune sensing pathways due to the absence of post-transcriptional modifications, and its structural conformation and mode of delivery may not fully reflect those of the endogenous RNA transported by EVs. These limitations are discussed in detail in Section 4.2. Acknowledged that our results suggest that *RPPH1* may contribute to the transcriptional response and macrophage recruitment induced by RLRs activation in response to melanoma-derived EVs, as inhibition of the candidate pathway reduces the effects of *RPPH1* injection. However, the precise role of *RPPH1* requires further experimental validation.

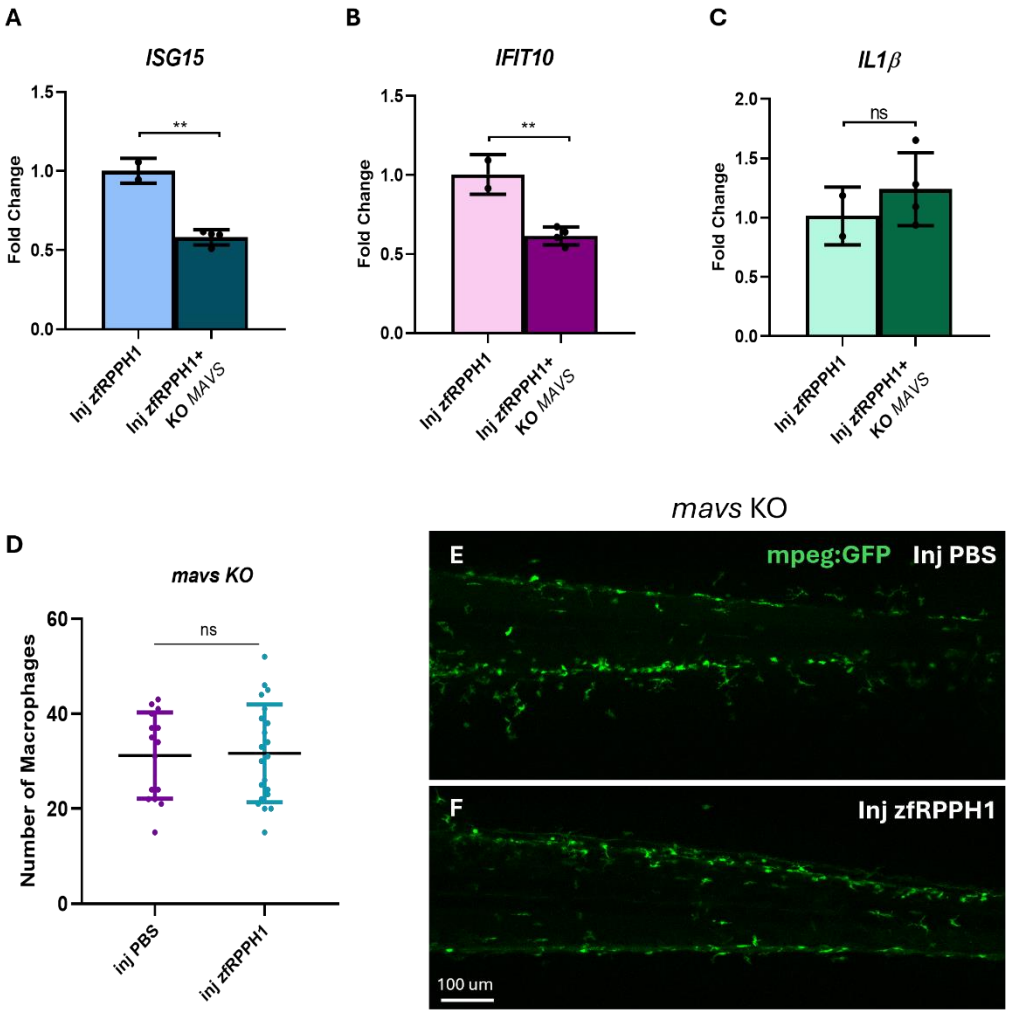

Figure 29. **Zebrafish larvae response to zf*RPPH1* injection**. **A**). Results of qPCR for *isg15*, **B**) *ifit10* and **C**) *il1β* in larvae transfused with synthetic zf*RPPH1* and in which RLRs pathway has been inhibited, compared to wild type larvae injected with zf*RPPH1*. Results are expressed as Fold Change and represent mean with SD. ***=p< 0.005* **D**) Counts of macrophages in the CHT of injected larvae. *Significative p-value set at >0.05* **E-F**) Representative confocal images of the CHT regions of 5 dpf *mavs* KO larvae injected with PBS (Inj PBS) or zf*RPPH1*.

3.3 Assessing the Response of Human Macrophages to Melanoma-Derived Extracellular Vesicles

Based on the observations made in the zebrafish model, we hypothesize that macrophages represent the primary cells within the tumor microenvironment responsible for the uptake of melanoma-derived EVs, thereby contributing to the activation of the subsequent responses. In the following section, we sought to validate macrophages as target cells for melanoma-derived EVs in human cell models. Specifically, we aimed to confirm in human macrophages the transcriptional response of ISGs and inflammatory cytokines that we had previously observed in zebrafish. Furthermore, we investigated the activation of RLRs and their downstream effectors and correlated RLRs pathway activation with the expression of the inflammatory genes.

3.3.1 Human macrophages as targets of melanoma-derived EVs

To validate macrophages as effectors of the inflammatory response activated by EVs that we reported *in vivo*, we took advantage of a human cell line model of macrophages. THP-1 cells are a human leukaemia monocytic cell line that is widely used in *in vitro* investigations on monocytic and macrophage behaviour. These cells have the advantage of being capable to differentiate from monocytes to M0, M1 or M2 macrophages (168).

THP-1 cells were differentiated into M0 macrophages and subsequently exposed to A375M-derived EVs. To isolate EVs from A375M culture media we performed differential ultracentrifugation (more detail in Chapter 5). To ensure that we were isolating the same population of vesicles (small vesicles, exosomes) that we previously characterized in (33), we analysed isolated EVs though Nanoparticle Tracking Analysis (NTA), showing that we are in fact isolating vesicles with a mean diameter of around 202 nm, confirming the enrichment of EVs (***Figure 30A***) , that we already characterized as exosomes (33). THP-1 cells were incubated with extracellular vesicles at a final ratio of 5,000-10000 EVs/cell, consistent with experimental conditions commonly adopted in the literature (169) (170). Following EVs exposure, the response of THP-1 cells was assessed by analysing the expression of ISGs and inflammatory cytokines through qPCR of total RNA extracted from EV-treated cells. In addition, we cloned the human *RPPH1* sequence into a plasmid that we used to transcribe *in vitro* the *RPPH1* RNA molecule (hsa*RPPH1*) as in section 3.2.4. Additional details regarding *RPPH1* cloning are provided in section 3.3.1.1 below. We then transfected hsa*RPPH1* into THP-1 cells using a lipid-based carrier to determine whether direct treatment of human macrophages with *RPPH1* could reproduce the effects observed with EVs. The amount of hsa*RPPH1* transfected in THP-1 cells was defined following manufacturer's instructions of the carrier employed, for an efficient delivery of the molecules (detailed information in Chapter 5). The same amount and protocol were used to deliver Poly(I:C) as a positive control for RNA sensing activation. We focused on the same genes that responded in zebrafish: *ISG15*, *IFIT1* (which in humans responds to stimuli similar to those activating zebrafish *ifit10* (171)), and

IL1β. Our results showed that THP-1 cells treated with A375M-derived EVs exhibited a significant increase in the expression of all the analysed genes compared to untreated cells. Transfection with hsa*RPPH1* induced overexpression of *ISG15* and *IFIT1*, while *IL1β* expression, although increased, did not show a statistically significant difference relative to control cells (***Figure 30B-D***). These findings demonstrate that both A375M-derived EVs and hsa*RPPH1* are capable of activating in human macrophages the same transcriptional response observed in the zebrafish model.

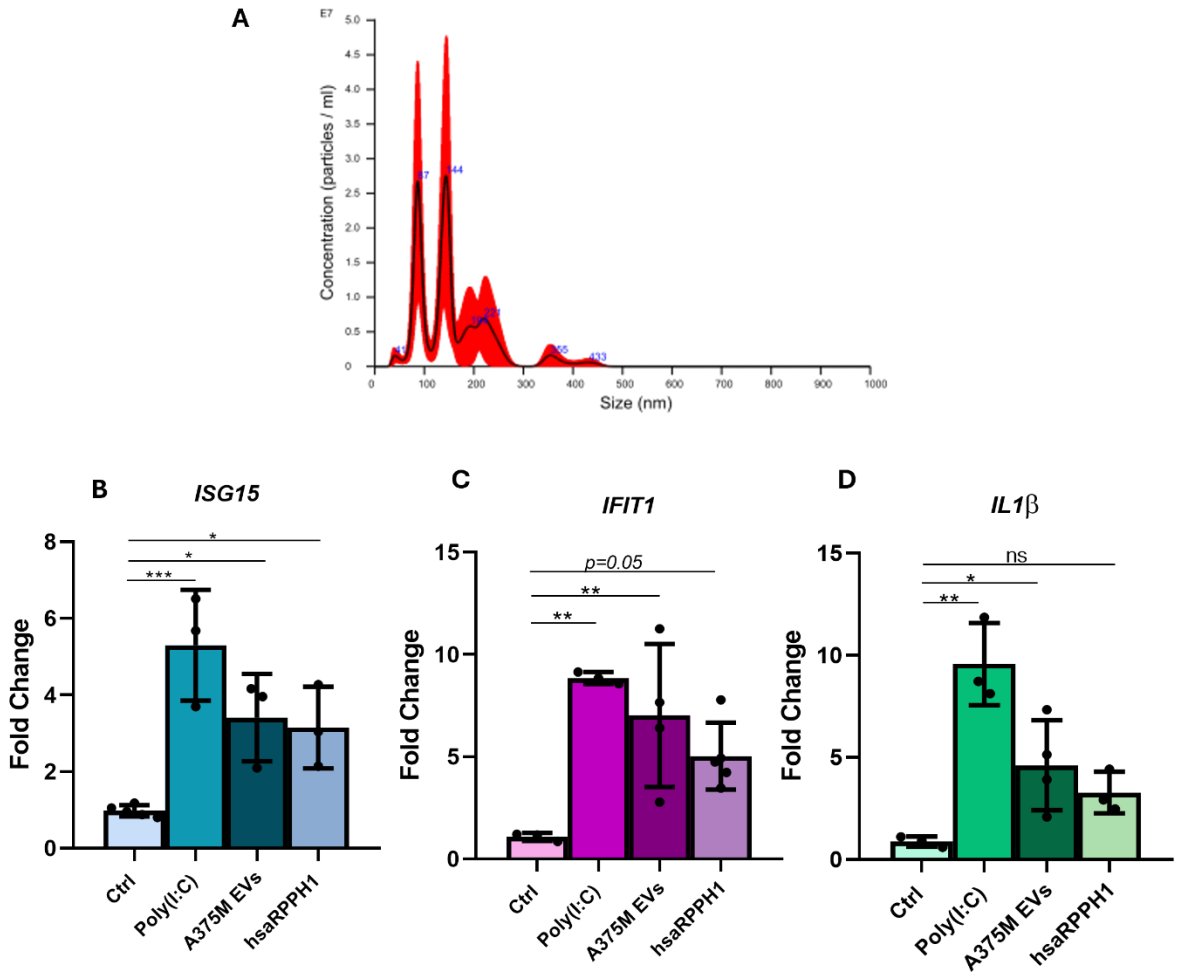

Figure 30. **THP-1 cells response to A375-derived EVs or hsa*RPPH1*. A)** Representative NTA on EVs isolated from A375M culture media by differential ultracentrifugation. The black curve indicated the mean of the three consecutive measurement made in the analysis, with SD in red. *n=5* **B**) Results of qPCR for *ISG15*, **C)** *IFIT1* and **D)** *IL1β* in M0 differentiated THP1-1 cells treated with Poly(I:C) as positive control, A375M-derived EVs or hsa*RPPH1*, compared to non-treated THP-1 cells. Results are showed as Fold Change and represent mean with SD. **= p< 0.05, **=p<0.005, ***=p<0.0005*

3.3.1.1 Cloning of RPPH1

To enable in vitro transcription of the *RPPH1* RNA molecule, its sequence was cloned into a vector containing SP6 and T7 promoters flanking the insertion site (***Figure 31***). This dual-promoter system allowed for transcription of the insert regardless of its orientation, by selecting the appropriate RNA polymerase. The *RPPH1* sequence was reverse-transcribed from total RNA extracted from A375M cells, and the resulting cDNA was amplified using Taq DNA polymerase with *RPPH1* specific primers. Due to primer design constraints, the amplified fragment corresponded to 294 nucleotides of the full 341-nucleotide human *RPPH1* transcript, lacking a small portion at the 5' end. The use of Taq polymerase results in PCR products with a single 3' A-overhang, which facilitated cloning into a linearized vector featuring complementary 3' T-overhangs at the insertion site.

The recombinant plasmid was subjected to Sanger sequencing, which confirmed successful cloning of the *RPPH1* insert. Sequence alignment demonstrated 100% identity with the corresponding region of the human *RPPH1* reference sequence (***Figure 31B***). Moreover, analysis of the sequencing data allowed us to verify that the insert was cloned in the correct orientation for transcription by T7 RNA polymerase.

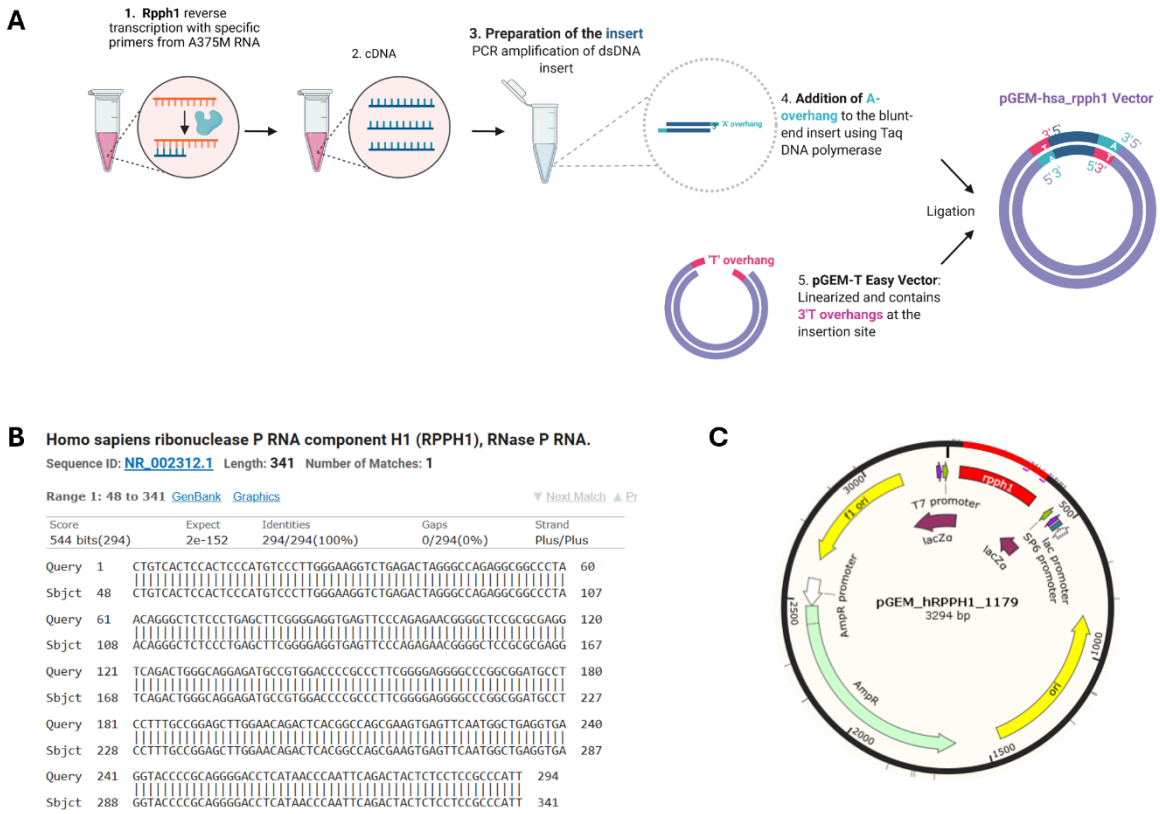

Figure 31. **Cloning of *RPPH1*. A**) Schematic representation of cloning workflow (*created with Biorender.com)* **B)** Alignment of the cloned and sequenced *RPPH1* insert showing 100% identity with the human *RPPH1*. Data obtained using NCBI Blast **C)** Map of the obtained plasmid, suitable for in vitro transcription of the inserted sequence.

3.3.2 Activation of the RLRs pathway in human macrophages

We wanted to verify whether A375M-derived EVs are actually able to activate the RLRs pathway in human macrophages. The RLRs pathway relies on a positive feedback loop; once it is activated through the recognition of PAMPs or DAMPs, the expression and production of receptors, along with downstream components of the pathway, are upregulated (83). Thus, one approach to investigate whether the pathway is activated is to assess the increased expression of proteins involved in it. In addition, transcription factors and activating kinases downstream of RIG-I and MDA5 are themselves activated through phosphorylation. To explore this, we performed Western blot analyses on M0 differentiated THP-1 cells treated with melanoma-derived EVs or transfected with hsa*RPPH1* or Poly(I:C) as positive control for the activation of the pathway.

In cells treated with A375M-derived EVs, WB analysis showed increased levels of both receptors of the RLRs pathway, RIG-I and MDA5, as well as an increase of the downstream activated transcription factor IRF3, in comparison to non-treated control cells. We also observed increased phosphorylation of the kinase TBK-1 and of IRF3 in comparison to control cells, meaning that in response to EV exposure these components of the RLRs pathway are activated in M0 THP1 cells. Transfection with hsa*RPPH1* produced a similar outcome, with increased production of RLRs; however, IRF3 was not overexpressed compared to control cells. On the other hand, its phosphorylation appeared to be enhanced upon treatment with hsa*RPPH1*, suggesting its activation, as was the case for TBK1 (***Figure 32***).

Overall, WB analysis on RLRs and downstream players of the pathway revealed that A375M-derived EVs, as well as hsa*RPPH1,* are able to trigger the activation of the RLRs pathway in human macrophages. This suggest that the involvement of the RLRs pathway in response to *RPPH1* and melanoma-derived EVs that we observed in zebrafish models is conserved in human macrophages.

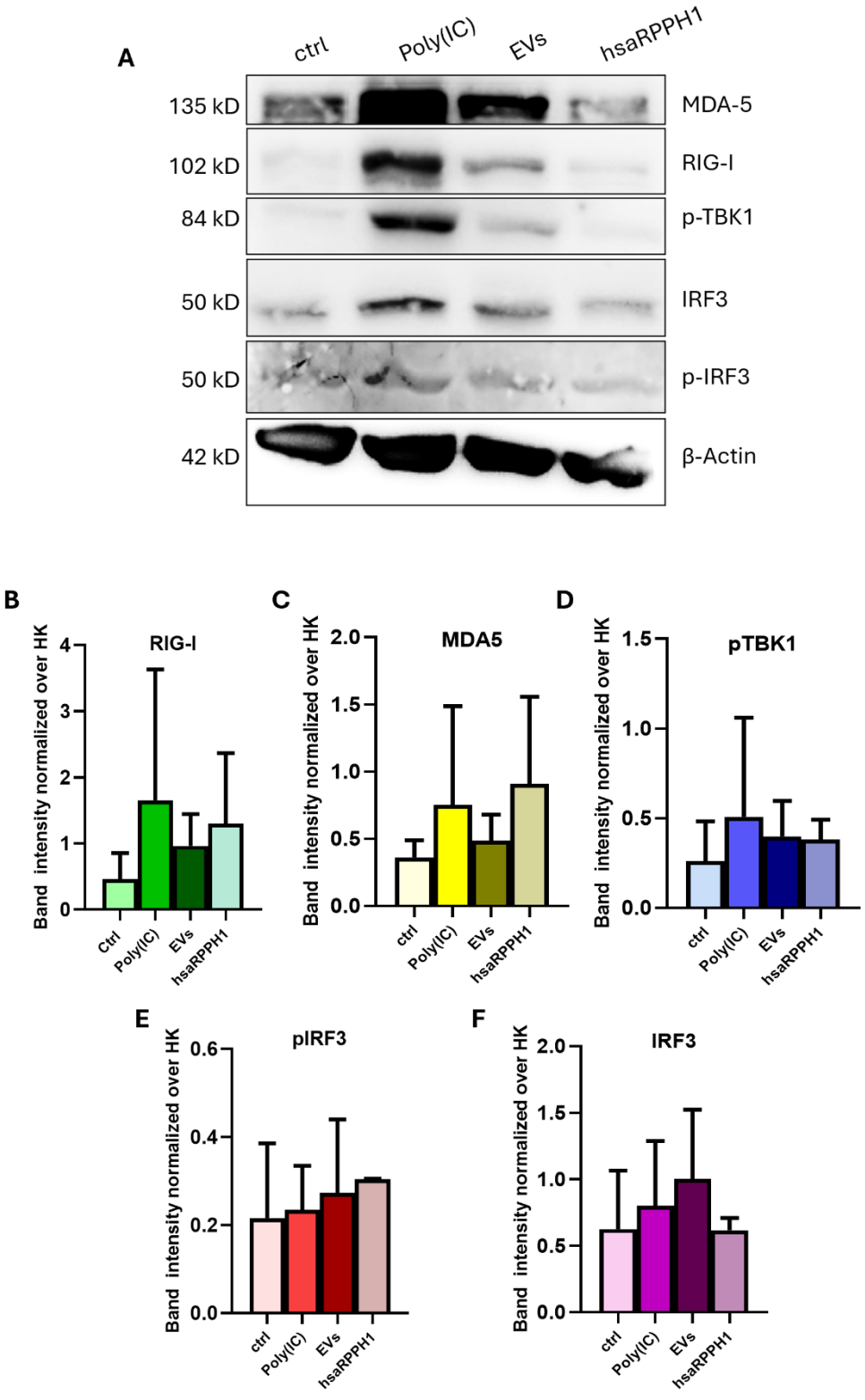

Figure 32 **Activation of RLRs pathway in THP-1 cells. A**) Representative image of WB analysis on THP-1 cells treated with Poly(I:C), A375M-derived EVs or hsa*RPPH1*, compared to non-treated controls. Analysis have been performed on MDA5, RIG-I, phosphorylated TBK1 (pTBK1), IRF3, phosphorylated IRF3 (pIRF3) and β-Actin as housekeeping protein **B-F)** WB volume band intensity quantification, normalised on β-Actin for RIG-I **(B),** MDA5 **(C),** pTBK1 **(D),** pIRF3 **(E)** and IRF3 **(F)** showing mean with SD. *n=3*

3.3.3 Correlation between activation of the RLRs pathway and transcriptional activation in response to melanoma-derived EVs in human macrophages

To test whether the increased transcription of ISGs and inflammatory cytokines correlates with activation of the RLR pathway in response to A375M-derived EVs in human macrophages, we knocked out *MAVS* in THP-1 cells (THP-1 KO *MAVS*) to generate cells in which the candidate pathway is inhibited. Further information about the KO of *MAVS* in THP-1 cells are reported in section 3.3.3.1 below.

We differentiated THP-1 KO *MAVS* cells into M0 macrophages and treated them with A375M-derived EVs or transfected them with *hsaRPPH1* and performed qPCR analysis to assess the expression of the ISGs and inflammatory cytokines of interest. Poly(I:C) was used as a positive control, and untreated THP-1 KO *MAVS* cells were used as negative control. Expression of *ISG15, IFIT1*, and *IL1β* in treated THP-1 KO *MAVS* cells was compared to the expression of the same genes in untreated THP-1 KO *MAVS* cells (Untreated). We observed that in macrophages with an inhibited RLRs pathway, neither A375M-derived EVs nor hsa*RPPH1* were able to induce the expression of *ISG15, IFIT1*, or *IL1β*, with expression levels remaining comparable to those of untreated cells. By contrast, Poly(I:C) retained the ability to increase *ISG15* and *IFIT1* expression, as expected, but, unexpectedly, not *IL1β* (***Figure 33***).

These results together with results in 3.3.1 and 3.3.2, suggest that melanoma-derived EVs and hsa*RPPH1* trigger the activation of ISGs and inflammatory cytokines by activating the RLR pathway.

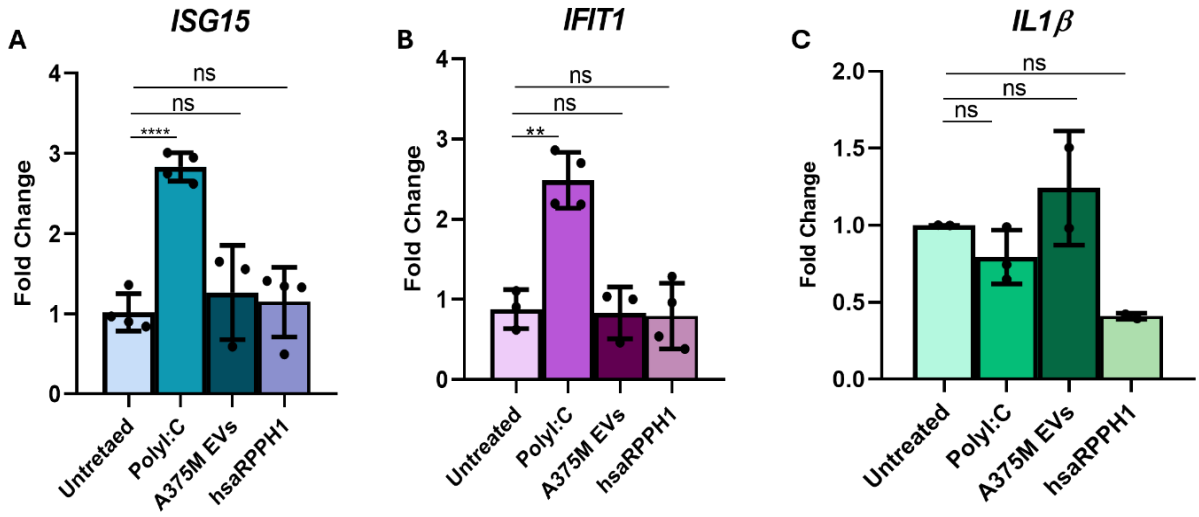

Figure 33. **THP-1 KO *MAVS* cells response to A375-derived EVs or hsa*RPPH1*. A)** qPCR results for ISG15, **B**) IFIT1 and **C**) IL1β in M0 differentiated THP1-1 KO MAVS cells treated with Poly(I:C) as a positive control, A375M-derived EVs or hsaRPPH1, compared to untreated THP-1 KO MAVS cells. Results are expressed as Fold Change and represent mean with SD. **= p< 0.05, **=p<0.005, ***=p<0.0005*

3.3.3.1 MAVS Knock-out in THP-1 cells

To generate a MAVS-deficient cellular model, we employed CRISPR/Cas9 genome-editing technology to knock out *MAVS* in THP-1 cells, in collaboration with Giorgia Pellizzaro (Harmenise-Harvard Laboratory of Cell Division, Cibio, University of Trento). The sequence of the guide RNA (Table 5.10,in Materials ad Methods) was designed to target exon six of *MAVS* sequence and, after the formation of gRNA-Cas9 Ribonucleoprotein complexes (RNPs), RNPs were delivered in THP-1 cells through electroporation as in (172) and (173).

We then assessed the efficiency of *MAVS* KO by sequencing genomic DNA extracted from the bulk population of electroporated cells. Results showed that we achieved a KO efficiency of 64,6%, with the majority of cells presenting deletions events (***Figure 34C-D***). Following the knockout, we also assessed MAVS protein expression in electroporated cells by Western blotting (WB), comparing the edited THP-1 cells (MAVS KO) with the corresponding wild-type THP-1 control. The analysis revealed a marked reduction in MAVS protein levels, with up to 94.5% depletion relative to wild-type cells (***Figure 34A-B***). This substantial decrease confirmed the successful knockout of MAVS in THP-1 cells. (166)

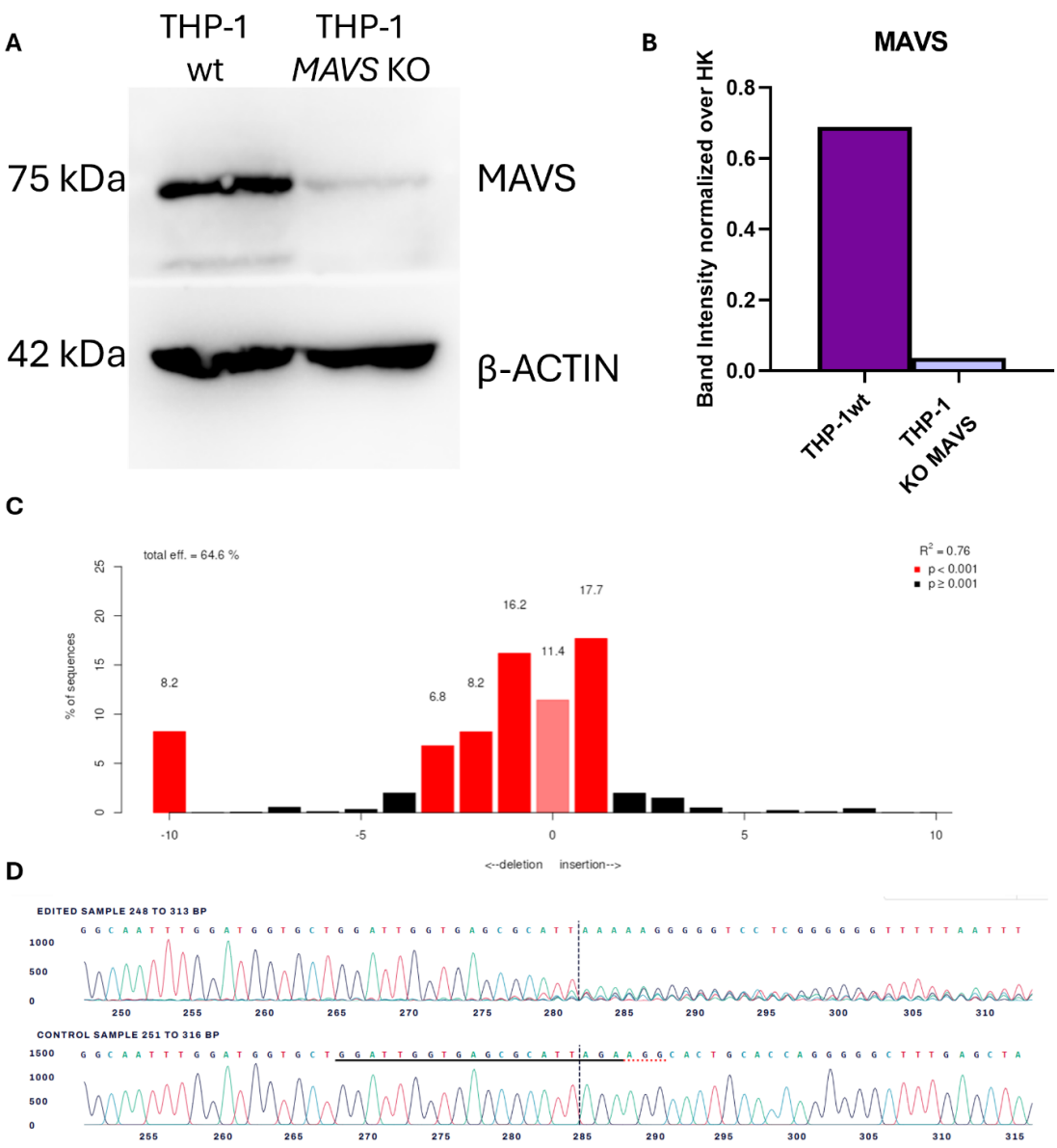

***Figure 34. MAVS* KO in THP-1 cells**. **A**) WB analysis for MAVS protein in THP-1 cells compared to THP-1 KO MAVS cells and **B**) Relative quantification showing a 94,5 % depletion of MAVS protein. Results are shown as volume band intensity normalised on the house keeping (β-Actin). **C**) Graph showing the MAVS total KO score and score for each type of mutation present in the bulk THP-1 MAVS KO population, (obtained with TIDE [*Brinkman et al., 2014*]). **D)** Electropherogram of sequenced cells showing a typical MAVS KO (upper row) sequence compared to wild type sequence (lower row).

3.3.4 Generic effects of synthetic mRNA on macrophages

The use of *in vitro*-transcribed hsa*RPPH1* introduces uncertainty, as its folding and resemblance to the endogenous EV-delivered molecule are unknown. Moreover, the transfection of synthetic RNA can, by itself, activate macrophage sensing pathways independently of the RNA sequence, since it lacks the post-transcriptional modifications that normally prevent self-recognition by the immune system.

To assess whether the response observed in THP-1 cells upon hsa*RPPH1* transfection was specific to this molecule, we performed a control experiment using an unrelated synthetic RNA. In particular, we transfected *in vitro*-transcribed GFP mRNA and evaluated the expression of *ISG15* and *IFIT1*, the two genes previously found to be significantly upregulated in response to hsa*RPPH1* (section 3.3.1). Results showed that there is a tendency for both *ISG15* and *IFIT1* expression to be increased in wt THP-1 cells upon transfection of GFP mRNA (***Figure 35A-B***).

To further investigate whether this effect was dependent on RLRs pathway activation, we repeated the experiment in THP-1 KO *MAVS* cells. Interestingly, in the KO background, GFP mRNA transfection triggered a significant increase in both *ISG15* and *IFIT1* expression probably by engaging MAVS-independent inflammatory pathways (***Figure 35C-D***). Of note, the same amount of synthetic RNA and the same protocol were used to transfect GFP and hsa*RPPH1* synthetic RNAs in THP-1 and THP-1 MAVS-KO cells as described in 3.3.1. Taken together, these findings indicate that while transfection of synthetic RNA can elicit a generic immune response in macrophages, the activation of the RLRs pathway appears to be specifically driven by ncRNA molecules, like hsa*RPPH1*.

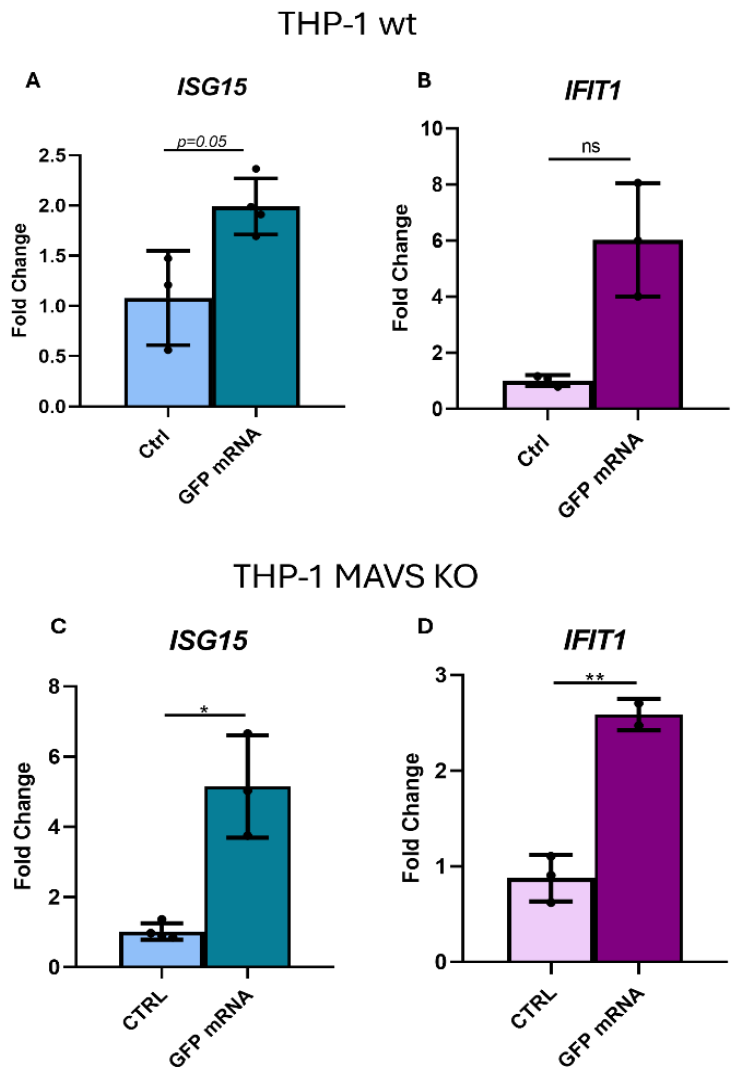

Figure 35. **THP-1 wt and KO MAVS cells response to synthetic GFP RNA**. **A**) Results of qPCR for *ISG15* and B) *IFIT1* in M0 differentiated THP1-1 wt treated with synthetic GFP mRNA compared to non-treated THP-1 wt cells. **C)** Results of qPCR for *ISG15* and D) *IFIT1* in M0 differentiated THP1-1 MAVS KO treated with synthetic GFP mRNA compared to non-treated THP-1 MAVS KO cells. Results are shown as Fold Change and showed as mean with SD. **= p< 0.05, **=p<0.005*

3.4 Response of Macrophages to RLRs Activation by Melanoma-Derived EVs

Macrophages represent the most abundant immune cell population within the TME. Owing to their close crosstalk with tumor cells, they actively contribute to cancer initiation and development, and are critically involved in processes such as tumor growth, angiogenesis, metastasis, and evasion of immune surveillance. Emerging evidence highlights that tumor-derived EVs play a pivotal role in shaping macrophage phenotypes by transferring diverse molecular cargos, thereby fostering tumor progression. Knowing that melanoma-derived EVs trigger the activation of the RLRs pathway in macrophages, we asked the question on what consequences the activation of the RLRs pathway has on macrophages differentiation. To investigate this point, we performed single cell RNA sequencing on human THP-1 cells exposed or not to melanoma-derived EVs. We analysed the transcriptional programs that are activated by this interaction to understand if exposure to melanoma derived EVs resulted in a homogeneous or heterogeneous population of macrophages. This part was performed in collaboration with Vittorio Bontempi, bioinformatician in our laboratory.

3.4.1 Single Cell RNA sequencing analysis

We differentiated THP-1 cells into M0 macrophages and then treated them with A375M-derived EVs. We then performed single cell RNA sequencing on untreated and EV-treated M0 THP-1 cells. Single Cell RNA sequencing analysis was performed in collaboration with Vittorio Bontempi, (Laboratory of Experimental Cancer Biology, University of Trento). After quality control (more information in Chapter 5, Materials and Methods), 4751 high quality cells were retained for further analysis (***Figure 36A***). Integrated Uniform Manifold Approximation and Projection (UMAP) visualization (***Figure 36B***) shows a great overlap between the two samples, suggesting a mild or partial response to the treatment.

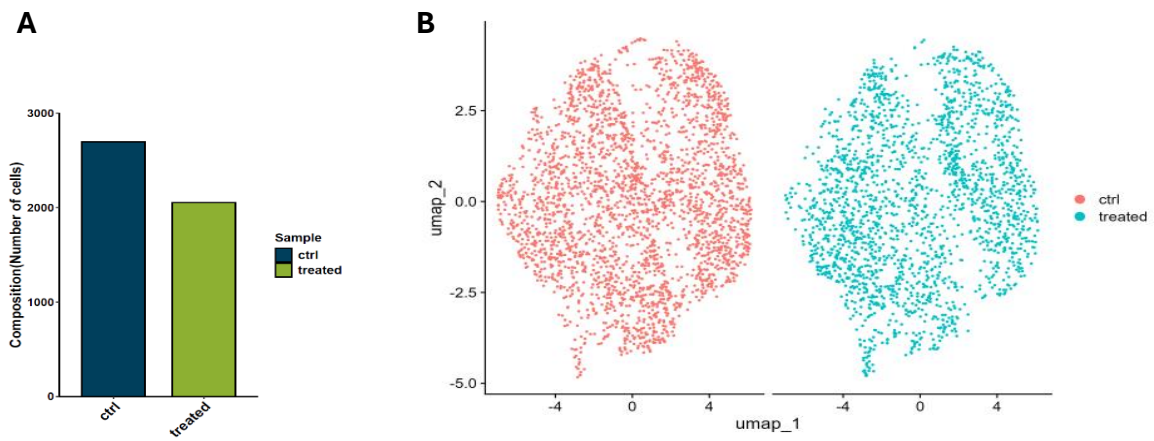

Figure 36. (A) Bar plot showing the total number of untreated (ctrl) and EV-treated cells in the samplesanalysed by sc-RNA Seq. (B) UMAP visualization of all cells colored by sample origin after dataset integration. Untreated (red) and treated (blue) cells are shown separately to show sample composition before clustering and cell type annotation

We first performed gene set enrichment analysis (GSEA) for Gene Ontology Biological processes (GO BP) on aggregated gene expression to identify biological processes that are differentially activated in EVs treated versus untreated M0 THP-1 cells. GSEA of GO BP reveals a clear shift in the cellular programs between untreated and treated cells. Untreated M0 THP1 cells show an enrichment of metabolic pathways, such as aerobic respiration, cellular respiration, oxidative phosphorylation, ATP synthesis and electron transport, indicating active energy production and a metabolically active state, that correlates with their M0 differentiation state (174). Overall, the untreated cells exhibit a metabolic and transcriptional profile consistent with resting macrophages under basal, non-inflammatory conditions.

In contrast, these metabolic pathways were markedly downregulated in macrophages exposed to A375M-derived extracellular vesicles. EVs treated cells display increase of immune-related processes, with an enrichment of genes involved in regulation of adaptive immunity and immune system processes, cytokines mediated signalling pathways, as well as macrophage activation and leukocytes migration pathways (***Figure 37A***). Concurrent downregulation of metabolic pathways involved in oxidative phosphorylation suggests a metabolic reprogramming toward glycolytic metabolism, an established feature not only of M1 pro-inflammatory macrophages, but also in Tumor Associated Macrophages (TAMs) (175). Overall, this observation indicates that uptake of A375M-derived EVs promotes macrophage activation, enhancing their inflammatory functions while suppressing energy-efficient mitochondrial metabolism in favour of immune effector responses.

Given our aim to investigate the effects of EVs on macrophages in terms of activation of innate immune pathways, we decided to further explore the genes that are involved in pathways related to cytokines mediated signalling, regulation of adaptive immune response

and regulation of immune system processes. We analysed genes overexpressed in treated cells that the GO analysis previously showed to be part of these categories and observed that some overexpressed genes correlate with the transcriptional program activated in Tumor Associated Macrophages (TAMs) (***Figure 37B***). TAMs are macrophages found within the tumor microenvironment that stimulate tumor tolerance in T-lymphocytes, thus promoting tumor growth and progression. They support processes such as angiogenesis, immune suppression, and metastasis, making them key contributors to cancer development and therapy resistance.

Among the upregulated genes, several are known to exert immunosuppressive functions typically associated with TAMs. *CSF1R*, encoding the receptor for macrophage colony-stimulating factor (M-CSF), is a key driver of macrophage polarization toward an immunoregulatory phenotype (176). *TFEB* and *ATG5*, two central regulators of the autophagy–lysosomal pathway, were also upregulated, supporting macrophage adaptation and survival within the hypoxic tumor microenvironment, a role previously described in breast cancer and lung adenocarcinoma, respectively (177) (178). Increased expression of *IL10RB*, a core subunit of the interleukin-10 receptor complex, suggests enhanced responsiveness to IL-10 signalling and reinforcement of the anti-inflammatory, immunoregulatory phenotype characteristic of TAMs (179). Furthermore, the upregulation of *TRIM14*, *TRIM56*, and *TRIM25* indicates activation of ubiquitin-mediated regulatory mechanisms that can influence TAM polarization and function. These TRIM family E3 ligases are known modulators of innate immune signalling, particularly the type I INF pathway, and their elevated expression may contribute to tune inflammatory responses and metabolic adaptation within the tumor microenvironment (180) (181). Of note, the responsiveness to INF signalling is further highlighted by the overexpression INF receptors. Chronic type I IFN signalling via *IFNAR1/2*, that we found overexpressed, may drive immune exhaustion or metabolic reprogramming that supports tumor progression (182). Similarly, IFN-γ signalling via IFNGR1/2 typically induces classical (M1-like) macrophage activation, but in many tumors this pathway becomes attenuated or tolerated, contributing to the persistence of an immunosuppressive TAM population (183). Additionally, increased signalling through IL-4 and its receptor IL-4R, which are well-established mediators of M2-like macrophage polarization, further supports the acquisition of a tumor-promoting, immunosuppressive phenotype by THP1 cells exposed to melanoma EVs, that contributes to immune evasion and resistance to immunotherapy (184) (185).

Overall, the observed transcriptional reprogramming of EV-treated macrophages toward glycolytic metabolism and TAM-associated gene expression signatures suggests that A375M-derived EVs may promote the acquisition of TAM-like characteristics, potentially contributing to a tumor-supportive microenvironment.

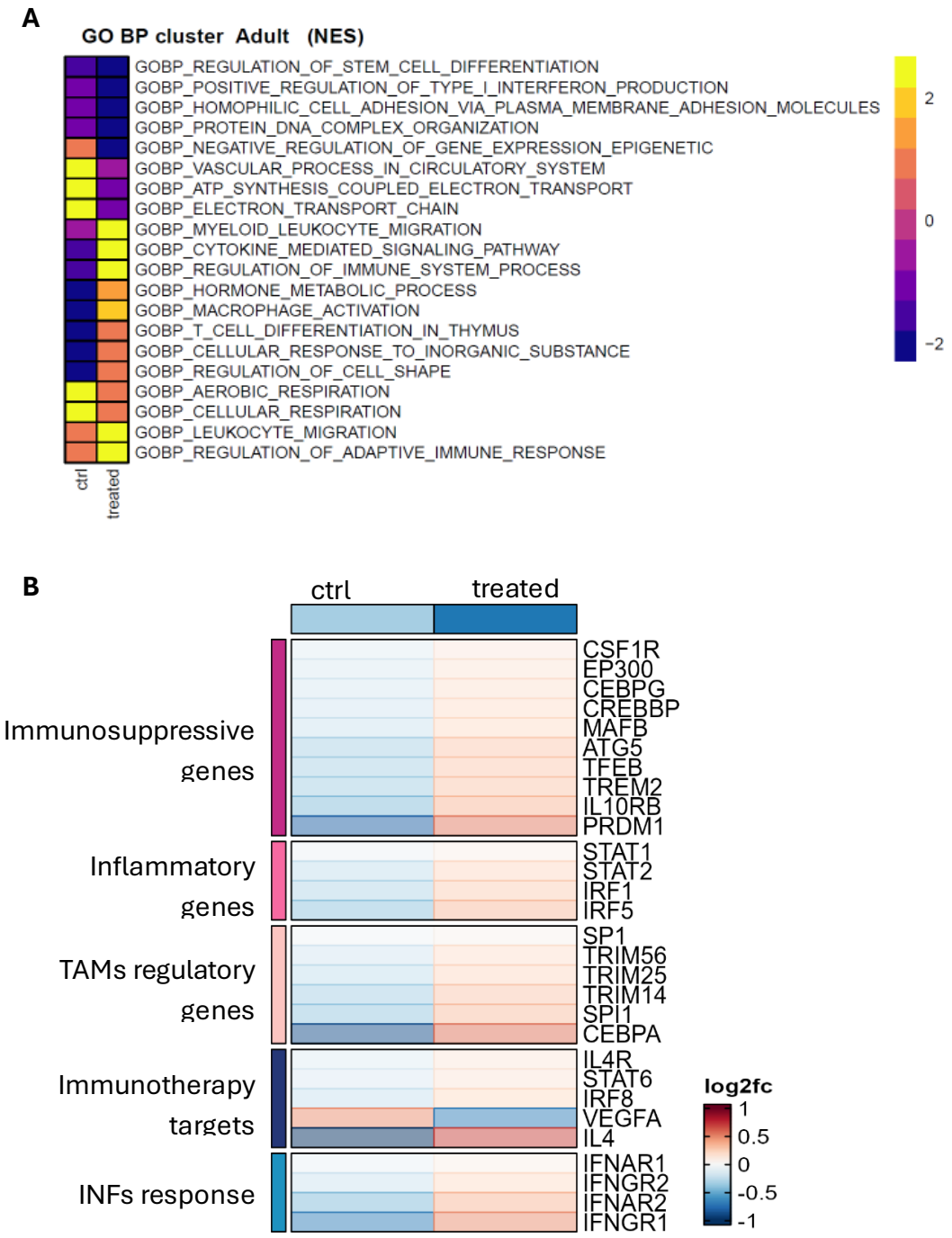

Figure 37. A) GSEA on Gene Ontology Biological Processes across the two conditions on aggregated data for each sample. The heatmap shows normalized enrichment score (NES), where positive values indicate enriched pathways. B) Heatmap showing the expression of genes associated with specific pathways in the two conditions. Expression shown by log2fc of normalized counts across all the genes and conditions. positive log2fc indicating higher expression while negative values indicate lower expression.

To explore potential heterogeneity in the response of M0 THP1 cells to EV treatment, we performed unsupervised clustering on the integrated single cell RNA sequencing data, which revealed 4 transcriptionally distinct cell clusters in both control and treated samples. Each cluster contributes equally to both the untreated and treated group (***Figure 38A, B***). Cell cycle analysis was carried out on all the clusters by calculating a score indicating the average expression of genes associated with the S and G2/M phase. The M1 cluster in both conditions is composed of both cells in the S and G2/M phase, indicating cycling cells. On the other hand, M2, M3 and M4 are negative for the G2M and S signatures, allocating them in the G1/G0 phase by exclusion (***Figure 38C***).

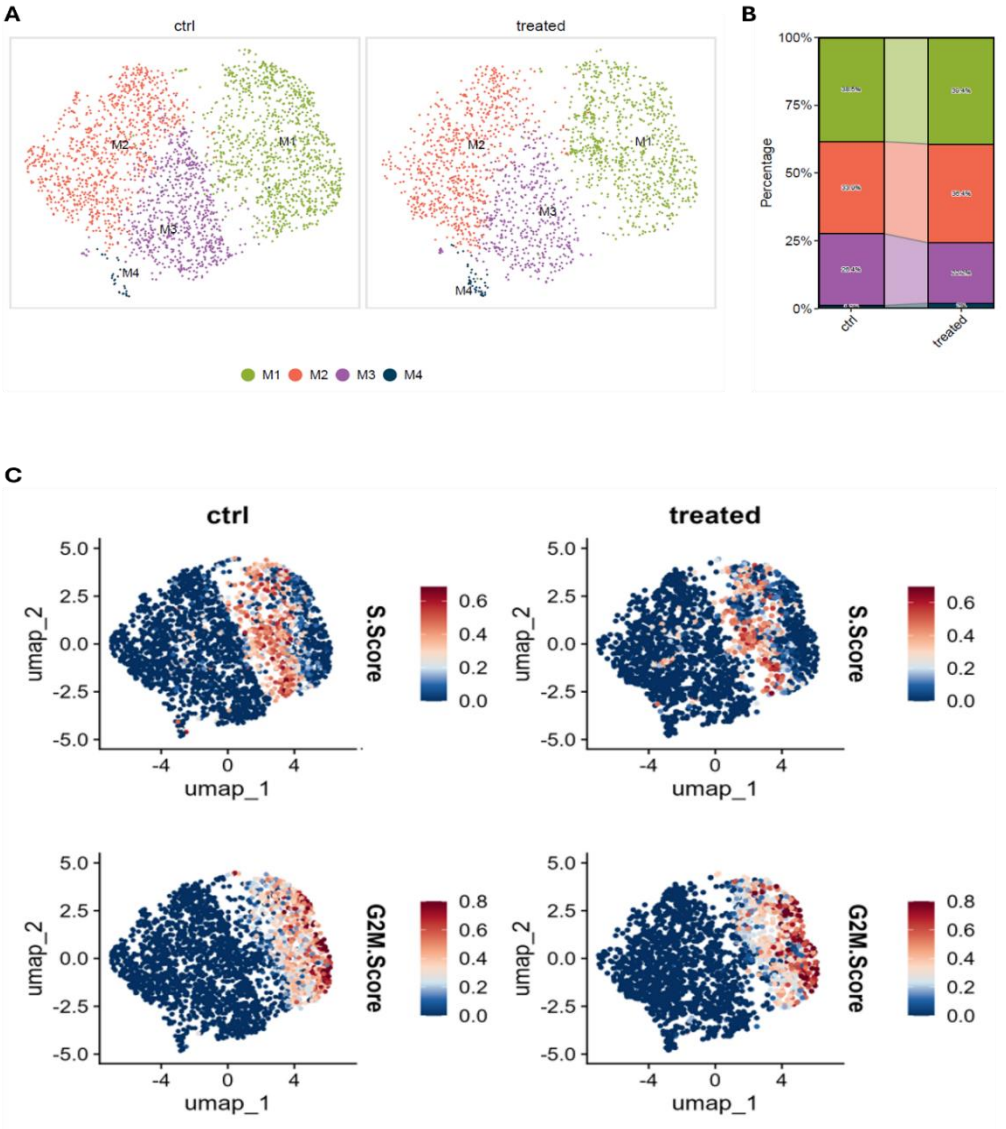

Figure 38. **A**) UMAP projection of 5.6k cells coming from the two conditions showing 4 transcriptionally different clusters. **B**) Barplot showing the cluster composition of the two conditions. **C**) Feature UMAP showing the S and G2M scores across all the cells and two conditions. Cells are colored according to the cell cycle score (red for high expression and blue for low expression). Regions in red represent cycling cells in the associated phase (S or G2M), while blue regions represent non dividing cells, either in the G0 or G1 phase. High score, in red, indicates the cell cycle state.

Aware that the definition of individual clusters appeared to be partially influenced by the cell cycle state of the cells, we sought to determine whether additional characteristics, particularly related to EVs uptake, might distinguish them. To address these differences, we carried out GSEA on the four identified clusters, focusing on pathways involved with the vesicle transport (***Fig. 39A***). This analysis showed a higher expression of pathways associated with vesicular trafficking in the M2 cluster in both the control and treated cells, with a remarkable overexpression in treated cells across most of the pathways examined, such as for example regulation of endosomal vesicles fusion, vesicles tethering, vesicles uncoating and vesicle transport. These findings suggest that cells within the M2 cluster are inherently predisposed to activate mechanisms related to vesicular trafficking, and this predisposition likely contributes to their enhanced activation upon extracellular vesicle uptake. The upregulation of these pathways also in the M1 cluster, which contains cells in the S/G2M phase, and in M2, together with low expression in the M3 cluster which, like M2 is mostly in the G1/G0 phase, suggest that, independently of the cell cycle stage of the cells, there is a subpopulation of macrophages, represented mainly by cluster M2, that is inherently predisposed to activate mechanisms related to vesicular trafficking and therefore is more responsive to vesicle uptake.

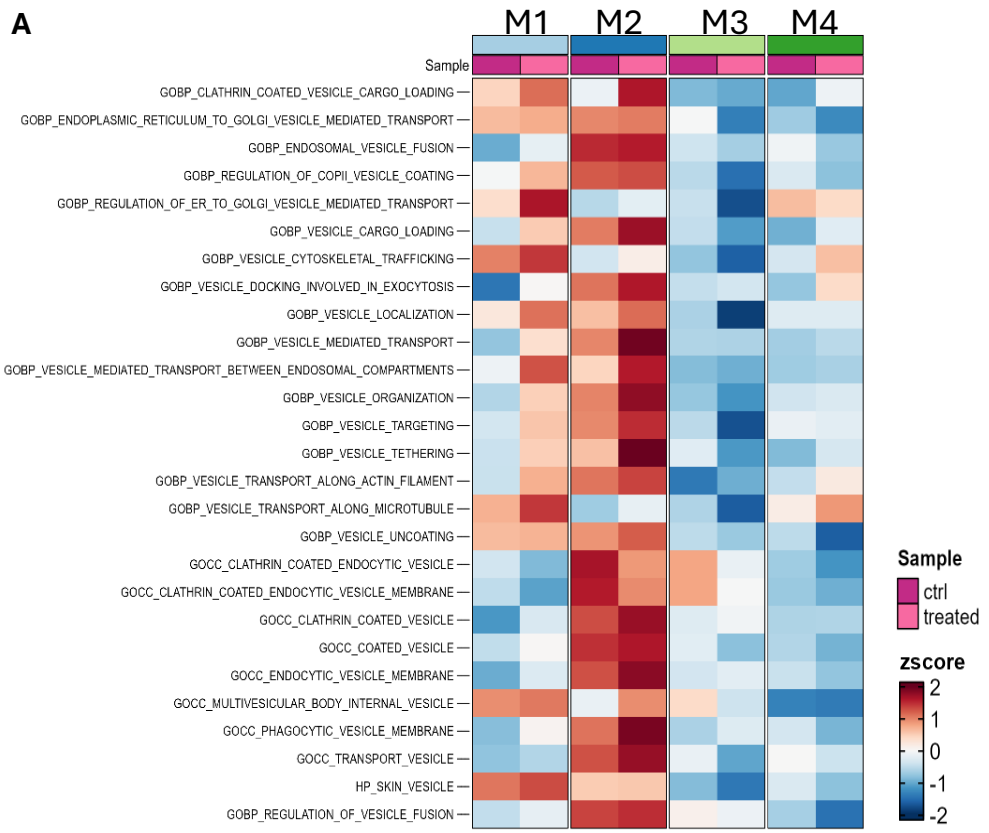

Figure 39. **A**) Heatmap showing the Z-score for Gene Ontologies involved with transport of vesicles. High z-score values indicate upregulation while low score downregulation.

We asked whether the difference in the EVs trafficking regulation between cluster M2 and M3, that is even more striking in treated cells, may reflect a difference in the activation of pathways related to immune activation and the TAMs-like state of treated macrophages. Focusing on treated cells, Gene Set Enrichment Analysis (GSEA) for the Hallmark pathways revealed pronounced differences between clusters M2 and M3, with cluster M2 exhibiting strong activation of inflammatory pathways, genes involved in the response to interferon-alpha and interferon-gamma, complement activation, to which TAMs are responsive to and can themselves initiate (186), and mTORC1 signalling, which has previously been reported to be activated in macrophages upon uptake of tumor-derived EVs (187) (***Figure 40A***). Moreover, gene set enrichment analysis of GO Biological Processes (GO BP) reveals a strong increase of the ribosomal compartment in M2 cluster of the treated cells compared to the M3, reflected by an enrichment of pathways involved in ribosome biogenesis and organization (***Figure 40B***), which has been previously reported to be associated with tumor associated macrophages in breast cancer (188). In conclusion, THP-1 macrophages seemed to respond heterogeneously to the treatment with A375M-derived EVs. Independently of the cell cycle phase, there is a subpopulation of THP-1 cells that showed a predisposition to upregulate pathways involved in EVs trafficking, and this predisposition correlates with a stronger shift towards a pro-tumorigenic profile, with the upregulation of specific metabolic pathways as well as the expression of inflammatory and interferon response genes.

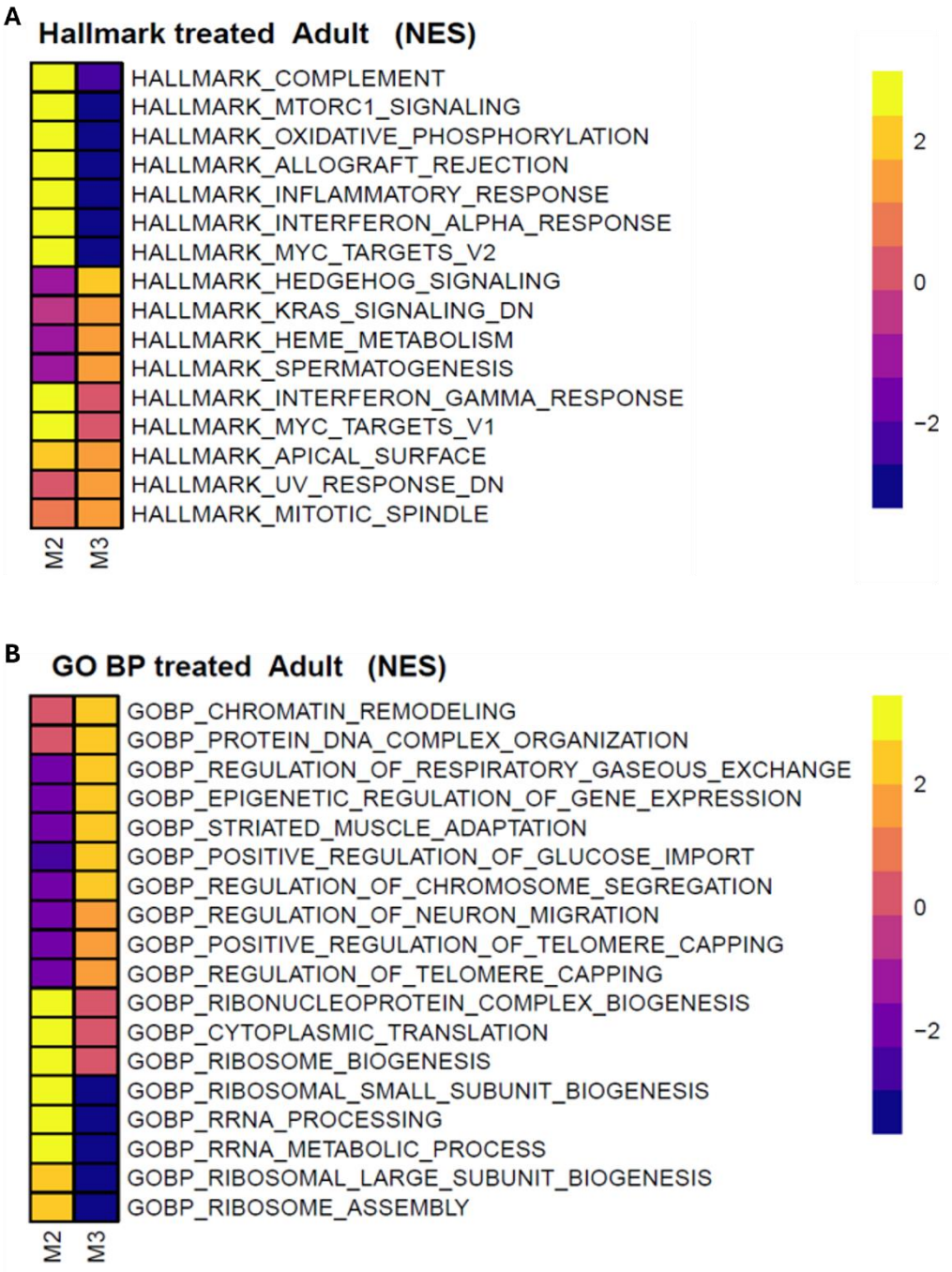

Figure 40. **A**) GSEA of Hallmark pathways comparing the clusters M2 and M3 in the EV treated sample, suggesting an inflammatory response in the M2 cluster. The heatmap shows normalized enrichment score (NES), where positive values indicate enriched pathways. **B**) GSEA on Gene Ontology Biological Processes comparing the clusters M2 and M3 in the EV treated sample, suggesting an activation of the ribosomal compartment in the M2 cluster. The heatmap shows normalized enrichment score (NES), where positive values indicate enriched pathways.

CHAPTER 4

Discussion and Future Perspectives

4. DISCUSSION AND FUTURE PERSPECTIVES

In this project, we investigated the role of melanoma-derived extracellular vesicles in eliciting a pro-tumorigenic response in innate immune cells within the tumor microenvironment. We show that EVs released by melanoma cells can activate the RIG-I-like receptor pathway in recipient macrophages, in both human and zebrafish models. EV uptake impacts macrophage cells fate by activating transcriptional programs that correlate with the cell identity of pro-tumorigenic Tumor Associated Macrophages (TAMs). Attention was given to the lncRNA *RPPH1* as a potential driver of this effect, since it represents an RNA cargo enriched in melanoma-derived EVs in the models we examined. Our analysis suggests that it can act as an RLRs ligand, owing to its secondary structure, and show that most of the responses triggered by EVs can be recapitulated by *RPPH1* itself. We also showed that *RPPH1* localisation is altered in melanoma cells, compared to normal melanocytes, with an accumulation in the cytoplasm of melanoma cells, increasing the likelihood of being packaged into EVs, and suggesting that, in melanoma, *RPPH1* may acquire novel functions, in addition to its well-characterized canonical roles.

4.1 *RPPH1* is overexpressed in melanoma and localizes to the cytoplasm of melanoma cells

In the first section (3.1) the objective of our investigation was to elucidate possible events that could enable the packaging of *RPPH1* in EVs in melanoma cells. Through the combined use of human melanoma cells and zebrafish melanoma models, we characterized *RPPH1* expression, localization, post transcriptional modifications and protein interactome to gain mechanistic insights into its regulation and potential functions.

We observed a marked overexpression of *RPPH1* in both human and zebrafish melanomas compared with non-malignant melanocytes. Overexpression of *RPPH1* has also been reported in several other cancer types, where elevated levels have been shown to correlate with cancer progression and poor prognosis (142). In hepatocellular carcinoma, *RPPH1* expression similarly influences the migratory and invasive capacities of malignant cells (28) and in colorectal cancer *RPPH1* is overexpressed and accumulates in tumor-derived EVs, through which it mediates polarization of macrophages in the TME (189). Although these findings demonstrate that *RPPH1* overexpression is a feature of many cancer cells, they do not elucidate the mechanisms leading to its overexpression, or whether this is associated to novel functions, or explain how *RPPH1* overexpression promotes its loading into extracellular vesicles (EVs). To further investigate *RPPH1* regulation in melanoma cells, we therefore examined other factors involved in its regulatory mechanisms.

Our results revealed a shift in *RPPH1* subcellular localization, with increased cytoplasmic accumulation in melanoma cells in comparison to normal melanocytes. This finding suggests a different post-transcriptional regulation for *RPPH1* in melanoma cells that influences its stability and localization opening the possibility of non-canonical roles for the lncRNA outside

the nucleus. In the context of ncRNA biology, cytoplasmic re-localization often reflects a functional adaptation, enabling participation in post-transcriptional regulation, mRNA stabilization, or association with ribonucleoprotein complexes involved in RNA transport or secretion (190). An example is *lincRNA-p21*, which is typically known for its role in transcriptional regulation within the nucleus but has been reported to accumulate in the cytoplasm of cervical cancer cells, where it functions as a post-transcriptional inhibitor of translation for specific mRNAs (191). Of note, recently, re-localization of *RPPH1* has already been reported in a non-physiological condition, such as in diabetic nephropathy (DN), where *RPPH1* showed an accumulation in the cytoplasm, where it interacts with the DN-related factor Gal-3, promoting inflammation and disease progression (192). In senescent fibroblast *RPPH1* accumulates in mitochondria, were it participate in the stabilization of different senescence-related mRNAs (6). Therefore, many non-canonical functions for *RPPH1* have been reported, yet they were not extensively studied beyond their influence on specific pathological contexts.

To understand the reasons for the re-localization of *RPPH1* in the cytoplasm of melanoma cells, we considered two of the most common RNA post-transcriptional modification that influence RNA stability and interactions, therefore also influencing its localization. Polyadenylation is a key post-transcriptional modification that adds a poly(A) tail to the 3' end of RNA transcripts, enhancing their stability, half-life, and translation efficiency, in the case of mRNAs (193). While most mRNAs undergo polyadenylation, certain noncoding RNAs, such as the lncRNA *RPPH1* transcribed by RNA polymerase III, lack this modification and are often used as markers of non-polyadenylated RNA (194). We showed that no significant difference between melanoma cells and healthy melanocytes in the state of polyadenylation of *RPPH1*, being the lncRNA prevalently not polyadenylated in both contexts. We also considered N6-methyladenosine (m6A), the most prevalent internal modification in eukaryotic RNAs, affecting stability, splicing, and nuclear export. m6A levels are dynamically regulated by specific writer, eraser, and reader enzymes, and dysregulation of this modification has been linked to cancer and other diseases (195). We predicted a very low probability for *RPPH1* to undergo m6A modification along its sequence. This was just an explorative investigation, based on computational prediction, that would need experimental validation. Of note, among the proteins that we retrieved in the proteomic analysis some have been reported to be involved in the recruitment of m6A regulators, such as SRSF7 (196). It is therefore possible that post-transcriptional modifications contribute to the delocalization of *RPPH1* in the cytoplasm, to its ability to bind new protein partners or gain new functions. Further studies are needed to clarify these events in more detail.

As *RPPH1* primarily functions as a catalytic RNA with intrinsic RNase activity, it may retain aspects of its canonical function in alternative locations and molecular contexts. *RPPH1* exhibits a well-characterized and specific ribonuclease activity within the RNase P complex, and substrate specificity is mainly dictated by the structural configuration of this complex, allowing recognition of specific tRNA-like structures within the catalytic pocket (151). It

appears unlikely, and not supported by current evidence, that its association with proteins other than those of the RNase P complex promotes the maintenance of its catalytically active structure. Rather, published studies on the non-canonical functions of *RPPH1* are mainly in support of the notion that *RPPH1* may function as an RNA scaffold, by recognizing target RNAs by sequence complementarity to recruit proteins involved in regulatory modifications (28). Though requiring further experimental validation, our proteomic analysis revealed an enrichment of proteins involved in mRNA regulation, both in the nucleus, with a great enrichment in proteins involved in the Spliceosome (**Section 3.4.1, Figure 7D**), and at a cytoplasmic level, such as SRSF7, SRSF3 and NCL which have been reported to be not only involved in the splicing of pre-mRNA, but also in their shuttling and stabilization of mRNAs in the cytoplasm (197) .

It remains to be determined whether *RPPH1* in melanoma is directly involved in the splicing of other RNAs, or whether its association with proteins implicated in this process reflects a mechanism through which *RPPH1* itself undergoes modifications that alter its function, a hypothesis that requires further experimental validation. To be noted the *RPPH1* sequence that we cloned for the experiments presented in this thesis, derives from RNA extracted from melanoma cells and showed a 100% match with the reference sequence deposited in public databases, at least within the region amplified by the primers employed in the cloning process. Although a small portion of the transcript was excluded in the amplicon, it nonetheless covers almost the entire length of *RPPH1.* Even if we cannot exclude the presence of shorter variants of RPPH1 non-detected in this study, it appears more plausible that the association of *RPPH1* with splicing-related proteins reflects its potential involvement in the regulation of other RNAs, rather than its own modification, in agreement with previous studies reporting such activity.

Our proteomic analysis revealed that some of the *RPPH1*-associated proteins are factors involved in ribosome biogenesis or functions, including EIF5B (198), TCOF1 (199) and of interest, NCL (200) cited above also between those proteins that can exert bot nuclear and cytosolic functions. Interestingly, our northern blot analysis, showed that some *RPPH1* molecules migrate at a position corresponding to the *18S* and *28S* rRNAs, suggesting a possible physical association with ribosomal or pre-ribosomal complexes. The functional enrichment of *RPPH1*-interacting proteins in pathways related to RNA metabolism and ribosome assembly therefore raises the possibility that *RPPH1* may transiently engage with ribosomal subunits. Such interactions could provide a mechanistic link between its cytoplasmic localization and vesicular packaging, as ribosome-associated RNAs and RNA-binding proteins are frequently enriched in extracellular vesicle cargo (201), as well as the *18S* RNAs that, even if to a lower extent than small RNA molecules, has been found in EVs in different contexts and also in melanoma-derived EVs (202). In previous works, all the proteins mentioned above, that we found to be *RPPH1* partners in melanoma cells have already been reported as cargo of melanoma-derived EVs in different models (203) (156) (155). Whether these proteins are also enriched in EVs derived from our melanoma models remains to be

validated through proteomic analyses of EV preparations. In addition, assessing their potential interaction with *RPPH1* in the EVs context would be a step forward to determine whether the inclusion of *RPPH1* in melanoma-derived EVs correlates with its association with one or more of these protein partners. At this stage of the investigation, elucidating these points could represent the most informative approach to advance our understanding of the mechanisms governing *RPPH1* loading into EVs in the context of melanoma cells.

It remains unclear whether the acquisition of novel functions by *RPPH1* in melanoma corresponds to a partial impairment of its canonical role within the RNase P complex. This aspect warrants further investigation. For instance, the impact on RNase P activity could be indirectly assessed by measuring global translation rates in melanoma cells or by sequencing and comparing the tRNA populations of melanoma cells and healthy melanocytes, to determine whether tRNA processing or abundance is altered. Such analyses could reveal whether dysregulation of RNase P function contributes to melanoma malignancy. Nonetheless, we can deduce that at least a basal level of RNase P activity is maintained, as this function is central in tRNA 5'-end processing and its absence would severely impact cell survival (204).

None of the known RNase P complex proteins were detected in our proteomic analysis. We propose that this absence results from the structural organization of the RNase P complex, in which the catalytic RNA component *RPPH1*, is highly folded and deeply embedded within the protein core. Crystallographic structure of human RNase P supports this interpretation, showing that the proteins subcomplexes that form the holoenzyme are organized in a hand-shaped structure that tightly wraps around the RNA moiety, occupying the space around it and leaving very low access to the RNA molecule. Moreover, even if very little is known to date about the process through which RNase P assembles around *RPPH1*, it has been reported in *Drosophila melanogaster* that the biogenesis of RNase P associated RNA (in Drosophila *RPR*) involves the association of a subset of the proteins of the complex (Rpps) to the nascent transcript. This association is fundamental for RPR maturation and to avoid its degradation (205). In Drosophila *RPR* biogenesis probably depends more critically on Rpps, as the RNA is released from an intron of a host gene and would otherwise be rapidly degraded by exonucleases in the absence of protective interactions with RNase P proteins. Nevertheless, although direct evidence for protection from exonucleolytic degradation in human *RPPH1* biogenesis is currently lacking, *in vitro* analyses have demonstrated that Rpp20–Rpp25 heterodimer, Pop5, Rpp21 and Rpp29 associate directly with *RPPH1* (206), probably at early stages of assembly, being also associated with chromatin (207) (208), shielding specific structural regions from nuclease cleavage. These findings support a model in which early association of Rpps with the nascent *RPPH1* transcript promotes correct folding and stabilization, thereby preventing premature degradation and facilitating incorporation into the mature holoenzyme. Consequently, it is unlikely that our RNA-targeting probes were able to efficiently access or capture the RNA molecules engaged in RNase P assembly.

4.2 Melanoma-derived EVs trigger the activation of RLRs in recipient macrophages

In our previous work (33), we demonstrated that melanoma-derived EVs, are enriched in the lncRNA *RPPH1* both in human and zebrafish models. These EVs when injected into the blood stream of healthy zebrafish larvae elicit an innate immune response characterized by the upregulation of some candidates interferon-stimulated genes (ISGs) and pro-inflammatory cytokines, as well as a marked recruitment of macrophages to the caudal hematopoietic tissue (CHT), where their numbers nearly doubled compared to PBS-injected controls (33). This type of response suggested the activation of Pattern Recognition Receptors (PPRs) in macrophages.

In section 3.2.1 we predicted that *RPPH1* predominantly adopts a double-stranded secondary structure, potentially serving as a ligand for a restricted subset of PRRs. We exploited zebrafish models, to investigate the involvement of candidate pathways, considering *RPPH1* as possible trigger of the response that we observed. We found that the RIG-I Like Receptors (RLRs) pathway plays a clear and essential role in mediating the response to melanoma-derived EVs. Specifically, knockout of its key downstream adaptor MAVS abolished both the induction of inflammatory genes and the recruitment of macrophages.

Our analysis revealed ambiguous effects of the pharmacological inhibition of the Toll Like Receptor 3 (TLR3) on IRG gene expression following melanoma-derived EV treatment. While *isg15* and *il1β* were upregulated, *ifit10* showed reduced induction in TLR3-inhibited larvae. This inconsistency may derive from the complexity of the zebrafish TLR system, particularly the presence of TLR22, which also recognizes double-stranded RNA. Unlike mammals, zebrafish possess multiple dsRNA-sensing TLRs, including TLR3 and TLR22 (165). This broader receptor repertoire enables zebrafish to detect dsRNA through partially overlapping pathways, that can result in compensatory or synergistic responses upon inhibition of a single receptor. As TLR22 signalling is not conserved in humans and its transcriptional outcomes remain undefined, compensatory activation of alternative TLRs may have contributed to the divergent gene expression patterns observed upon TLR3 inhibition.

In contrast, humans rely primarily on TLR3 and cytosolic RNA sensors such as MDA5 and RIG-I for dsRNA detection. The absence of TLR22 in mammals may limit redundancy within the TLR-mediated dsRNA recognition system, leading to a more defined and compartmentalized antiviral response. Consequently, the transcriptional effects of TLR3 inhibition observed in zebrafish may not be directly replicable in humans. For this reason, we did not explore this discrepancy further and did not investigate the TLR3 pharmaceutical inhibition in human cells, as our primary aim was to translate these findings into a human-relevant context and given the more clear and specific result that we observed for RLRs inhibition through *mavs* KO.

It is important to note that we employed two distinct approaches to inhibit the target pathways, and technical differences between these methods may have contributed to the

observed discrepancies in the results. The TLR3 inhibitor used in this study acts as a receptor antagonist, occupying the ligand-binding pocket and thereby preventing interaction with its natural ligands. This mechanism could lead to the accumulation of unbound TLR3 ligands, originating from both external stimuli and endogenous sources, which may in turn account for the ambiguous response observed (Section 3.2.2). On the other hand, inhibition of the RLR pathway was achieved through knockout of *mavs*, which functions downstream of the receptors RIG-I and MDA5. This strategy allows ligand recognition and binding to occur normally while specifically blocking the propagation of the signal to downstream effectors. Consequently, this approach minimizes the potential accumulation of ligand molecules and reduces the risk of off-target effects.

Nonetheless, even if we cannot exclude an involvement of TLR3 in the response to molecular stimuli coming from melanoma-derived EVs, the results obtained through *mavs* KO clearly highlighted the involvement of RLRs pathway in the effects that we were observing, not only in terms of transcriptional activation of inflammatory genes, but also in respect to the recruitment of macrophages.

It has been observed that the RLRs pathway can be activated in cancer cells by endogenous molecules released as a result of cellular damage induced by radiotherapy or chemotherapy (209). Such activation exerts an anti-tumor effect by promoting a pro-inflammatory response that enhances immune-mediated tumor clearance, thereby contributing to the overall therapeutic efficacy. For instance, activation of RLRs in pancreatic cancer cells has been shown to induce immunogenic cell death and increase their susceptibility to $CD8^+$ T cell–mediated cytotoxicity (210). Considering that, the RLR pathway has gained considerable interest as a therapeutic target, both for the development of adjuvant agents that can potentiate existing treatments and as a promising avenue for immunotherapeutic intervention (211). In this direction most studies have focused primarily on the cell-autonomous effects of RLRs activation within cancer cells themselves, on how RLR signalling influences the fate of tumor cells directly. However, the growing interest in the tumor microenvironment (TME) and in the mechanisms regulating tumor progression and therapeutic efficacy beyond cancer cells has raised important questions regarding the consequences of RLRs activation in non-malignant cells within the surrounding microenvironment.

Persistent activation of the RLRs pathway can sustain type I interferon and NF-κB signalling, leading to a state of chronic inflammation that favours the establishment of a tumor-promoting microenvironment. One of the downstream effects of RLRs, is the activation of NF-kB signalling. Chronic NF-κB signalling sustains unresolved inflammation that leads to tumor progression, supporting immune suppression, angiogenesis, and fibrosis within the tumor microenvironment (212). Several studies indicate that RLRs-linked chronic type I interferons (INF)/ NF-κB signalling in non-malignant stromal or immune cells can foster tumor progression and metastasis. For example, cancer-activated astrocytes generate a sustained, low-level type

I IFN microenvironment that promotes brain metastasis by recruiting monocytic myeloid cells (213). Thus, RLRs activation represents a double-edged sword in cancer biology, capable of eliciting potent anti-tumor immunity yet, under chronic or dysregulated conditions, fostering a pro-tumorigenic microenvironment, and therefore underscores the need for careful investigation in the context of tumor-derived signals shaping the tumor microenvironment, such as extracellular vesicles. Given all the above, the involvement of RLRs in the response to melanoma-derived EVs that we observed in zebrafish highlighted an interesting point for our investigation.

In Section 3.2.3, we showed that in *mavs* KO *mpeg:GFP* larvae, injection of either melanoma-derived EVs or the synthetic *RPPH1* molecule did not induce macrophage recruitment. Interestingly, upon *mavs* KO we observed a decrease in the number of macrophages in the CHT of zebrafish larvae, regardless of any treatment or external stimuli (section 3.2.2.1).

MAVS is a key adaptor molecule downstream of RLRs, essential for initiating type I interferon and pro-inflammatory responses following the activation of RIG-I-like receptors by viral or endogenous RNAs. In cells of the innate immune system, MAVS plays a central role in coordinating antiviral defence, cytokine production, and inflammatory signalling (214). In macrophages, MAVS depletion disrupts RLR-mediated signalling, leading to impaired activation of NF-κB and IRF3/7, and consequently reduced secretion of interferons and pro-inflammatory cytokines (215). MAVS-deficient macrophages display altered functional polarization and metabolic activity, often exhibiting a diminished ability to mount effective immune responses, but there are no evidence linking MAVS loss to alteration of physiological cellular processes in macrophages, such as proliferation. In infection models, MAVS deficiency has been associated with defective macrophage recruitment and impaired inflammatory responses, underscoring its importance in maintaining macrophage activation and antiviral competence within the innate immune network (216). Overall, MAVS deficiency is expected to specifically impair the ability of macrophages to respond to stimuli that engage MAVS-dependent inflammatory signalling, but not the ability of macrophages to proliferate and circulate. Nevertheless, RLRs signalling has been demonstrated to be crucial for the formation of hematopoietic stem and progenitor cells (HSPCs) during development. In zebrafish, loss of *rig-I* or *mda5* impairs HSPC formation, with endogenous repetitive element–derived RNAs activating the RLRs–MAVS pathway to regulate inflammatory signalling required for HSPC specification, highlighting a developmental role for this pathway (217). Therefore, the observed reduction in CHT macrophage numbers in *mavs* knockout *mpeg:GFP* larvae may be a consequence of impaired development of the hematopoietic lineage in crispant larvae as well as may reflect a basal defect in responding to endogenous signals that are physiologically active in the larvae under normal conditions.

The tumor microenvironment constitutes a highly dynamic and complex ecosystem in which immune cells play a central role in modulating tumor behaviour and progression. Among these, macrophages represent the most abundant immune cell population and, through their

crosstalk with tumor cells, they actively participate in cancer initiation and progression. Increasing evidence indicates that tumor-derived EVs critically influence macrophage functional states by delivering diverse molecular cargos, thereby contributing to the establishment of a tumor-promoting microenvironment. In Section 3.3, we transitioned to human models, focusing on macrophages as target cells for melanoma-derived extracellular vesicles. We demonstrated that EVs released from the A375M melanoma cell line, previously shown to be enriched in *RPPH1*, as well as in vitro–synthesized *RPPH1*, induce the expression of interferon-stimulated genes and pro-inflammatory cytokines in human macrophages through the activation of the RLRs pathway. This highlights macrophages as key target cells for molecular signals released by melanoma cells through EVs within the surrounding microenvironment.

We employed in vitro–synthesized *RPPH1* in both zebrafish models and human cell lines to investigate whether the effects observed in response to melanoma-derived EVs could be specifically attributed to this molecule, previously identified as enriched in melanoma-derived EVs. To assess the specificity of *RPPH1*-mediated effects, we performed control experiments using a generic mRNA, as described in Section 3.3.4. These experiments revealed that synthetic RNA transfection alone can induce a baseline immune response in macrophages, but that activation of the RLRs pathway is more specifically triggered by *RPPH1.*

With regard to *in vivo* experiments (section 3.2.4), it should be noted that introducing in zebrafish larvae synthetic RNA can inherently trigger the immune sensing pathways due to its possible immunogenic effects, as it lacks the post-transcriptional modifications that normally prevent self-recognition by the immune system, regardless of its specific sequence. In this study, we generated the *RPPH1* transcripts through *in vitro* transcription; however, the precise structural conformation of the RNA remains unknown. Although we can speculate that synthetic *RPPH1* RNA assumes the predicted folding described in Section 3.2.1, this has not been experimentally confirmed. Additionally, it is uncertain whether the synthetic transcript accurately replicates the endogenous *RPPH1* delivery to recipient cells via extracellular vesicles (EVs), leaving open the possibility that the observed responses may not fully represent the physiological situation. In fact, to date we do not know how the *RPPH1* molecules are transferred to melanoma-derived EVs and if associated with other molecules, such as protein partners or other RNAs, that can influence the lncRNA stability and conformation in the context of EVs, as well as post-transcriptional modification.

In section 3.1.4 we identified several proteins that are *RPPH1* interactors in melanoma cells, the majority of which are reported to be also cargo of melanoma-derived EVs in many models. We can hypothesize that among these protein interactors there may be factors involved in escorting *RPPH1* during its incorporation into EVs, as discussed in Section 4.1. With respect to the conformational state of *RPPH1* within EVs, and consequently the form in which it is delivered to recipient cells, its association with specific protein partners may play a role in stabilizing the RNA molecule and shaping its structural conformation. As previously noted,

experimental evidence identifying *RPPH1*-interacting proteins in the context of melanoma-derived EVs is currently lacking. Nevertheless, RNA molecules are inherently unstable, and cells have evolved multiple mechanisms to enhance RNA stability and enable functional persistence while preventing rapid degradation. These mechanisms include post-transcriptional modifications as well as interactions with RNA-binding proteins. (218). For these reasons, it is unlikely that *RPPH1* can be efficiently incorporated into EVs or exert a role in cell–cell communication in the absence of protective factors. Accordingly, when interpreting the results obtained from the injection of in vitro–synthesized *RPPH1* into zebrafish larvae, as well as from its transfection into THP-1 cells, it is important to acknowledge that the synthetic RNA lacks both interacting partners and potential post-transcriptional modifications. The absence of these features may influence the observed biological effects, which may therefore not precisely recapitulate the signalling mechanisms mediated by EV uptake in recipient cells.

Moreover, we know that *RPPH1* transcript is enriched in melanoma-derived EVs, compared to the melanoma cells that generate them (33), nonetheless we do not know how many molecules of transcript transported by EVs are involved in the signalling to macrophages. Treatments with synthetic RNA molecules were performed *in vivo* following our previously published approach (33), resulting in the administration of higher RNA doses compared with the amount of RNA retrieved in EVs. For experiments conducted in human cells, transfection efficiency and the biological responses obtained with the positive control poly(I:C) were used as reference, as described in Section 3.3.1, to ensure that a functionally relevant amount of RNA reached its intracellular targets. Consequently, our analysis does not fully recapitulate the mechanism through which *RPPH1* is delivered to cells through EVs-mediated transport. In conclusion, even if this approach represents a valid proof of concept to validate whether our candidate RNA is capable of activating the molecular pathway under investigation, it does not comprehensively reflect the physiological mode of *RPPH1* signalling, highlighting the need for further investigation.

As a future perspective, an important next step in dissecting the communication mechanisms between tumor cells and macrophages would be to demonstrate a direct interaction between *RPPH1* and the RLR sensors RIG-I and/or MDA5. This could be achieved through *in vitro* binding assays designed to determine whether *RPPH1* can function as a bona fide ligand of RLRs and imaging-based analyses in macrophages exposed to melanoma-derived EVs.

4.3 Melanoma-derived EVs activate a TAMs-like signature in recipient macrophages

Emerging evidence indicates that tumor-derived extracellular vesicles play a crucial role in shaping macrophage phenotypes by transferring diverse molecular cargos that promote tumor progression. Depending on microenvironmental cues, macrophages can acquire distinct functional states and EVs-related lncRNAs have recently emerged as key regulators of macrophage polarization. For example, lncRNA *TUC339*, enriched in hepatocellular carcinoma–derived EVs, drives macrophages toward an M2-like phenotype (219), an effect that in colorectal cancer (CRC) has been reported to be driven by CRC–derived EVs carrying *RPPH1* (31). Macrophages are commonly classified into two main polarization states: M1, with pro-inflammatory and anti-tumor properties, and M2, with immunosuppressive and tumor-promoting functions. However, research advances have revealed that macrophage polarization exists along a spectrum of intermediate activation states, rather than as strictly defined M1 or M2 phenotypes (220). Within the TME, these cells are more broadly referred to as tumor-associated macrophages (TAMs). TAMs represent a major immune cell population within the TME, where they play diverse roles in promoting tumor progression, acquiring immunosuppressive and tumor-supportive phenotypes, fostering T-cell tolerance and enhancing tumor growth and survival (221).

In section 3.4 we showed that the uptake of melanoma-derived EVs by THP-1 macrophages results in a transcriptional reprogramming toward a glycolytic metabolic profile and TAM-associated gene expression signatures, suggesting that A375M-derived EVs may drive the acquisition of TAM-like features, thereby potentially contributing to the establishment of a tumor-supportive microenvironment.

The impact of melanoma-derived EVs on macrophage cell fate can be studied by single cell transcriptome analysis. We found that M0 THP-1 cells respond heterogeneously to melanoma-derived EVs. Although cell lines are often considered homogeneous, they can display intrinsic heterogeneity. Individual cells within the same population may differ in cell-cycle phase, metabolic state influencing their responsiveness to external stimuli and resulting in transcriptional and functional heterogeneity (222). Accounting for this variability can provide deeper insights into the underlying mechanisms sustaining heterogeneity and can inform us on the processes that take place in vivo. We found that, independently of the cell cycle phase of M0 THP-1 cells, there is a subpopulation of macrophages that upregulate pathways involved in EVs trafficking, and this correlates with a stronger shift towards a pro-tumorigenic profile, with the upregulation of specific metabolic pathways as well as the expression of inflammatory and interferon response genes. The observation that the most pronounced immune responses occur, upon treatment with EVs, within the cluster where vesicle-associated pathways are active, suggest that the transcriptional activation that we observe is driven by melanoma-derived EVs and that macrophages which are able to quicky upregulate endocytic pathways may be more responsive to EVs signalling and may undergo

transformation in TAMs. Given that this ability is not dependent on the cell cycle (section 3.4), it would be of great interest to further investigate differences that characterize each of the identified clusters to define what may determine this heterogeneity and investigate how it may reflect events happening *in vivo* and provide further insights into the mechanisms underlying the pro-tumorigenic education of immune cells by tumor cell signalling.

Signalling from tumor cells to immune cells through EVs often promotes metastasis formation through multiple mechanisms. One mechanism involves the modulation of the TME, where EV-mediated communication influences TAMs to promote metastasis by inducing epithelial–mesenchymal transition (EMT), supporting tumor cell intravasation and migration in distant sites. However, EVs are released also into biofluids such as blood, enabling them to reach distant sites. At these locations, tumor-derived EVs can interact with immune cells, contributing to the establishment of an inflammatory microenvironment that supports the formation of a pre-metastatic niche (223). Collectively, these activities position TAMs as central orchestrators of tumor progression, immune suppression, and therapy resistance. As a further future perspective for this part of the project, it would be interesting to investigate *in vivo* how melanoma-derived extracellular vesicles (EVs) influence metastasis formation, and whether the activation of the RLR pathway in recipient cells is involved in this process. The model established in this thesis, based on EV injection into the bloodstream of *mavs* KO larvae, could be employed to perform in vivo metastasis assays aimed at exploring this aspect. Gaining a deeper understanding of the mechanisms through which tumor cells modulate the tumor microenvironment and promote metastasis in melanoma via extracellular vesicles and their RNA cargo will provide valuable insights into the cell-to-cell communication pathways and the specific molecular players involved. Such knowledge could be strategically exploited to develop novel therapeutic approaches.

To conclude, in this PhD work we demonstrated that the long non-coding RNA *RPPH1* is overexpressed and predominantly localized in the cytoplasm of melanoma cells compared to non-malignant melanocytes. This observation, together with the proteomic analysis of *RPPH1*-interacting partners, suggests the acquisition of novel, non-canonical functions for *RPPH1* within melanoma cells, which may, in turn, contribute to its accumulation in EVs.

We demonstrated that melanoma-derived extracellular vesicles, likely through their *RPPH1* cargo, are capable of activating the RIG-I-like receptor pathway in recipient macrophages, thereby inducing an inflammatory response characterized by the upregulation of interferon-stimulated genes (ISGs) and pro-inflammatory cytokines. The uptake of melanoma-derived EVs by macrophages leads to a transcriptional reprogramming consistent with the polarization of these immune cells toward a tumor-supportive phenotype.

CHAPTER 5

Materials and Methods

5. MATERIALS AND METHODS

Zebrafish lines and Maintenance

Adult zebrafish (*Danio rerio*) were housed at the Department of Cellular, Computational and Integrative Biology (CIBIO), University of Trento, and maintained in the Model Organism Facility under standard laboratory conditions (224). All zebrafish experimental procedures adhered to the European law on Animal Protection and were authorized under permit no. 425/2024-PR by the Italian Ministry of Health issued to M.C. Mione. The following transgenic zebrafish lines were used in this study:

- *Et(kita:Gal4TA4, UAS:mCherry)^{hzm1}*; *p53-/-*, referred to as *kita:Gal4* (137)
- *Tg(UAS:egfp-HRAS^V12G)^{io006}*; *p53-/-,* referred to as *UAS:RAS* (137),
- *Tg(mpeg1:GFP)^{gl22Tg},* referred to as *mpeg:GFP* (225).
- *Et(kita:GalTA4,UAS:mCherry)hzm1xtg(UAS:eGFP-H-RASV12)io6; p53-/-,* referred to as *Kita-GFP-RAS;p53-/-* (137).

Cell lines, culture and treatments

A375M cells were cultured in DMEM medium (high glucose) supplemented with 10% FBS, 2 mM L-glutamine, and 2 mM of penicillin/streptomycin. NHEM cells were cultured in DMEM-F12 supplemented with 10% FBS, 2 mM L-glutamine, and 2 mM of penicillin/streptomycin.SK-MEL-5 and THP-1 cells were cultured in suspension in RPMI supplemented with 10% FBS, 2 mM L-glutamine, and 2 mM of penicillin/streptomycin. Cells were maintained at 37 °C in a humified atmosphere containing 5% CO2.

THP-1 cells were differentiated into M0 macrophages by adding to their complete medium 10 ng/ml Phorbol 12-Myristate 13-Acetate (PMA) [MedChemExpress] for 24h. Upon treatment cells attach to culture plate and after 24 h medium was changed with complete medium without PMA and other treatments were performed as follows:

EVs treatments were performed on M0 THP-1 cells by adding EVs isolated from A375M cells as in *EVs isolation from cell culture media* below, to the complete medium of THP-1 cells. EVs were added in order to treat with 5000-10000 EVs/cell. Poly(I:C) HMW [Invivogen] and in vitro transcribed RNAs were transfected in cells at a concentration of 1 ug/ul using Lipofectamine 3000 [Invitrogen] according to manufacturer instruction.

EVs isolation from zebrafish melanoma

Zebrafish melanomas were dissected and cut in small fragments. Fragments were incubated in Collagenase 2 mg/ml and Dnase I 10U/ml in RPMI without phenol red, for 30 minutes at room temperature in gentle rotation on a tube rotator [VWR]. Samples were filtered using a 40 ul cell strainer and tissue and cells debris were removed through sequential centrifugation:

300xg for 10 minutes, followed by 2000xg for 20 minutes. EVs were then captured from the resulting supernatant through nickel-based isolation (NBI) as described in (33) and resuspended in 1x sterile PBS.

EVs isolation from cell culture media

When cells at 80% confluency were washes twice with PBS and a medium made of DMEM, L-Glutamine and Pen/Strep was added to cells. After 24h, the medium was collected and subjected to differential centrifugation to obtain small EVs. First supernatant is first centrifuged at 300 *x g* for 10 minutes at 4°C. Supernatant is collected and centrifuged again at 2000xg for 10 minutes at 4°C. The resulting supernatant is collected and centrifuged at 10 000xg for 30 minutes at 4°C. Finally, to isolate small EVs the remaining supernatant was centrifuged at 100 000xg for 70 minutes at 4°C and EVs pellet was resuspended in 1x sterile PBS. EVs were quantified using NanoSight NS300 [Malvern Panalytical].

Nanoparticle Tracking Analysis (NTA)

EVs size distribution and particle concentration were assessed using a NanoSight NS300 system (Malvern Panalytical) in accordance with the manufacturer's guidelines. Pellets obtained by differential centrifugation were resuspended in PBS and diluted to a final volume of 1 mL prior to analysis. For each sample dilution, a minimum of four 60-second videos was acquired and subsequently analysed using NanoSight NS300 NTA software version 3.4 (Build 3.4.003; Malvern Panalytical).

RNA extraction from zebrafish larvae and cultured cells

Each zebrafish larvae sample was collected as pools of larvae (10-15) in a 1.5 ml tube and resuspended in 0.5 ml TripleXtractor reagent for RNA isolation [GRiSP]. Samples were mechanically disaggregated in TripleXtractor using a homogenizer. Cultured cells were washed with 1x PBS and detached through incubation in Trypsin-EDTA [Gibco] for 5 min, centrifuged 200x g, 5 min (RT). Cell pellets were washed in 0.5 ml 1x PBS, centrifuged 200x g, 5 min (RT) resuspended in 0.5 ul TripleXtractor. After 5 min of incubation at RT, 100 uL of chloroform were added, the tubes were vortexed and incubated 15 min at room temperature, to be centrifuged for 15 min at 4 C, 12000 *xg*. 250 uL of 100% isopropanol were added to the supernatant, samples were vortexed, incubated 10 min at room temperature and centrifuged for 10 min at 4 C, 12000 *xg*. Pellets were washed with 500 uL of 70% v/v ethanol by centrifugations of 5 min at 4 C, 7500 *xg* before resuspension in the appropriate volume of nuclease-free H2O. RNA concentration was assessed with the NanoDrop Lite spectrophotometer [Thermo Scientific]

Rpph1 levels of expression in zebrafish and human cells though qPCR

Melanoma samples were collected from adult *kita:RAS* zebrafish, with each tumor representing one biological replicate. Healthy tissue samples were dissected from the trunk

region of adult *UAS:RAS* zebrafish, with one fish considered as one biological replicate. Immediately after dissection, tissues were resuspended in 500 µL of TripleXtractor reagent [GRiSP] for RNA isolation and mechanically homogenized using a tissue homogenizer. Human cell lines NHEM, A375M, and SK-MEL-5 were cultured as previously described (*Cell lines and culture*). For RNA extraction, each biological replicate (corresponding to one 10 cm culture plate at 80% confluency) was washed with 1X PBS and lysed with 500 µL of TripleXtractor reagent [GRiSP]. RNA was purified described above (*RNA extraction from zebrafish larvae and cultured cells*).

RNA was reverse-transcribed using ReverTra Ace™ qPCR RT Master Mix with gDNA Remover [Toyobo] according to manufacturer's instructions. RT reaction was used for the qPCR experiments which were performed in triplicates using qPCRBIO SyGreen® Mix [PCR Biosystem] in a CFX96 Thermo Cycler [Bio-Rad]. The results were analysed with Bio-Rad CFX Manager, version 2.1. The relative expression was calculated according to the $2^{-\Delta\Delta Ct}$ method normalized on b-actin mRNA for human samples and RSP11 for zebrafish samples. Primers used are reported in **Table 5.1**. Statistical analysis was performed with GraphPad Prism 8, performing Normality test and non-parametric t-test (no Gaussian distribution).

Table 5.1

Primer	**Sequence**
hsa_RPPH1 FW	TATCCCGCCTCCCTTCGA
hsa_RPPH1 RV	AATGGGCGGAGGAGAGTAGT
hsa_Actin FW	ACCCATTGGCAATGAGCGGTTC
hsa_Actin RV	AGGTCTTTGCGGATGTCCACGT
zf_rpph1 FW	AGCGGAAGGAAGCTCACTG
zf_rpph1 RV	GGGAGAGTAGTCTGAATTGG
zf_rps11_FW	ACAGAAATGCCCCTTCACTG
Zf_rps11 RV	GCCTCTTCTCAAAACGGTTG

Northern Blot

Total RNA was isolated as in *RNA extraction from zebrafish larvae and cultured cells*. For each sample, 1 µg of RNA was diluted in NorthernMax™-Gly Sample Loading Dye [Invitrogen] according to manifacturer's instruction, incubated for 30 min at 50 °C and resolved on a denaturing MOPS agarose gel (1% agarose [Sigma-Aldrich], 50 mM MOPS [Fisher BioReagents], 5 mM Sodium Acetate, 1mM EDTA in H_2O).

Electrophoresis was carried out for 2,5 h at 85 V, after which the RNA was transferred overnight at room temperature (RT) onto a Cytiva Membrane Amersham™ Hybond™ -N+ [Fisher Scientific] by capillary transfer, using membranes pre-equilibrated in H_2O and 20× SSC. The next day, membranes were UV crosslinked for 3 min at 1500 mJ/cm² using a UVP CL-

1000L Longwave Crosslinker [Fisher Scientific]. Membranes were then pre-hybridized in hybridization buffer (5× SSC, 0.1% Sarkosyl, 0.04% SDS) for 1 h at 42 °C in a UVP HB1000 Hybridizer oven [Fisher Scientific], followed by overnight hybridization in the same buffer containing 10 nM BIOTEG-labeled *RPPH1* probe (**Table 5.2**)

Following hybridization, membranes were washed twice in 2× SSC/0.1% SDS for 10 min at 42°, twice in 0.5× SSC/0.1% SDS for 10 min at 42°, and twice in 0.2× SSC/0.1% SDS at 42° °C for 15 min, followed by a brief rinse in 2× SSC at RT. Membranes were then blocked for 15 min at RT in Blocking Buffer (Part of Chemiluminescent Nucleic Acid Detection Module Kit [Thermo Scientific]), and subsequently incubated for 15 min at RT in the same solution supplemented with Streptavidine-HRP (Part of Chemiluminescent Nucleic Acid Detection Module Kit [Thermo Scientific]). After five washes of 15 min each in Wash Buffer (Part of Chemiluminescent Nucleic Acid Detection Module Kit [Thermo Scientific]), membranes were equilibrated for 2 min at RT in Substrate Equilibration Buffer (part of Chemiluminescent Nucleic Acid Detection Module Kit [Thermo Scientific]). Detection was performed using CDP-Star Chemiluminescence Substrate [Roche] according to the manufacturer's instructions, and signals were visualized with the ChemiDoc XRS$^+$ system [Bio-Rad].

Table 5.2

Probe	**Sequence**
RPPH1 probe	[BIOTEG] AGGACGCACTCAGCTCGTGGCC

Isolation of poly(A)+ and poly(A)- RNA fractions

Total RNA was purified from A375M and NHEM cells as described in *RNA extraction from zebrafish larvae and cultured cells*, treated with DNase I. RNA samples were processed by Poly(A) RNA Selection Kit (Lexogen) following manufacturer's protocol. Briefly, Poly(A)+ RNA fraction was obtained by eluting the RNA bound to the oligo-dT resin. Poly(A)- RNA fraction was isolated by precipitating the RNA from washes using 1 volume of isopropanol O/N at -80C in the presence of glycogen. Total RNA, poly(A)+ and poly(A)- RNA fractions were reverse transcribed either with *RPPH1* primers, for *RPPH1* detection and random hexamers, for GAPDH and 18S rRNA detection, using the Superscript IV RT enzyme (Invitrogen). cDNA was analysed by qPCR. The relative enrichment of transcripts was calculated as a percentage of total RNA and normalized over the poly(A).

M^{6}A prediction

Prediction of m6A modifications putative sites was performed using the online tool deepSRAMP (http://www.cuilab.cn/deepsramp/) (226). Both zebrafish (NR_036645.1) and human (NR_002312.1) *RPPH1* sequences were submitted as queries selecting "Other organism" and "Full transcript mode" as setup for prediction.

Single Molecule Inexpensive FISH (smiFISH)

Single molecule RNA FISH against Rpph1 was performed according to the method described in (2) with some modifications. NHEM ad A375M cells were plated on acid washed glass coverslips (22x22mm no1.5) and fixed in 4% paraformaldehyde for 20 minutes at RT. Cells were then permeabilized in 0.5% Triton X-100 at RT for 5 minutes and transferred to 1X SSC 15% formamide solution for hybridization. A 4 *RPPH1* smiFISH probe set was designed on regions predicted as single stranded in section 3.2.1 (**Table 5.3**). The *RPPH1* probe sets were annealed to a FLAP-Cy5 oligo in NEB buffer 3 (100 mM NaCl, 50 mM Tris-HCl, 10 mM $MgCl_2$, 1 mM DTT, pH 7.9) [New England Biolabs] as follows: 3 min at 85°; 3min at 65°; 5 min at 25°. Rpph1-FLAP-Cy5 hybridization was carried out overnight at 37° in a humidified chamber. Cells were washed with 1X SSC 15% formamide solution once 25 min at 37° and again for 20 min at 37°. Cells were rinsed twice with 1x PBS. Lastly, cells were stained with HOECST 0.5µg/ml in PBS [Life Technologies], washed twice with 1x PBS and mounted with ProLong™ Glass Antifade Mountant [Invitrogen] for 24 hours prior to image acquisition. Acquisition was performed using a a Leica TCS SP8 inverted confocal microscope [Leica Microsystem], using a HC PL APO 63x/1.40 Oil CS2 objective [Leica Microsystem] on a z-projection.

Table 5.3

Probe	**Sequence**
Rpph1 smiFISH_1	ACTCAGCTCGTGGCCCCACTGATTACACTCGGACCTCGTCGACATGCATT
Rpph1 smiFISH_2	CATGGGAGTGGAGTGACAGGACTTACACTCGGACCTCGTCGACATGCATT
Rpph1 smiFISH_3	CCCAGTCTGACCTCGCGCGGAGCTTACACTCGGACCTCGTCGACATGCATT
Rpph1 smiFISH_4	AGGGCGGGGTCCACGGCATCTCCTTACACTCGGACCTCGTCGACATGCATT

iDRIP

A375M cells were cultured in order to obtain 150 million cells (around 18 cell culture dishes 10 cm) per biological replicate and iDRIP was performed as in (149) with some modification. Briefly Cells were washed three times with ice cold PBS and cross-linked with 0.3 J/m^2 using a Stratalinker® UV Crosslinker [Stratagene], scraped, washed in ice cold 1x PBS and centrifuged 3 min, 800 xg, 4°. Cells were resuspended in DNase Digestion Buffer (Tris-HCl 50 mM, 0,5% NP-40, 0,1% Sarkosyl, DNase I 200U/ml of lysate) and incubated 1h at 37°. Samples were added with Lysis Buffer I (1% Sarkoyl, 0,1% Sodium deoxycholate, 0,5 M LiCl, 20 mM EDTA, 20 mM EGTA), vortexed and incubated 5 min, 37°. Lysates were centrifuged 5 min, 21 000 xg, 4°C and supernatant was recovered and kept in ice. Pellets were resuspended in a Lysis Buffer II (Tris-HCl 50 mM, NP-40 0,5 %, 0,5 M LiCl, 20 mM EDTA, 20 mM EGTA), incubated in ice for 10 min and then at 65° for 5 min, centrifuged 5 min, 21 000 xg, 4°C and supernatant was recovered and kept in ice. The two supernatants were combined. Lysates were precleared for 20 min under gentle rotation with 40 ul of Dynabeads™ Streptavidin Magnetic Beads [Invitrogen™], previously washed and resuspended in Lysis buffer II. Beads were discarded

with magnetic rack. 80 ul/sample of Dynabeads™ Streptavidin Magnetic Beads were washed and resuspended in Binding Buffer (Tris-HCl 5mM, EDTA 0,5 mM, NaCL 1 M), added of 160 pmol/condition of iDRIP probe (**Table 5.5**) and incubated 20 min under gentle rotation. Beads were collected using a magnetic rack and resuspended in Lysis Buffer II. Lysates and conjugated beads were pre-warmed at 65° for 5 min and then beads were added to lysates, incubated at 65°, 15 minutes. Temperature was gradually decreased to 37° and lysates +beads were incubated at 37° under 500 rpm agitation for 1 h. Beads were collected and washed three times with Wash Buffer I (Tris-HCl 50 mM, LiCl 0.3 M, EDTA 5 mM, SDS 1%, NP-40 0,5%, DTT 1mM, PMSF 1mM, protease inhibitors cocktail [MedChemExpress] according to manufacturer instructions). Beads were resuspended in DNase Digestion Buffer and incubated 10 min, 37°, then washed twice with Wash Buffer I and once with Wash Buffer II (SDS 1%, NaCl 150 mM, EDTA 5 mM, DTT 1mM, PMSF 1mM). Beads were eluted in Elution Buffer (Tris-HCl 10 mM, EDTA 1 mM, Triton-X 0,05%) 5 min at 70° and immediately collected with magnetic rack. Supernatant was collected and destined to Proteomic analysis. 10% of lysates were treated with Proteinase K and RNA was extracted to evaluate *RPPH1* capture efficiency. The efficiency of RPPH1 retrieval in the iDRIP assay was calculated as the percentage of total input RNA recovered in the iDRIP fraction, as described in (149).

Table 5.5

Probe	**Sequence**
RPPH1_ AntiSense (AS) probe	[BIOTEG] AGGACGCACTCAGCTCGTGGCC
RPPH1_ Sense	[BIOTEG] GGCCACGAGCTGAGTGCGTCCT

Proteomic Analysis

Sample preparation: Proteins enriched after iDRiP capture were suspended in a solution of 2.5% SDS and 50 mM triethylammonium bicarbonate buffer (TEAB). Subsequently, the disulfide bonds were reduced with 5 mM Tris(2-carboxyethyl)phosphine hydrochloride (TCEP) for 30 minutes at room temperature (RT), and then alkylated with 20 mM iodoacetamide (IAA) for 20 minutes in the dark at RT. The samples were then processed using S-Trap Micro Columns [ProtiFi, USA] according to the manufacturer's protocol. Briefly, the samples were acidified with phosphoric acid (final concentration of approximately 1.2%) and mixed with six volumes of binding buffer (90% methanol and 100 mM TBEA). The protein solution was then loaded onto the S-trap filters by centrifugation at 4000×g for 1 min. The loaded proteins were washed three times with a solution of 90:10 methanol:50 mM TEAB, then digested by adding 25 µL of digestion buffer (1.5 µg Trypsin-LysC, 50 mM TEAB, pH 8) and incubating at 37 °C for 18 hours. Peptides were eluted using three elution steps: 50 mM TEAB in water, 0.2% formic acid in water, and 50% acetonitrile in water. The three eluates were pooled, vacuum-centrifuged to dryness, and desalted using homemade C18 StageTips. The cleaned peptides were then suspended in 15 µL of water containing 0.1% formic acid for LC-MS/MS analysis.

Liquid chromatography–mass spectrometry and data dependent analysis: Peptides were separated on an Easy-nLC 1200 HPLC system [Thermo Scientific]. A 28 cm reversed-phase column with an integrated electrospray emitter (ID 75 µm, 1.7 µm, 100 Å, CoAnn Technologies), heated to 40°C, was used for peptide separation. A two-component mobile phase system was employed: 0.1% formic acid in water (buffer A) and 0.1% formic acid in 80% acetonitrile (buffer B). Peptides were eluted using a gradient of 5% to 25% buffer B over 52 minutes, followed by 25% to 40% over 8 minutes, and 40% to 98% over 10 minutes at a flow rate of 200 nL/min. Peptide analysis was performed on an Orbitrap Fusion Tribrid mass spectrometer [Thermo Fisher Scientific] in data-dependent acquisition mode. Full MS scans were acquired at a resolving power of 120,000 FWHM (mass range: 350–1200 m/z, AGC target: 1 × 10^6 ions, maximum injection time: 50 ms). Each full scan was followed by a set of HCD MS/MS scans within a 3-second cycle, using a collision energy of 27%. Fragment ions were acquired in the Orbitrap analyzer (AGC target: 2.5 × 10^4 ions, resolution: 30,000 FWHM, maximum injection time: 54 ms). The ion transfer tube temperature was set to 200°C. Dynamic exclusion was enabled with a duration of 40 seconds and a mass tolerance of 5 ppm. Data acquisition was controlled using Xcalibur 4.3 and Tune 3.3 software [Thermo Fisher Scientific]. QCloud was employed throughout the project to monitor long-term instrument performance using quality control standards (227). All proteomic data were searched against an in-silico digested UniProt Homo sapiens database (downloaded August 2024), including major known contaminants and reversed sequences. Proteome Discoverer v3.1 [Thermo Scientific] with the MASCOT search engine (v2.6.2, MatrixScience) was used for protein identification (precursor mass tolerance: 10 ppm; fragment mass tolerance: 0.02 Da). Carbamidomethylation (C) was set as a static modification, while oxidation (M) and N-terminal protein acetylation were set as variable modifications. False discovery rate (FDR) was set at < 1% for both peptides and proteins, and contaminants

MS computational analyses: Downstream analysis was performed using the ProTN proteomics pipeline (https://github.com/TebaldiLab/ProTN). Peptide intensities were log2-transformed, median-normalized, and summarized into proteins using median sweeping via functions in the DEqMS Bioconductor package (228). Missing intensity values were imputed using the PhosR package (229). Differential analysis was conducted with DEqMS (228); proteins with an absolute log2 fold change > 0.75 and P-value < 0.05 were considered significant. Functional enrichment analysis of differentially expressed proteins was performed using EnrichR (230). Enriched terms with P-value < 0.05 and an overlap size > 4 were considered significant.

Prediction of *RPPH1* secondary structure

Secondary structure prediction of human and zebrafish RPPH1 sequence was performed using three computational tools: RNAfold from the ViennaRNA package (158), RNAstructure (159), and MXFold . RNAfold was employed to calculate minimum free energy (MFE) structures and base-pairing probabilities based on the nearest-neighbour thermodynamic model.

RNAstructure was used to predict MFE structures. Predicted structures were exported in dot-bracket notation and, with ViennaRNAfold, linear color-coded base pairing probability representation. 2D secondary structure prediction was generated using MXFold.

Injections in 48 hpf Zebrafish

Injections were performed in the Duct of Couvier of anaesthetized 48 hpf zebrafish *tg(mpeg:GFP)*^{gl222} larvae using a glass capillary connected to a FemtoJet microinjector [Eppendorf], as described in (6). For injections of EVs, we used volumes of 4 nL of a EVs resuspension in PBS. Purified synthetic zfRPPH1, GFP RNA and Poly(I:C)(HMW)-LyoVec [InVivoGen] were injected as 1ng/nl solution with Poly (I:C) (4 nl).

Inhibition of TLR3 in zebrafish

TLR3 was inhibited in zebrafish larvae by adding CU-CPT 4a (TLR3-IN-1) [MedChemExpress] at a final concentration of 10 uM to the water of zebrafish larvae.

KO of *mavs* in zebrafish larvae

crRNAs were designed (**Table 4.6**) in collaboration with Irene Pecchini (PhD student in the Lab of Experimental Cancer Biology, Cibio, Unitn). To knock out mavs we used a CRISPR/Cas9 approach using the Alt-R CRISPR/Cas9 system [IDT] according to manufacturer instructions. Briefly, to form guideRNAs (gRNA) each 100 µM Alt-RTM CRISPR-Cas9 crRNA (**Table 4.6**) was mixed with 100 µM Alt-RTM CRISPR-Cas9 tracrRNA [IDT custom] in a 1:1 ratio, annealed for 5 min at 95° and then cooled in ice. RNPs were assembled combining formed gRNAs with 500 ng/ul Cas9 protein (donated by Harmenise-Harvard Laboratory of Cell Division, Cibio, Unitn), Nuclease-free duplex buffer [IDT] and 0.2 ul of phenol red and kept at RT. RNPs were injected in 1 cell-stage zebrafish embryos in 0.1-0.13 nm diameter drops. Knock out specimens were then selected observing the golden phenotype at 48 hpf. Genomic DNA was extracted from a pool of 5 KO larvae using *Quick*-DNA Miniprep Plus Kit [Zymo Research], mavs sequence was amplified using EmeraldAmpGT PCR Master mix [Takara Bio] using primers listed in **Table 5.6** and KO efficiency was evaluated through Sanger sequencing.

Table 5.6

Probe	**Sequence**
crRNA mavs (gRNAzf01)	TGGGAAGGTGCTATAACTTG [IDT custom]
crRNAgolden (gRNAzf02)	GGTCTCTCGCAGGATGTTGC [IDT custum]
zf_mavs FW primer	CTCTAGCTCCTTCTTTAACTGGAG
zf_mavs RV primer	CTCATTTGCAATTGGGTCGGAA

qPCR for ISGs and Inflammatory cytokynes

THP-1 cells were cultured in 12 wells plates were washed with 1X PBS, lysed with 500ul of TripleXtractor reagent per biological replicate (6 wells-1200000 cells/condition). Pools of 15-20 larvae were resuspended in TripleXtractor reagent (Grisp) and mechanically dissociated. Total RNA was purified from cells or larvae using TripleXtractor reagent for RNA isolation [GRiSP] as reviewed above (*RNA extraction from zebrafish larvae and cultured cells*).

RNA was reverse-transcribed using ReverTra Ace™ qPCR RT Master Mix with gDNA Remover [Toyobo] according to manufacturer's instructions. RT reaction was used for the qPCR experiments which were performed in triplicates using qPCRBIO SyGreen® Mix [PCR Biosystem] in a CFX96 Thermo Cycler [Bio-Rad]. The results were analysed with Bio-Rad CFX Manager, version 2.1. The relative expression was calculated according to the $-2^{\Delta\Delta Ct}$ method normalized on *b-actin* mRNA for human samples and *rps11* mRNA for zebrafish samples. Primers used for genes of interests are reported in **Table 5.7**. Statistical analysis was performed with GraphPad Prism 8, performing ordinary one-way Anova.

Table 5.7

Primer	**Sequence**
hsa_isg15 FW	GAGAGGCAGCGAACTCATCT
hsa_isg15 RV	CTTCAGCTCTGACACCGACA
hsa_ifit1 FW	GGCTGCCTAATTTACAGCAACC
hsa_ifit1 RV	GGCATTTCATCGTCATCAATGG
hsa_il-1β FW	CCAGCTACGAATCTCCGACC
hsa_il-1β RV	GGGAACTGGGCAGACTCAAA
hsa_β-actin FW	ACCCATTGGCAATGAGCGGTTC
hsa_β-actin RV	AGGTCTTTGCGGATGTCCACGT
zf_isg15 FW	ATGATGTGGACGCCAACGAG
zf_isg15 RV	TCCTGCAACTTCATGCCAGAC
zf_ifit10 FW	CAC GAG AAA GCA CAT CAG AGC C
zf_ifit10 RV	TCCATCCCTTCTCACCAAGCACT
zf_il-1β FW	TCATCATCGCCCTGAACAGA
zf_il-1β RV	CATGTCCAGCACCTCTTTTTCTC
zf_rps11 FW	ACAGAAATGCCCCTTCACTG
zf_rps11 RV	GCCTCTTCTCAAAACGGTTG

Confocal imaging and macrophages count

72 hours post injection; zebrafish *tg(mpeg:GFP)*^{gl222} larvae were anesthetised and observed using a confocal microscope. Confocal microscopy was carried out with a Leica TCS SP8 inverted confocal microscope [Leica Microsystem], using a HC PL FLUOTAR 10x/0.30 objective

[Leica Microsystem] and on a z-projection. Fluorescent macrophages in the Caudal Hematopoietic Tissue of acquired larvae were counted manually, and statistical analysis was performed using GraphPad Prism 8.

Statistical Analysis

In all cases, *n* numbers refer to biological replicates unless otherwise stated. All the graphs and the statistical analyses were generated and calculated using GraphPad Prism software version 8.0. All the graphs represent mean +/− SD, unless otherwise stated. Data were analysed against controls with one-way ANOVA. To verify normality of data Shapiro-Wilk, D'Agostino & Pearson and Kolmogorov-Smirov tests were employed.

Protein extraction and Western Blot

Western blot analysis was carried out using standard methods. Briefly, cells and EV pellets were lysed on ice with RIPA buffer (NaCl 150 mM, TrisHCl 50 mM pH 8 , NP40 1%, Sodium deoxycholate 0.5% , SDS 0.1%, 0.1 mg/mL phenylmethylsulfonyl fluoride [MedChem Express], protease cocktail inhibitor [MedChemExpress], phosphatase inhibitor cocktail [MedChemExpress]. For Western blots, equal protein concentrations (quantified with the Pierce BCA Protein assay kit [Thermo Scientific]) were resolved via 10% SDS–PAGE and transferred to PVDF membranes [Biorad Laboratories]. Antibodies used are listed in **Table 5.8**. ECL Western blotting substrate [GeneTex] was added before detection with a ChemiDoc MP Imaging System [Biorad Laboratories]. Quantification was made using ImageLab version 3.0 using volume tools to quantify band intensity, normalized on the house keeping protein (βACTIN).

Table 5.8.

Target	**Antibody**
RIG-I	Rig-I (D14G6) #3743 [Cell Signaling]
MDA5	MDA-5 (D74E4) #5321 [Cell Signaling]
IRF3	IRF-3 (D6I4C) #11904 [Cell Signaling]
Phospho-IRF3	Phospho-IRF-3 (Ser396) (4D4G) #4947 [Cell Signaling]
Phosphor-TBK1	Phospho-TBK1/NAK (Ser172) (D52C2) #5483 [Cell Signaling]
B-ACTIN	anti-ACTIN (Clone C4) [MP Biomedicals]
MAVS	MAVS #3993 [Cell Signaling]

Cloning of human *RPPH1*

Human *RPPH1* was reverse-transcribed from total RNA extracted from A375M cells using the primers reported in **Table 5.9**. The sequence was cloned in pGEM®-T Easy Vector System

[Promega] following the manufacturer's instructions. Correct clones and orientations were confirmed by Sanger sequencing.

Table 5.9

Target	Antibody
hsa_RPPH1_cloningFW	TATCCCGCCTCCCTTCGA
hsa_RPPH1_cloningRV	AATGGGCGGAGGAGAGTAGT

***In vitro* synthesis of RNA molecules**

Plasmid DNA was linearized using a restriction enzyme that cuts uniquely within the plasmid backbone and immediately downstream the sequence of interest. Linearized DNA was purified using a phenol-chloroform-isopropanol extraction method. Briefly, to DNA was added 1/10 volume of 3 M sodium acetate and phenol:chloroform:isoamyl alcohol. DNA was pelleted by centrifugation (15,000 × g, 15–20 min, 4 °C), washed with 70% ethanol, air-dried, and resuspended in nuclease-free water to a final concentration of 0.5–1 µg/µL. In vitro transcription was performed using purified linearized plasmid using mMessage mMachine T7/SP6 kit [Ambion] according to manufacturer's instruction.

KO of *MAVS* in THP-1 cells

To KO *MAVS* in THP-1 cells, we employed CRISPR/Cas9 genome-editing technology to knock cells, in collaboration with Giorgia Pellizzaro (Harmenise-Harvard Laboratory of Cell Division, Cibio, Univeristy of Trento) and performed as in (3). cRNA, tracrRNA and Cas9 protein were donated by Harmenise-Harvard Laboratory of Cell Division (Cibio, Unitn). The guide RNA sequence was designed to target exon six of *MAVS* sequence (**Table 5.10)**. To form guideRNAs (gRNA) 100 crRNA was mixed with 100 tracrRNA in a 1:1 ratio, annealed for 5 min at 95° and then cooled in ice. RNPs were assembled combining formed 150 pmol gRNA with 120 pmol Cas9 protein in Nuclease-free duplex buffer [IDT] and incubated for 20 min at RT. The RNPs obtained were electroporated in THP-1 cells using Cell Line Nucleofector® Kit V [Lonza] according to manufacturer's instruction in a 4D-Nucleofector® X Unit [Lonza]. After two cells passages proteins and genomic DNA were extracted. Genomic DNA was extracted using *Quick*-DNA Miniprep Plus Kit [Zymo Research], mavs sequence was amplified using PCR Master mix [Takara Bio] using primers listed in **Table 4.10** and KO efficiency was evaluated through Sanger sequencing. Proteins were extracted and MAVS depletion was analysed through Western Blot as described in *Protein extraction and Western Blot.*

Table 5.10

Probe	Sequence
crRNA mavs	GGATTGGTGAGCGCATTAGA
hsa_mavs FW primer	CAGGCCGAGCCTATCATCTG
hsa_mavs RV primer	CTGCATGAGGCTGGTTCTCA

Single-cell RNA sequencing

Single-cell RNA data collection: M0 THP-1 differentiated cells Untreated and treated with melanoma-derived EVs ad indicated above were washed with sterile PBS at room temperature, detached by incubation in Trypsin-EDTA (Gibco, cat. 25200072) for 3.5 minutes at 37°C and collected them in a 15ml falcon tube adding 2ml of complete medium and centrifuged for 5 minutes, 200xg (RT). Cell pellet was washed in 5 ml 1x sterile PBS, centrifuged for 5 minutes, 200 xg (RT) and resuspended in 1 ml complete medium and counted using a Burker chamber.

2500 targeted cells per sample were pooled together with 7500 cells coming from zebrafish samples. Cells were tagged with oligo labelling prior to pooling following manufacturer instructions (CG0000391 Rev B protocol). Cells were loaded on the 10x chromium controller and Single cell RNA sequencing libraries were created using the Chromium Next GEM Single cell 3' Reagent kits v3.1 (Dual Index) with Feature Barcode technology for Cell Multiplexing (CG0000388 RevD) according to the manufacturer instructions. Both the gene expression and feature barcode libraries were then sequenced with 100bp paired end reads on NOVAseq6000.

*Single-cell RNA sequencing analysis: r*aw Illumina sequencing reads were aligned independently to both the zebrafish reference (GRCz11) and human reference (GRCh38) using the count function of Cell Ranger v9.0.1 using default parameters. Only the barcodes aligning to human reference were taken into consideration for further analysis, discarding barcodes present in both alignments. High-quality cells containing <10% mitochondrial transcript, >200 number of genes and total transcripts between 1000 and 80000 were retained for downstream analysis. Also, genes expressed in less than 3 cells were discarded. Doublets were removed using db_scDblFinder from the SCP R package (version 0.5.6) with expected percentage of doublets of 1% for every 1000cells. Counts were normalized to the size of the library, scaled on all the genes and principal components analysis was performed on the 3000 most variable genes. Samples were integrated using harmony 1.2.3 with the RunHarmony R function. Clusters were defined using Seurat 5.1.0 with a resolution of 0.2. Cell cycle scoring was calculated using the CellCycleScoring function from the Seuat 5.1.0 R package. Heatmaps showing the expression of genes were done using the SCP:GroupHeatmap function visualizing the log2fc on normalized counts.

Gene set enrichment analysis: Gene Set enrichment analysis (GSEA) was carried out on differentially expressed genes between groups of interest using the wilcoxauc function (presto R package 1.0.0). Differentially expressed genes were filtered for adjusted pvalue < 0.05 and logFC > 0.1. GSEA was conducted with the fgsea function (fgsea 1.32.4 R package) using the GO BP and Hallmark gene sets obtained from the MSigDB. Normalized enriched scores (NES) were calculated and results shown using heatmaps (pheatmap 1.0.12). For each group, the top upregulated and downregulated pathways were chosen for visualization. Regarding the GSEA specific for the vesicles transport processes, only the pathways containing the word “vesicle” were used for downstream analysis.

REFERENCES

1. Mattick JS, Amaral PP, Carninci P, Carpenter S, Chang HY, Chen LL, et al. Long non-coding RNAs: definitions, functions, challenges and recommendations. Nat Rev Mol Cell Biol. 2023 Jun;24(6):430–47.

2. Bartkiewicz M, Gold H, Altman S. Identification and characterization of an RNA molecule that copurifies with RNase P activity from HeLa cells. Genes Dev. 1989 Apr;3(4):488–99.

3. Baer M, Nilsen TW, Costigan C, Altman S. Structure and transcription of a human gene for Hi RNA, the RNA component of human RNase P.

4. Altman S. Ribonuclease P. Philos Trans R Soc Lond B Biol Sci. 2011 Oct 27;366(1580):2936–41.

5. Mann H, Ben-Asouli Y, Schein A, Moussa S, Jarrous N. Eukaryotic RNase P: Role of RNA and Protein Subunits of a Primordial Catalytic Ribonucleoprotein in RNA-Based Catalysis. Molecular Cell. 2003 Oct 1;12(4):925–35.

6. Lee JW, Chun YL, Kim AY, Lloyd LT, Ko S, Yoon JH, et al. Accumulation of Mitochondrial RPPH1 RNA Is Associated with Cellular Senescence. Int J Mol Sci. 2021 Jan 14;22(2):782.

7. Zhang P, Sun Y, Peng R, Chen W, Fu X, Zhang L, et al. Long non-coding RNA Rpph1 promotes inflammation and proliferation of mesangial cells in diabetic nephropathy via an interaction with Gal-3. Cell Death Dis. 2019 Jul 8;10(7):1–16.

8. Zhu Yang, Gia-Phong Vu, Hua Qian, Yuan-Chuan Chen, Yu Wang, Michael Reeves, Ke Zen, Fenyong Liu. Engineered RNase P Ribozymes Effectively Inhibit Human Cytomegalovirus Gene Expression and Replication. Viruses. 2014. 10.3390/v6062376

9. Howard MJ, Liu X, Lim WH, Klemm BP, Fierke CA, Koutmos M, et al. RNase P enzymes. RNA Biology. 2013 Jun 1;10(6):909–14.

10. Ziehler WA, Day JJ, Fierke CA, Engelke DR. Effects of 5‘ Leader and 3‘ Trailer Structures on Pre-tRNA Processing by Nuclear RNase P. Biochemistry. 2000 Aug 1;39(32):9909–16.

11. Guerrier-Takada C, Gardiner K, Marsh T, Pace N, Altman S. The RNA moiety of ribonuclease P is the catalytic subunit of the enzyme. Cell. 1983 Dec 1;35(3):849–57.

12. Orlovetskie N, Mani D, Rouvinski A, Jarrous N. Human RNase P exhibits and controls distinct ribonucleolytic activities required for ordered maturation of tRNA. Proceedings of the National Academy of Sciences. 2023 Oct 17;120(42):e2307185120.

13. Kikovska E, Svärd SG, Kirsebom LA. Eukaryotic RNase P RNA mediates cleavage in the absence of protein. Proceedings of the National Academy of Sciences. 2007 Feb 13;104(7):2062–7.

14. Wu J, Niu S, Tan M, Huang C, Li M, Song Y, et al. Cryo-EM Structure of the Human Ribonuclease P Holoenzyme. Cell. 2018 Nov;175(5):1393-1404.e11.

15. Yun-Tzai Lee, Maximilia F. S. Degenhardt, Ilias Skeparnias, Hermann F. Degenhardt, Yuba R. Bhandari, Ping Yu, Jason R. Stagno, Lixin Fan, Jinwei Zhang, Yun-Xing Wang. The conformational space of RNase P RNA in solution. Nature. Jan 2025. 10.1038/s41586-024-08336-6

16. Altman S, Wesolowski D, Guerrier-Takada C, Li Y. RNase P cleaves transient structures in some riboswitches. Proc Natl Acad Sci U S A. 2005 Aug 9;102(32):11284–9.

17. Coughlin DJ, Pleiss JA, Walker SC, Whitworth GB, Engelke DR. Genome-wide search for yeast RNase P substrates reveals role in maturation of intron-encoded box C/D small nucleolar RNAs. Proc Natl Acad Sci U S A. 2008 Aug 26;105(34):12218–23.

18. Wilusz JE, Freier SM, Spector DL. 3' end processing of a long nuclear-retained noncoding RNA yields a tRNA-like cytoplasmic RNA. Cell. 2008 Nov 28;135(5):919–32.

19. Reiner R, Ben-Asouli Y, Krilovetzky I, Jarrous N. A role for the catalytic ribonucleoprotein RNase P in RNA polymerase III transcription. Genes Dev. 2006 Jun 15;20(12):1621–35.

20. Abu-Zhayia ER, Khoury-Haddad H, Guttmann-Raviv N, Serruya R, Jarrous N, Ayoub N. A role of human RNase P subunits, Rpp29 and Rpp21, in homology directed-repair of double-strand breaks. Sci Rep. 2017 Apr 21;7(1):1002.

21. Chu S, Archer RH, Zengel JM, Lindahl L. The RNA of RNase MRP is required for normal processing of ribosomal RNA. Proceedings of the National Academy of Sciences. 1994 Jan 18;91(2):659–63.

22. Zhou B, Wan F, Lei KX, Lan P, Wu J, Lei M. Coevolution of RNA and protein subunits in RNase P and RNase MRP, two RNA processing enzymes. Journal of Biological Chemistry. 2024 Mar 1. 10.1016/j.jbc.2024.105729

23. Garcia PD, Zakian VA. A new role for proteins subunits of RNase P: stabilization of the telomerase holoenzyme. Microbial Cell. 2020 Jun 17;7(9):250–4.

24. Jorge Ferrer, Nadya Dimitrova. Transcription regulation by long non-coding RNAs: mechanisms and disease relevance | Nature Reviews Molecular Cell Biology. May 2024. 10.1038/s41580-023-00694-9

25. Pisignano G, Ladomery M. Epigenetic Regulation of Alternative Splicing: How LncRNAs Tailor the Message. Noncoding RNA. 2021 Mar 11;7(1):21.

26. Chenguang Gong, Lynne E Maquat. lncRNAs transactivate STAU1-mediated mRNA decay by duplexing with 3' UTRs via Alu elements | Nature . Feb 2011. 10.1038/nature09701

27. Liu SJ, Dang HX, Lim DA, Feng FY, Maher CA. Long noncoding RNAs in cancer metastasis. Nat Rev Cancer. 2021 Jul;21(7):446–60.

28. Zhou J, Shi K, Huang W, Zhang Y, Chen Q, Mou T, et al. LncRNA RPPH1 acts as a molecular sponge for miR-122 to regulate Wnt1/β-catenin signaling in hepatocellular carcinoma. International Journal of Medical Sciences. 2023 Jan 1;20(1):23–34.

29. Huang Y, Zheng W, Ji C, Wang X, Yu Y, Deng X, et al. Circular RNA circRPPH1 promotes breast cancer progression via circRPPH1-miR-512-5p-STAT1 axis. Cell Death Discov. 2021 Dec 6;7(1):376.

30. Zhang C, Yu Z, Yang S, Liu Y, Song J, Mao J, et al. ZNF460-mediated circRPPH1 promotes TNBC progression through ITGA5-induced FAK/PI3K/AKT activation in a ceRNA manner. Molecular Cancer. 2024 Feb 14;23(1):33.

31. Liang Z xing, Liu H shan, Wang F wei, Xiong L, Zhou C, Hu T, et al. LncRNA RPPH1 promotes colorectal cancer metastasis by interacting with TUBB3 and by promoting exosomes-mediated macrophage M2 polarization. Cell Death Dis. 2019 Nov 4;10(11):1–17.

32. Ning W, Yang J, Ni R, Yin Q, Zhang M, Zhang F, et al. Hypoxia induced cellular and exosomal RPPH1 promotes breast cancer angiogenesis and metastasis through stabilizing the IGF2BP2/FGFR2 axis. Oncogene. 2025 Feb;44(3):147–64.

33. Biagini V, Busi F, Anelli V, Kerschbamer E, Baghini M, Gurrieri E, et al. Zebrafish Melanoma-Derived Interstitial EVs Are Carriers of ncRNAs That Induce Inflammation. IJMS. 2022 May 14;23(10):5510.

34. Kalluri R, LeBleu VS. The biology, function, and biomedical applications of exosomes. Science. 2020 Feb 7;367(6478):eaau6977.

35. Théry C, Witwer KW, Aikawa E, Alcaraz MJ, Anderson JD, Andriantsitohaina R, et al. Minimal information for studies of extracellular vesicles 2018 (MISEV2018): a position statement of the International Society for Extracellular Vesicles and update of the MISEV2014 guidelines. J Extracell Vesicles. 2018 Nov 23;7(1):1535750.

36. Del Conde I, Shrimpton CN, Thiagarajan P, López JA. Tissue-factor-bearing microvesicles arise from lipid rafts and fuse with activated platelets to initiate coagulation. Blood. 2005 Sep 1;106(5):1604–11.

37. Wang T, Gilkes DM, Takano N, Xiang L, Luo W, Bishop CJ, et al. Hypoxia-inducible factors and RAB22A mediate formation of microvesicles that stimulate breast cancer invasion and metastasis. Proc Natl Acad Sci U S A. 2014 Aug 5;111(31):E3234-3242.

38. Clancy JW, Schmidtmann M, D'Souza-Schorey C. The ins and outs of microvesicles. FASEB BioAdvances. 2021;3(6):399–406.

39. Tricarico C, Clancy J, D'Souza-Schorey C. Biology and biogenesis of shed microvesicles. Small GTPases. 2016 Aug 5;8(4):220–32.

40. Abels ER, Breakefield XO. Introduction to Extracellular Vesicles: Biogenesis, RNA Cargo Selection, Content, Release, and Uptake. Cell Mol Neurobiol. 2016 Apr 6;36(3):301–12.

41. Teng F, Fussenegger M. Shedding Light on Extracellular Vesicle Biogenesis and Bioengineering. Advanced Science. 2021;8(1):2003505.

42. Santavanond JP, Rutter SF, Atkin-Smith GK, Poon IKH. Apoptotic Bodies: Mechanism of Formation, Isolation and Functional Relevance. Subcell Biochem. 2021;97:61–88.

43. Jiang D, Jiang Z, Lu D, Wang X, Liang H, Zhang J, et al. Migrasomes provide regional cues for organ morphogenesis during zebrafish gastrulation. Nat Cell Biol. 2019 Aug;21(8):966–77.

44. Minciacchi VR, You S, Spinelli C, Morley S, Zandian M, Aspuria PJ, et al. Large oncosomes contain distinct protein cargo and represent a separate functional class of tumor-derived extracellular vesicles. Oncotarget. 2015 Mar 14;6(13):11327–41.

45. Zaborowski MP, Balaj L, Breakefield XO, Lai CP. Extracellular Vesicles: Composition, Biological Relevance, and Methods of Study. Bioscience. 2015 Aug 1;65(8):783–97.

46. Esmaeili A, Baghaban Eslaminejad M, Hosseini S. Biomolecular corona potential in extracellular vesicle engineering for therapeutic applications. Biomedicine & Pharmacotherapy. 2025 Jul 1;188:118202.

47. Tassoni S, Bergese P, Radeghieri A. The extracellular vesicle biomolecular corona: current insights and diagnostic potential. Nanomedicine (Lond). 2025 Aug;20(16):2013–21.

48. Ghadami S, Dellinger K. The lipid composition of extracellular vesicles: applications in diagnostics and therapeutic delivery. Front Mol Biosci [Internet]. 2023 Jul 13 [cited 2026 Jan 25];10. Available from: https://www.frontiersin.org/journals/molecular-biosciences/articles/10.3389/fmolb.2023.1198044/full

49. Feng D, Zhao WL, Ye YY, Bai XC, Liu RQ, Chang LF, et al. Cellular Internalization of Exosomes Occurs Through Phagocytosis. Traffic. 2010;11(5):675–87.

50. Haraszti RA, Didiot MC, Sapp E, Leszyk J, Shaffer SA, Rockwell HE, et al. High-resolution proteomic and lipidomic analysis of exosomes and microvesicles from different cell sources. J Extracell Vesicles. 2016 Nov 17;5:10.3402/jev.v5.32570.

51. Dorado E, Doria ML, Nagelkerke A, McKenzie JS, Maneta-Stavrakaki S, Whittaker TE, et al. Extracellular vesicles as a promising source of lipid biomarkers for breast cancer detection in blood plasma. J Extracell Vesicles. 2024 Mar;13(3):e12419.

52. Mir B, Goettsch C. Extracellular Vesicles as Delivery Vehicles of Specific Cellular Cargo. Cells. 2020 Jul;9(7):1601.

53. Pedro Lorite, Jorge N. Domínguez,Teresa Palomeque and María Isabel Torres. Extracellular Vesicles: Advanced Tools for Disease Diagnosis, Monitoring, and Therapies. *Int. J. Mol. Sci.* Dec 2024. https://doi.org/10.3390/ijms26010189

54. Jankovičová J, Sečová P, Michalková K, Antalíková J. Tetraspanins, More than Markers of Extracellular Vesicles in Reproduction. Int J Mol Sci. 2020 Oct 14;21(20):7568.

55. Buzas EI. Opportunities and challenges in studying the extracellular vesicle corona. Nat Cell Biol. 2022 Sep;24(9):1322–5.

56. Wolf M, Poupardin RW, Ebner-Peking P, Andrade AC, Blöchl C, Obermayer A, et al. A functional corona around extracellular vesicles enhances angiogenesis, skin regeneration and immunomodulation. Journal of Extracellular Vesicles. 2022;11(4):e12207.

57. Valadi H, Ekström K, Bossios A, Sjöstrand M, Lee JJ, Lötvall JO. Exosome-mediated transfer of mRNAs and microRNAs is a novel mechanism of genetic exchange between cells. Nat Cell Biol. 2007 Jun;9(6):654–9.

58. Dellar ER, Hill C, Melling GE, Carter DRF, Baena-Lopez LA. Unpacking extracellular vesicles: RNA cargo loading and function. J Extracell Biol. 2022 May 2;1(5):e40.

59. Lazo S, Noren Hooten N, Green J, Eitan E, Mode NA, Liu Q, et al. Mitochondrial DNA in extracellular vesicles declines with age. Aging Cell. 2021 Jan;20(1):e13283.

60. Tsering T, Nadeau A, Wu T, Dickinson K, Burnier JV. Extracellular vesicle-associated DNA: ten years since its discovery in human blood. Cell Death Dis. 2024 Sep 12;15(9):668.

61. Moonmuang S, Chaiyawat P, Jantrapirom S, Pruksakorn D, Lo Piccolo L. Circulating Long Non-Coding RNAs as Novel Potential Biomarkers for Osteogenic Sarcoma. Cancers (Basel). 2021 Aug 21;13(16):4214.

62. Sork H, Conceicao M, Corso G, Nordin J, Lee YXF, Krjutskov K, et al. Profiling of Extracellular Small RNAs Highlights a Strong Bias towards Non-Vesicular Secretion. Cells. 2021 Jun;10(6):1543.

63. Ding J, Teng Y, Cui R, Liu J, Xiao K, Dong Z, et al. LncRNAs in serum-derived extracellular vesicles are potential biomarker and correlated with immune infiltration in gastric cancer. Front Immunol. 2025 Jan 24 https://doi.org/10.3389/fimmu.2025.1533111

64. O'Grady T, Njock MS, Lion M, Bruyr J, Mariavelle E, Galvan B, et al. Sorting and packaging of RNA into extracellular vesicles shape intracellular transcript levels. BMC Biol. 2022 Mar 24;20(1):72.

65. Spanos M, Gokulnath P, Chatterjee E, Li G, Varrias D, Das S. Expanding the horizon of EV-RNAs: LncRNAs in EVs as biomarkers for disease pathways. Extracell Vesicle. 2023 Dec;2:100025.

66. Weissinger H, Bobbili MR, Yan Y, Gockert M, Arcalis E, Grillari J, et al. Native extracellular vesicles display surface bound RNAs that are co-delivered to cells. bioRxiv; 2025. https://www.biorxiv.org/content/10.64898/2025.12.17.694909v1

67. Desrochers LM, Bordeleau F, Reinhart-King CA, Cerione RA, Antonyak MA. Microvesicles provide a mechanism for intercellular communication by embryonic stem cells during embryo implantation. Nat Commun. 2016 Jun 15;7(1):11958.

68. Cocucci E, Racchetti G, Meldolesi J. Shedding microvesicles: artefacts no more. Trends Cell Biol. 2009 Feb;19(2):43–51.

69. Cristina Villa del Campo, Norman Y Liaw, Mala Gunadasa-Rohling, Moritz Matthaei, Luca Braga, Tahnee Kennedy, Gabriela Salinas, Niels Voigt, Mauro Giacca, Wolfram-Hubertus Zimmermann, Paul Richard Riley. Regenerative potential of epicardium-derived extracellular vesicles mediated by conserved miRNA transfer. Cardiovascular Research. Feb 2021. 10.1093/cvr/cvab054

70. Sun LH, Tian D, Yang ZC, Li JL. Exosomal miR-21 promotes proliferation, invasion and therapy resistance of colon adenocarcinoma cells through its target PDCD4. Sci Rep. 2020 May 19;10:8271.

71. Ren W, Hou J, Yang C, Wang H, Wu S, Wu Y, et al. Extracellular vesicles secreted by hypoxia pre-challenged mesenchymal stem cells promote non-small cell lung cancer cell growth and mobility as well as macrophage M2 polarization via miR-21-5p delivery. J Exp Clin Cancer Res. 2019 Feb 8;38(1):62.

72. Omarini C, Catani V, Mastrolia I, Toss A, Banchelli F, Isca C, et al. Extracellular vesicles-derived miR-21 as a biomarker for early diagnosis and tumor activity in breast cancer subtypes. Biomarker Research. 2025 Jan 23;13(1):14.

73. Ko SY, Lee W, Kenny HA, Dang LH, Ellis LM, Jonasch E, et al. Cancer-derived small extracellular vesicles promote angiogenesis by heparin-bound, bevacizumab-insensitive VEGF, independent of vesicle uptake. Commun Biol. 2019 Oct 18;2(1):386.

74. Skog J, Würdinger T, van Rijn S, Meijer DH, Gainche L, Curry WT, et al. Glioblastoma microvesicles transport RNA and proteins that promote tumour growth and provide diagnostic biomarkers. Nat Cell Biol. 2008 Dec;10(12):1470–6.

75. Karama Asleh, Valerie Dery, Catherine Taylor, Michelle Davey, Marie-Ange Djeungoue-Petga, Rodney J Ouellette. Extracellular vesicle-based liquid biopsy biomarkers and their application in precision immuno-oncology. Biomarker Research. Nov 2023. 10.1186/s40364-023-00540-2

76. Chang WH, Cerione RA, Antonyak MA. Extracellular Vesicles and Their Roles in Cancer Progression. Methods Mol Biol. 2021;2174:143–70.

77. Abd Elmageed ZY, Yang Y, Thomas R, Ranjan M, Mondal D, Moroz K, et al. Neoplastic Reprogramming of Patient-Derived Adipose Stem Cells by Prostate Cancer Cell-Associated Exosomes. Stem Cells. 2014 Apr 1;32(4):983–97.

78. Zhou W, Fong MY, Min Y, Somlo G, Liu L, Palomares MR, et al. Cancer-secreted miR-105 destroys vascular endothelial barriers to promote metastasis. Cancer Cell. 2014 Apr 14;25(4):501–15.

79. Mary B, Asokan N, Jerabkova-Roda K, Larnicol A, Busnelli I, Stemmelen T, et al. Blood flow diverts extracellular vesicles from endothelial degradative compartments to promote angiogenesis. bioRxiv; 2022. 10.1101/2022.12.19.521008v1

80. Franz L Ricklefs, Quazim Alayo, Harald Krenzlin, Ahmad B Mahmoud, Maria C Speranza, Hiroshi Nakashima , Josie L Hayes , Kyungheon Lee, Leonora Balaj, Carmela

Passaro , Arun K Rooj, Susanne Krasemann, Bob S Carter, Clark C Chen, Tyler Steed, Jeffrey Treiber, Scott Rodig, Katherine Yang, Ichiro Nakano, Hakho Lee, Ralph Weissleder, Xandra O Breakefield, Jakub Godlewski, Manfred Westphal, Katrin Lamszus, Gordon J Freeman, Agnieszka Bronisz, Sean E Lawler, Antonio Chiocca. Immune evasion mediated by PD-L1 on glioblastoma-derived extracellular vesicles. Sci Adv. 2018 Mar 7;4(3):eaar2766. doi: 10.1126/sciadv.aar2766

81. Fabbri M, Paone A, Calore F, Galli R, Gaudio E, Santhanam R, et al. MicroRNAs bind to Toll-like receptors to induce prometastatic inflammatory response. Proc Natl Acad Sci U S A. 2012 Jul 31;109(31):E2110–6.

82. Li D, Wu M. Pattern recognition receptors in health and diseases. Sig Transduct Target Ther. 2021 Aug 4;6(1):291.

83. Uehata T, Takeuchi O. RNA Recognition and Immunity—Innate Immune Sensing and Its Posttranscriptional Regulation Mechanisms. Cells. 2020 Jul 16;9(7):1701.

84. Vesely MD, Kershaw MH, Schreiber RD, Smyth MJ. Natural innate and adaptive immunity to cancer. Annu Rev Immunol. 2011;29:235–71.

85. Satoh T, Kato H, Kumagai Y, Yoneyama M, Sato S, Matsushita K, et al. LGP2 is a positive regulator of RIG-I– and MDA5-mediated antiviral responses. Proc Natl Acad Sci U S A. 2010 Jan 26;107(4):1512–7.

86. Kato H, Takeuchi O, Mikamo-Satoh E, Hirai R, Kawai T, Matsushita K, et al. Length-dependent recognition of double-stranded ribonucleic acids by retinoic acid–inducible gene-I and melanoma differentiation–associated gene 5. J Exp Med. 2008 Jun 30;205(7):1601–10.

87. Hornung V, Ellegast J, Kim S, Brzózka K, Jung A, Kato H, et al. 5′-Triphosphate RNA Is the Ligand for RIG-I. Science. 2006 Nov 10;314(5801):994–7.

88. Paz S, Vilasco M, Arguello M, Sun Q, Lacoste J, Nguyen TLA, et al. Ubiquitin-Regulated Recruitment of IκB Kinase ε to the MAVS Interferon Signaling Adapter. Mol Cell Biol. 2009 Jun;29(12):3401–12.

89. Liu Y, Olagnier D, Lin R. Host and Viral Modulation of RIG-I-Mediated Antiviral Immunity. Front Immunol. 2017 Jan 3 /10.3389/fimmu.2016.00662/

90. El-Zayat SR, Sibaii H, Mannaa FA. Toll-like receptors activation, signaling, and targeting: an overview. Bulletin of the National Research Centre. 2019 Dec 12;43(1):187.

91. Yang Y, Li H, Fotopoulou C, Cunnea P, Zhao X. Toll-like receptor-targeted anti-tumor therapies: Advances and challenges. Frontiers in Immunology. 2022 /10.3389/fimmu.2022.1049340

92. Pirher N, Pohar J, Manček-Keber M, Benčina M, Jerala R. Activation of cell membrane-localized Toll-like receptor 3 by siRNA. Immunol Lett. 2017 Sep;189:55–63.

93. Marit Bugge, Bjarte Bergstrom, Oda K Eide, Helene Solli, Ingrid F Kjønstad, Jørgen Stenvik, Terje Espevik, Nadra J Nilsen. Surface Toll-like receptor 3 expression in metastatic intestinal epithelial cells induces inflammatory cytokine production and promotes invasiveness. J Biol Chem. 2017 Sep 15;292(37):15408-15425

94. CHEN Y, LIN J, ZHAO Y, MA X, YI H. Toll-like receptor 3 (TLR3) regulation mechanisms and roles in antiviral innate immune responses. J Zhejiang Univ Sci B. 2021 Aug 15;22(8):609–32.

95. Zhao H, Wu L, Yan G, Chen Y, Zhou M, Wu Y, et al. Inflammation and tumor progression: signaling pathways and targeted intervention. Sig Transduct Target Ther. 2021 Jul 12;6(1):263.

96. Jones SA, Jenkins BJ. Recent insights into targeting the IL-6 cytokine family in inflammatory diseases and cancer. Nat Rev Immunol. 2018 Dec;18(12):773–89.

97. Liu W, Wang H, Bai F, Ding L, Huang Y, Lu C, et al. IL-6 promotes metastasis of non-small-cell lung cancer by up-regulating TIM-4 via NF-κB. Cell Prolif. 2020 Mar;53(3):e12776.

98. Le Noci V, Tortoreto M, Gulino A, Storti C, Bianchi F, Zaffaroni N, et al. Poly(I:C) and CpG-ODN combined aerosolization to treat lung metastases and counter the immunosuppressive microenvironment. Oncoimmunology. 2015 Oct;4(10):e1040214.

99. Howe K, Clark MD, Torroja CF, Torrance J, Berthelot C, Muffato M, et al. The zebrafish reference genome sequence and its relationship to the human genome. Nature. 2013 Apr;496(7446):498–503.

100. Bertrand JY, Chi NC, Santoso B, Teng S, Stainier DYR, Traver D. Haematopoietic stem cells derive directly from aortic endothelium during development. Nature. 2010 Mar;464(7285):108–11.

101. Franza M, Varricchio R, Alloisio G, De Simone G, Di Bella S, Ascenzi P, et al. Zebrafish (Danio rerio) as a Model System to Investigate the Role of the Innate Immune Response in Human Infectious Diseases. International Journal of Molecular Sciences. 2024 Jan;25(22):12008.

102. Gore AV, Pillay LM, Venero Galanternik M, Weinstein BM. The zebrafish: A fintastic model for hematopoietic development and disease. Wiley Interdiscip Rev Dev Biol. 2018 May;7(3):e312.

103. Lam SH, Chua HL, Gong Z, Lam TJ, Sin YM. Development and maturation of the immune system in zebrafish, *Danio rerio*: a gene expression profiling, in situ hybridization and immunological study. Developmental & Comparative Immunology. 2004 Jan 1;28(1):9–28.

104. Shan Nan Chen, Peng Fei Zou, Pin Nie. Retinoic acid-inducible gene I (RIG-I)-like receptors (RLRs) in fish: current knowledge and future perspectives. Immunology. 2017 May;151(1):16-25. doi: 10.1111/imm.12714

105. Nie L, Zhang Y sheng, Dong W ren, Xiang L xin, Shao J zhong. Involvement of zebrafish RIG-I in NF-κB and IFN signaling pathways: Insights into functional conservation of RIG-I in antiviral innate immunity. Developmental & Comparative Immunology. 2015 Jan 1;48(1):95–101.

106. Zou PF, Chang MX, Li Y, Huan Zhang S, Fu JP, Chen SN, et al. Higher antiviral response of RIG-I through enhancing RIG-I/MAVS-mediated signaling by its long insertion variant in zebrafish. Fish & Shellfish Immunology. 2015 Mar 1;43(1):13–24.

107. Gabor KA, Charette JR, Pietraszewski MJ, Wingfield DJ, Shim JS, Millard PJ, et al. A DN-mda5 transgenic zebrafish model demonstrates that Mda5 plays an important role in snakehead rhabdovirus resistance. Dev Comp Immunol. 2015 Aug;51(2):298–304.

108. Zou PF, Chang MX, Xue NN, Liu XQ, Li JH, Fu JP, et al. Melanoma differentiation-associated gene 5 in zebrafish provoking higher interferon-promoter activity through signalling enhancing of its shorter splicing variant. Immunology. 2014 Feb;141(2):192–202.

109. Gong XY, Zhang QM, Zhao X, Li YL, Qu ZL, Li Z, et al. LGP2 is essential for zebrafish survival through dual regulation of IFN antiviral response. iScience. 2022 Jul 30;25(8):104821.

110. Chen SN, Zou PF, Nie P. Retinoic acid-inducible gene I (RIG-I)-like receptors (RLRs) in fish: current knowledge and future perspectives. Immunology. 2017 May;151(1):16–25.

111. Li Y, Li Y, Cao X, Jin X, Jin T. Pattern recognition receptors in zebrafish provide functional and evolutionary insight into innate immune signaling pathways. Cell Mol Immunol. 2017 Jan;14(1):80–9.

112. Mogensen TH. Pathogen recognition and inflammatory signaling in innate immune defenses. Clin Microbiol Rev. 2009 Apr;22(2):240–73, Table of Contents.

113. Meijer AH, Gabby Krens SF, Medina Rodriguez IA, He S, Bitter W, Ewa Snaar-Jagalska B, et al. Expression analysis of the Toll-like receptor and TIR domain adaptor families of zebrafish. Mol Immunol. 2004 Jan;40(11):773–83.

114. Zhang J, Kong X, Zhou C, Li L, Nie G, Li X. Toll-like receptor recognition of bacteria in fish: ligand specificity and signal pathways. Fish Shellfish Immunol. 2014 Dec;41(2):380–8.

115. Matsuo A, Oshiumi H, Tsujita T, Mitani H, Kasai H, Yoshimizu M, et al. Teleost TLR22 recognizes RNA duplex to induce IFN and protect cells from birnaviruses. J Immunol. 2008 Sep 1;181(5):3474–85.

116. Sullivan C, Charette J, Catchen J, Lage CR, Giasson G, Postlethwait JH, et al. The gene history of zebrafish tlr4a and tlr4b is predictive of their divergent functions. J Immunol. 2009 Nov 1;183(9):5896.

117. Gill S, Catchpole R, Forterre P. Extracellular membrane vesicles in the three domains of life and beyond. FEMS Microbiol Rev. 2018 Nov 21;43(3):273–303.

118. Zhao N, Deng Q, Zhu C, Zhang B. Application of Extracellular Vesicles in Aquatic Animals: A Review of the Latest Decade. Reviews in Fisheries Science & Aquaculture. 2022 Sep 13;30(4):447–66.

119. Bai X, Shi Y, Tarique I, Vistro WA, Huang Y, Chen H, et al. Multivesicular bodies containing exosomes in immune-related cells of the intestine in zebrafish (*Danio rerio*): Ultrastructural evidence. Fish & Shellfish Immunology. 2019 Dec 1;95:644–9.

120. Mulzer LM, Felger T, Muñoz LE, Engl G, Reutter H, Schiffer M, et al. Dynamic changes of extracellular vesicles during zebrafish organogenesis. Cell Commun Signal. 2025 Feb 3;23(1):60.

121. Gatta AT, Carlton JG. The ESCRT-machinery: closing holes and expanding roles. Current Opinion in Cell Biology. 2019 Aug 1;59:121–32.

122. Scott A, Sueiro Ballesteros L, Bradshaw M, Tsuji C, Power A, Lorriman J, et al. In Vivo Characterization of Endogenous Cardiovascular Extracellular Vesicles in Larval and Adult Zebrafish. Arterioscler Thromb Vasc Biol. 2021 Sep;41(9):2454–68.

123. Verweij FJ, Revenu C, Arras G, Dingli F, Loew D, Pegtel DM, et al. Live Tracking of Inter-organ Communication by Endogenous Exosomes In Vivo. Dev Cell. 2019 Feb 25;48(4):573-589.e4.

124. Mary B, Asokan N, Jerabkova-Roda K, Larnicol A, Busnelli I, Stemmelen T, et al. Blood flow diverts extracellular vesicles from endothelial degradative compartments to promote angiogenesis. EMBO reports. 2023 Dec 6;24(12):e57042.

125. Hyenne V, Ghoroghi S, Collot M, Bons J, Follain G, Harlepp S, et al. Studying the Fate of Tumor Extracellular Vesicles at High Spatiotemporal Resolution Using the Zebrafish Embryo. Dev Cell. 2019 Feb 25;48(4):554-572.e7.

126. Bray F, Laversanne M, Sung H, Ferlay J, Siegel RL, Soerjomataram I, et al. Global cancer statistics 2022: GLOBOCAN estimates of incidence and mortality worldwide for 36 cancers in 185 countries. CA: A Cancer Journal for Clinicians. 2024;74(3):229–63.

127. Massand S, Neves RI. Emerging Therapies in the Treatment of Advanced Melanoma. Clin Plast Surg. 2021 Oct;48(4):713–33.

128. Anna Fateeva , Kevinn Eddy, Suzie Chen. Current State of Melanoma Therapy and Next Steps: Battling Therapeutic Resistance. Cancers. 2024 Apr 19;16(8):1571. doi: 10.3390/cancers16081571

129. Anderson NM, Simon MC. Tumor Microenvironment. Curr Biol. 2020 Aug 17;30(16):R921–5.

130. Larkin J, Chiarion-Sileni V, Gonzalez R, Grob JJ, Rutkowski P, Lao CD, et al. Five-Year Survival with Combined Nivolumab and Ipilimumab in Advanced Melanoma. N Engl J Med. 2019 Oct 17;381(16):1535–46.

131. Frantz WT, Ceol CJ. From Tank to Treatment: Modeling Melanoma in Zebrafish. Cells. 2020 May 22;9(5):1289.

132. Yin J, Zhao G, Kalirai H, Coupland SE, Jochemsen AG, Forn-Cuní G, et al. Zebrafish Patient-Derived Xenograft Model as a Preclinical Platform for Uveal Melanoma Drug Discovery. Pharmaceuticals (Basel). 2023 Apr 15;16(4):598.

133. Lorenzini F, Marines J, Le Friec J, Do Khoa N, Nieto MA, Sanchez-Laorden B, et al. Melanoma innervation, noradrenaline and cancer progression in zebrafish xenograft model. Cell Death Discov. 2025 May 31;11(1):260.

134. Usai A, Di Franco G, Piccardi M, Cateni P, Pollina LE, Vivaldi C, et al. Zebrafish Patient-Derived Xenografts Identify Chemo-Response in Pancreatic Ductal Adenocarcinoma Patients. Cancers. 2021 Jan;13(16):4131.

135. Patton EE, Widlund HR, Kutok JL, Kopani KR, Amatruda JF, Murphey RD, et al. BRAF mutations are sufficient to promote nevi formation and cooperate with p53 in the genesis of melanoma. Curr Biol. 2005 Feb 8;15(3):249–54.

136. Michael Dovey, Richard Mark White, Leonard I Zon. Oncogenic NRAS Cooperates with p53 Loss to Generate Melanoma in Zebrafish | Zebrafish. 2009 Dec;6(4):397-404. doi: 10.1089/zeb.2009.0606.

137. Santoriello C, Gennaro E, Anelli V, Distel M, Kelly A, Köster RW, et al. Kita Driven Expression of Oncogenic HRAS Leads to Early Onset and Highly Penetrant Melanoma in Zebrafish. PLOS ONE. 2010 Dec 10;5(12):e15170.

138. Distel M, Wullimann MF, Köster RW. Optimized Gal4 genetics for permanent gene expression mapping in zebrafish. Proceedings of the National Academy of Sciences. 2009 Aug 11;106(32):13365–70.

139. Anelli V, Santoriello C, Distel M, Köster RW, Ciccarelli FD, Mione M. Global repression of cancer gene expression in a zebrafish model of melanoma is linked to epigenetic regulation. Zebrafish. 2009 Dec 1;6(4):417–24.

140. Notarangelo M, Zucal C, Modelska A, Pesce I, Scarduelli G, Potrich C, et al. Ultrasensitive detection of cancer biomarkers by nickel-based isolation of polydisperse extracellular vesicles from blood. EBioMedicine. 2019 May;43:114–26.

141. Mayrhofer M, Gourain V, Reischl M, Affaticati P, Jenett A, Joly JS, et al. A novel brain tumour model in zebrafish reveals the role of YAP activation in MAPK- and PI3K-induced malignant growth. Dis Model Mech. 2017 Jan 1;10(1):15–28.

142. Yue K. LncRNA RPPH1 predicts poor prognosis and regulates cell proliferation and migration by repressing P21 expression in gastric cancer.

143. Parker DM, Winkenbach LP, Parker A, Boyson S, Nishimura EO. Improved Methods for Single-Molecule Fluorescence In Situ Hybridization and Immunofluorescence in Caenorhabditis elegans Embryos. Current Protocols. 2021;1(11):e299.

144. Passmore LA, Coller J. Roles of mRNA poly(A) tails in regulation of eukaryotic gene expression. Nat Rev Mol Cell Biol. 2022 Feb;23(2):93–106.

145. Zhang XO, Yin QF, Chen LL, Yang L. Gene expression profiling of non-polyadenylated RNA-seq across species. Genom Data. 2014 Aug 3;2:237–41.

146. Jiang X, Liu B, Nie Z, Duan L, Xiong Q, Jin Z, et al. The role of m6A modification in the biological functions and diseases. Sig Transduct Target Ther. 2021 Feb 21;6(1):1–16.

147. The role of m6A modification in the biological functions and diseases | Signal Transduction and Targeted Therapy [Internet]. [cited 2025 Sep 23]. Available from: https://www.nature.com/articles/s41392-020-00450-x

148. Jaffrey SR, Kharas MG. Emerging links between m6A and misregulated mRNA methylation in cancer. Genome Medicine. 2017 Jan 12;9(1):2.

149. Chu HP, Minajigi A, Chen Y, Morris R, Guh CY, Hsieh YH, et al. iDRiP for the systematic discovery of proteins bound directly to noncoding RNA. Nat Protoc. 2021 Jul;16(7):3672–94.

150. Desideri F, D'Ambra E, Laneve P, Ballarino M. Advances in endogenous RNA pull-down: A straightforward dextran sulfate-based method enhancing RNA recovery. Front Mol Biosci. 2022 Oct 19 doi.org/10.3389/fmolb.2022.1004746

151. Perederina A, Li D, Lee H, Bator C, Berezin I, Hafenstein SL, et al. Cryo-EM structure of catalytic ribonucleoprotein complex RNase MRP. Nat Commun. 2020 Jul 10;11(1):3474.

152. Kalra H, Simpson RJ, Ji H, Aikawa E, Altevogt P, Askenase P, et al. Vesiclepedia: a compendium for extracellular vesicles with continuous community annotation. PLoS Biol. 2012;10(12):e1001450.

153. Hurwitz SN, Rider MA, Bundy JL, Liu X, Singh RK, Meckes DG. Proteomic profiling of NCI-60 extracellular vesicles uncovers common protein cargo and cancer type-specific biomarkers. Oncotarget. 2016 Dec 27;7(52):86999–7015.

154. Peinado H, Alečković M, Lavotshkin S, Matei I, Costa-Silva B, Moreno-Bueno G, et al. Melanoma exosomes educate bone marrow progenitor cells toward a pro-metastatic phenotype through MET. Nat Med. 2012 Jun;18(6):883–91.

155. Suárez H, Andreu Z, Mazzeo C, Toribio V, Pérez-Rivera AE, López-Martín S, et al. CD9 inhibition reveals a functional connection of extracellular vesicle secretion with mitophagy in melanoma cells. J Extracell Vesicles. 2021 May;10(7):e12082.

156. Liang Y, Eng WS, Colquhoun DR, Dinglasan RR, Graham DR, Mahal LK. Complex N-Linked Glycans Serve as a Determinant for Exosome/Microvesicle Cargo Recruitment. J Biol Chem. 2014 Nov 21;289(47):32526–37.

157. RNA secondary structure prediction using deep learning with thermodynamic integration | Nature Communications [Internet]. [cited 2025 Oct 28]. Available from: https://www.nature.com/articles/s41467-021-21194-4

158. ViennaRNA Package 2.0 | Algorithms for Molecular Biology | Full Text [Internet]. [cited 2025 Oct 28]. Available from: https://almob.biomedcentral.com/articles/10.1186/1748-7188-6-26

159. Reuter JS, Mathews DH. RNAstructure: software for RNA secondary structure prediction and analysis. BMC Bioinformatics. 2010 Mar 15;11(1):129.

160. Liu YJ, Wang C. A review of the regulatory mechanisms of extracellular vesicles-mediated intercellular communication. Cell Communication and Signaling. 2023 Apr 13;21(1):77.

161. Alaimo A, Genovesi S, Annesi N, De Felice D, Subedi S, Macchia A, et al. Sterile inflammation via TRPM8 RNA-dependent TLR3-NF-kB/IRF3 activation promotes antitumor immunity in prostate cancer. EMBO J. 2024 Feb 5;43(5):780–805.

162. Mulcahy LA, Pink RC, Carter DRF. Routes and mechanisms of extracellular vesicle uptake. J Extracell Vesicles. 2014;3.

163. Boelens MC, Wu TJ, Nabet BY, Xu B, Qiu Y, Yoon T, et al. Exosome Transfer from Stromal to Breast Cancer Cells Regulates Therapy Resistance Pathways. Cell. 2014 Oct 23;159(3):499–513.

164. Cheng K, Wang X, Yin H. Small Molecule Inhibitors of the TLR3/dsRNA Complex. J Am Chem Soc. 2011 Mar 23;133(11):3764–7.

165. Li Y, Li Y, Cao X, Jin X, Jin T. Pattern recognition receptors in zebrafish provide functional and evolutionary insight into innate immune signaling pathways. Cell Mol Immunol. 2017 Jan;14(1):80–9.

166. Brinkman EK, Chen T, Amendola M, van Steensel B. Easy quantitative assessment of genome editing by sequence trace decomposition. Nucleic Acids Res. 2014 Dec 16;42(22):e168.

167. Lim CS, Jang YH, Lee GY, Han GM, Jeong HJ, Kim JW, et al. TLR3 forms a highly organized cluster when bound to a poly(I:C) RNA ligand. Nat Commun. 2022 Nov 12;13(1):6876.

168. Chanput W, Mes JJ, Wichers HJ. THP-1 cell line: An in vitro cell model for immune modulation approach. International Immunopharmacology. 2014 Nov 1;23(1):37–45.

169. Deschamps T, Kalamvoki M. Extracellular Vesicles Released by Herpes Simplex Virus 1-Infected Cells Block Virus Replication in Recipient Cells in a STING-Dependent Manner. J Virol. 2018 Aug 29;92(18):e01102-18.

170. Hagey DW, Ojansivu M, Bostancioglu BR, Saher O, Bost JP, Gustafsson MO, et al. The cellular response to extracellular vesicles is dependent on their cell source and dose. Science Advances. 2023 Sep;9(35):eadh1168.

171. Varela M, Diaz-Rosales P, Pereiro P, Forn-Cuní G, Costa MM, Dios S, et al. Interferon-Induced Genes of the Expanded IFIT Family Show Conserved Antiviral Activities in Non-Mammalian Species. PLOS ONE. 2014 Jun 20;9(6):e100015.

172. Rizzotto D, Vigorito V, Rieder P, Gallob F, Moretta GM, Soratroi C, et al. Caspase-2 kills cells with extra centrosomes. Science Advances. 2024 Oct 30;10(44):eado6607.

173. Ablain J, Durand EM, Yang S, Zhou Y, Zon LI. A CRISPR/Cas9 vector system for tissue-specific gene disruption in zebrafish. Dev Cell. 2015 Mar 23;32(6):756–64.

174. Hickman E, Smyth T, Cobos-Uribe C, Immormino R, Rebuli ME, Moran T, et al. Expanded characterization of in vitro polarized M0, M1, and M2 human monocyte-derived macrophages: Bioenergetic and secreted mediator profiles. PLOS ONE. 2023 Mar 2;18(3):e0279037.

175. Cao J, Zeng F, Liao S, Cao L, Zhou Y. Effects of glycolysis on the polarization and function of tumor-associated macrophages (Review). Int J Oncol. 2023 May 4;62(6):70.

176. Lv Q, Zhang Y, Gao W, Wang J, Hu Y, Yang H, et al. CSF1R inhibition reprograms tumor-associated macrophages to potentiate anti-PD-1 therapy efficacy against colorectal cancer. Pharmacol Res. 2024 Apr;202:107126.

177. Li Y, Hodge J, Liu Q, Wang J, Wang Y, Evans TD, et al. TFEB is a master regulator of tumor-associated macrophages in breast cancer. Journal for ImmunoTherapy of Cancer. 2020 Jun 2;8(1):e000543.

178. Wang K, Chen X. Autophagic tumor-associated macrophages promote the endothelial mesenchymal transition in lung adenocarcinomas through the FUT4/p-ezrin pathway. Journal of Thoracic Disease [Internet]. 2021 Oct [cited 2025 Oct 31];13(10). Available from: https://jtd.amegroups.org/article/view/57564

179. Sun J, Corradini S, Azab F, Shokeen M, Muz B, Miari KE, et al. IL-10R inhibition reprograms tumor-associated macrophages and reverses drug resistance in multiple myeloma. Leukemia. 2024 Nov;38(11):2355–65.

180. Li X, Zhou F, Niu K, Wang Y, Shi Y, Li Y, et al. Emerging discoveries on the role of TRIM14: from diseases to immune regulation. Cell Death Discov. 2024 Dec 24;10:513.

181. Cao Y, Kong L, Zhai Y, Hou W, Wang J, Liu Y, et al. Comprehensive analysis of TRIM56's prognostic value and immune infiltration in Pan-Cancer. Sci Rep. 2025 Apr 21;15(1):13673.

182. Gong W, Donnelly CR, Heath BR, Bellile E, Donnelly LA, Taner HF, et al. Cancer-specific type-I interferon receptor signaling promotes cancer stemness and effector CD8+ T-cell exhaustion. Oncoimmunology. 2021;10(1):1997385.

183. Ding H, Wang G, Yu Z, Sun H, Wang L. Role of interferon-gamma (IFN-γ) and IFN-γ receptor 1/2 (IFNγR1/2) in regulation of immunity, infection, and cancer development:

IFN-γ-dependent or independent pathway. Biomedicine & Pharmacotherapy. 2022 Nov 1;155:113683.

184. Kwaśniak K, Czarnik-Kwaśniak J, Maziarz A, Aebisher D, Zielińska K, Karczmarek-Borowska B, et al. Scientific reports concerning the impact of interleukin 4, interleukin 10 and transforming growth factor β on cancer cells. Cent Eur J Immunol. 2019;44(2):190–200.

185. Mollaoglu G, Tepper A, Falcomatà C, Potak HT, Pia L, Amabile A, et al. Ovarian cancer-derived IL-4 promotes immunotherapy resistance. Cell. 2024 Dec 26;187(26):7492-7510.e22.

186. Ain D, Shaikh T, Manimala S, Ghebrehiwet B. The role of complement in the tumor microenvironment. Fac Rev. 2021 Nov 29;10:80.

187. Kersten K, You R, Liang S, Tharp KM, Pollack J, Weaver VM, et al. Uptake of tumor-derived microparticles induces metabolic reprogramming of macrophages in the early metastatic lung. Cell Reports [Internet]. 2023 Jun 27. 10.1016/j.celrep.2023.112582

188. Metge BJ, Williams L, Swain CA, Hinshaw DC, Elhamamsy AR, Chen D, et al. Ribosomal RNA Biosynthesis Functionally Programs Tumor-Associated Macrophages to Support Breast Cancer Progression. Cancer Res. 2025 Apr 15;85(8):1459–78.

189. Qu L, Ding J, Chen C, Wu ZJ, Liu B, Gao Y, et al. Exosome-Transmitted lncARSR Promotes Sunitinib Resistance in Renal Cancer by Acting as a Competing Endogenous RNA. Cancer Cell. 2016 May 9;29(5):653–68.

190. Yoon JH, Abdelmohsen K, Gorospe M. Post-transcriptional gene regulation by long noncoding RNA. J Mol Biol. 2013 Oct 9;425(19):3723–30.

191. Yoon JH, Abdelmohsen K, Srikantan S, Yang X, Martindale JL, De S, et al. LincRNA-p21 Suppresses Target mRNA Translation. Molecular Cell. 2012 Aug 24;47(4):648–55.

192. Zhang P, Sun Y, Peng R, Chen W, Fu X, Zhang L, et al. Long non-coding RNA Rpph1 promotes inflammation and proliferation of mesangial cells in diabetic nephropathy via an interaction with Gal-3. Cell Death Dis. 2019 Jul 8;10(7):1–16.

193. Juan B Rodríguez-Molina, Matti Turtola. Birth of a poly(A) tail: mechanisms and control of mRNA polyadenylation -FEBS Open Bio. 2023 Jul;13(7):1140-1153. doi: 10.1002/2211-5463.13528

194. Sihang Zhou, Kevin Van Bortle. The Pol III transcriptome: Basic features, recurrent patterns, and emerging roles in cancer. Wiley Interdiscip Rev RNA. 2023 Sep-Oct;14(5):e1782. doi: 10.1002/wrna.178

195. Cusenza VY, Tameni A, Neri A, Frazzi R. The lncRNA epigenetics: The significance of m6A and m5C lncRNA modifications in cancer. Front Oncol. 2023 Mar 9;13:1063636.

196. Cun Y, An S, Zheng H, Lan J, Chen W, Luo W, et al. Specific Regulation of m6A by SRSF7 Promotes the Progression of Glioblastoma. genom proteom bioinform. 2023 Aug 1;21(4):707–28.

197. Müller-McNicoll M, Botti V, Domingues AM de J, Brandl H, Schwich OD, Steiner MC, et al. SR proteins are NXF1 adaptors that link alternative RNA processing to mRNA export. Genes Dev. 2016 Jan 3;30(5):553–66.

198. Lee JH, Pestova TV, Shin BS, Cao C, Choi SK, Dever TE. Initiation factor eIF5B catalyzes second GTP-dependent step in eukaryotic translation initiation. Proceedings of the National Academy of Sciences. 2002 Dec 24;99(26):16689–94.

199. Grzanka M, Piekiełko-Witkowska A. The Role of TCOF1 Gene in Health and Disease: Beyond Treacher Collins Syndrome. International Journal of Molecular Sciences. 2021 Jan;22(5):2482.

200. Sun L, Meng H, Liu T, Zhao Q, Xia M, Zhao Z, et al. Nucleolin malonylation as a nuclear-cytosol signal exchange mechanism to drive cell proliferation in Hepatocarcinoma by enhancing AKT translation. J Biol Chem. 2024 Sep 19;300(10):107785.

201. Padilla JCA, Barutcu S, Malet L, Deschamps-Francoeur G, Calderon V, Kwon E, et al. Profiling the polyadenylated transcriptome of extracellular vesicles with long-read nanopore sequencing. BMC Genomics. 2023 Sep 22;24(1):564.

202. Lunavat TR, Cheng L, Kim DK, Bhadury J, Jang SC, Lässer C, et al. Small RNA deep sequencing discriminates subsets of extracellular vesicles released by melanoma cells – Evidence of unique microRNA cargos. RNA Biology. 2015 Aug 3;12(8):810–23.

203. Hurwitz SN, Rider MA, Bundy JL, Liu X, Singh RK, Meckes DG. Proteomic profiling of NCI-60 extracellular vesicles uncovers common protein cargo and cancer type-specific biomarkers. Oncotarget. 2016 Dec 27;7(52):86999–7015.

204. Jarrous N, Liu F. Human RNase P: overview of a ribonuclease of interrelated molecular networks and gene-targeting systems. RNA. 2023 Mar;29(3):300–7.

205. Palsule G, Gopalan V, Simcox A. Biogenesis of RNase P RNA from an intron requires co-assembly with cognate protein subunits. Nucleic Acids Res. 2019 Sep 19;47(16):8746–54.

206. Reiner R, Alfiya-Mor N, Berrebi-Demma M, Wesolowski D, Altman S, Jarrous N. RNA binding properties of conserved protein subunits of human RNase P. Nucleic Acids Res. 2011 Jul 1;39(13):5704–14.

207. Shastrula PK, Lund PJ, Garcia BA, Janicki SM. Rpp29 regulates histone H3.3 chromatin assembly through transcriptional mechanisms. J Biol Chem. 2018 Aug 10;293(32):12360–77.

208. Reiner R, Krasnov-Yoeli N, Dehtiar Y, Jarrous N. Function and Assembly of a Chromatin-Associated RNase P that Is Required for Efficient Transcription by RNA Polymerase I. PLOS ONE. 2008 Dec 30;3(12):e4072.

209. Ranoa DRE, Parekh AD, Pitroda SP, Huang X, Darga T, Wong AC, et al. Cancer therapies activate RIG-I-like receptor pathway through endogenous non-coding RNAs. Oncotarget. 2016 May 3;7(18):26496–515.

210. Duewell P, Steger A, Lohr H, Bourhis H, Hoelz H, Kirchleitner SV, et al. RIG-I-like helicases induce immunogenic cell death of pancreatic cancer cells and sensitize tumors toward killing by CD8+ T cells. Cell Death Differ. 2014 Dec;21(12):1825–37.

211. Yang R, Yu S, Xu T, Zhang J, Wu S. Emerging role of RNA sensors in tumor microenvironment and immunotherapy. Journal of Hematology & Oncology. 2022 Apr 12;15(1):43.

212. Zhang T, Ma C, Zhang Z, Zhang H, Hu H. NF-κB signaling in inflammation and cancer. MedComm (2020). 2021 Dec 16;2(4):618–53.

213. Ma W, Oliveira-Nunes MC, Xu K, Kossenkov A, Reiner BC, Crist RC, et al. Type I interferon response in astrocytes promotes brain metastasis by enhancing monocytic myeloid cell recruitment. Nat Commun. 2023 May 6;14(1):2632.

214. Seth RB, Sun L, Ea CK, Chen ZJ. Identification and Characterization of MAVS, a Mitochondrial Antiviral Signaling Protein that Activates NF-κB and IRF3. Cell. 2005 Sep 9;122(5):669–82.

215. Sun Q, Sun L, Liu HH, Chen X, Seth RB, Forman J, et al. The specific and essential role of MAVS in antiviral innate immune responses. Immunity. 2006 May;24(5):633–42.

216. Stone AEL, Green R, Wilkins C, Hemann EA, Gale M. RIG-I-like receptors direct inflammatory macrophage polarization against West Nile virus infection. Nat Commun. 2019 Aug 13;10(1):3649.

217. Lefkopoulos S, Polyzou A, Derecka M, Bergo V, Clapes T, Cauchy P, et al. Repetitive Elements Trigger RIG-I-like Receptor Signaling that Regulates the Emergence of Hematopoietic Stem and Progenitor Cells. Immunity. 2020 Nov 17;53(5):934-951.e9.

218. Kornienko IV, Aramova OYu, Tishchenko AA, Rudoy DV, Chikindas ML. RNA Stability: A Review of the Role of Structural Features and Environmental Conditions. Molecules. 2024 Dec 18;29(24):5978.

219. Li X, Lei Y, Wu M, Li N. Regulation of Macrophage Activation and Polarization by HCC-Derived Exosomal lncRNA TUC339. Int J Mol Sci. 2018 Sep 28;19(10):2958.

220. Hume DA. The Many Alternative Faces of Macrophage Activation. Front Immunol. 2015 Jul 22;6:370.

221. Habib S, Osborn G, Willsmore Z, Chew MW, Jakubow S, Fitzpatrick A, et al. Tumor associated macrophages as key contributors and targets in current and future therapies for melanoma. Expert Review of Clinical Immunology. 2024 Aug 2;20(8):895–911.

222. Zhu Q, Zhao X, Zhang Y, Li Y, Liu S, Han J, et al. Single cell multi-omics reveal intra-cell-line heterogeneity across human cancer cell lines. Nat Commun. 2023 Dec 9;14:8170.

223. Wang Y, Jia J, Wang F, Fang Y, Yang Y, Zhou Q, et al. Pre-metastatic niche: formation, characteristics and therapeutic implication. Sig Transduct Target Ther. 2024 Sep 25;9(1):236.

224. Monte Westerfield, Leonard I. Zon, H. William Detrich III. Essential Zebrafish Methods: Cell and Developmental Biology. 1st Edition

225. Ellett F, Pase L, Hayman JW, Andrianopoulos A, Lieschke GJ. mpeg1 promoter transgenes direct macrophage-lineage expression in zebrafish. Blood. 2011 Jan 27;117(4):e49-56.

226. Fan R, Cui C, Kang B, Chang Z, Wang G, Cui Q. A combined deep learning framework for mammalian m6A site prediction. Cell Genomics. 2024 Dec 11;4(12):100697.

227. Chiva C, Olivella R, Borràs E, Espadas G, Pastor O, Solé A, et al. QCloud: A cloud-based quality control system for mass spectrometry-based proteomics laboratories. PLOS ONE. 2018 Jan 11;13(1):e0189209.

228. Zhu Y, Orre LM, Zhou Tran Y, Mermelekas G, Johansson HJ, Malyutina A, et al. DEqMS: A Method for Accurate Variance Estimation in Differential Protein Expression Analysis. Mol Cell Proteomics. 2020 Jun;19(6):1047–57.

229. Kim HJ, Kim T, Hoffman NJ, Xiao D, James DE, Humphrey SJ, et al. PhosR enables processing and functional analysis of phosphoproteomic data. Cell Rep. 2021 Feb 23;34(8):108771.

230. Chen EY, Tan CM, Kou Y, Duan Q, Wang Z, Meirelles GV, et al. Enrichr: interactive and collaborative HTML5 gene list enrichment analysis tool. BMC Bioinformatics. 2013 Apr 15;14:128.